

1 How unstable was the environment during the Penultimate Glacial in
2 the South-Western Mediterranean? Vegetation, climate and human
3 dynamics during MIS 6.
4

5 **Charton Liz^{1,2}, Combourieu-Nebout Nathalie¹, Bertini Adele², Peyron Odile³, Robles Mary³,**
6 **Lebreton Vincent¹, Moncel, Marie-Hélène¹.**

7 1 : UMR 7194 HNHP- « Histoire Naturelle des Humanités Préhistoriques », MNHN / CNRS / UPVD, Paris, France.
8 liz.charton@mnhn.fr

9 2 : Dipartimento di Scienze della Terra, Università degli Studi di Firenze, Florence, Italy.

10 3: UMR 5554, ISEM-Institut des Sciences de l'Evolution de Montpellier, CNRS, Université de Montpellier, Montpellier, France.

11

12 **Correspondance** : Liz Charton (liz.charton@mnhn.fr)

13 Abstract

14 The impact of rapid climate variability on Neanderthal population in Europe during the Last
15 Glacial (Marine Isotope Stages 4-2), including Dansgaard-Oeschger cycles and Heinrich events, has
16 been the subject of a long-standing debate. However, few studies have focused on the nature and
17 impact of such rapid variations on human population during earlier periods. A growing number of high-
18 resolution paleoclimatic archives supports the persistence of rapid oscillations during the penultimate
19 glaciation (MIS 6), and the close response of Mediterranean ecosystems to these. Still, few
20 palynological sequences in the Mediterranean region offer sufficient resolution to document
21 vegetation dynamics during this time. Pollen records are especially lacking in the western
22 Mediterranean, a key region to understand the connection between North Atlantic and Mediterranean
23 climatic influences. This region is also traditionally considered a climatic refugium for human
24 population during unfavourable periods. We provide new palynological data covering MIS 6 from the
25 long and continuous marine record of ODP 976 in the Alboran Sea. A total of 200 samples, spanning
26 the interval from 196 to 127 ka Before Present (BP), reveal both long-term trends and rapid
27 fluctuations in regional vegetation composition. A multi-method approach, including modern
28 analogues, regression, and machine learning approaches, was applied to ODP 976 pollen assemblages
29 to reconstruct the annual/seasonal temperatures and precipitation. Results show that three phases
30 can be identified. The first phase (187-166 ka BP) is characterized by significant oscillations of
31 temperate trees and rather cool and humid conditions during early MIS 6, coincident with a sapropel
32 layer deposition in both the western and eastern Mediterranean. In the second phase (165-144 ka BP),
33 arid herbaceous vegetation is dominant, marking the main imprint of glacial maxima conditions and

34 reduced climate variability. The third phase (144-129 ka BP) is marked by the development of Ericaceae
35 and increased annual precipitation. At the end of MIS 6 glaciation, an episode of strong cooling and
36 steppe and semi-desert expansion is identified as Heinrich Stadial 11 (135-129 ka BP), marking a
37 distinct pattern for Termination II in the Western Mediterranean. Rapid oscillations appear like a
38 pervasive feature of the Penultimate glacial in the SW Mediterranean, though they present reduced
39 amplitude and frequency compared to the Last Glacial. A synthesis of human occupation during MIS 6
40 shows that a mosaic of traditional (Mode 2) and innovative (Mode 3) lithic technological features is
41 observed in the archaeological record. Although the data are scarce, Neanderthals seem to have
42 continuously inhabited Western Mediterranean regions across the penultimate glacial. The severe
43 climate conditions during Heinrich Stadial 11 (~133-129 ka BP) might have played a role in the apparent
44 population contraction at the end of MIS 6, and perhaps also in the definitive abandonment of Lower
45 Palaeolithic industries.

46 1. Introduction

47 Rapid climate oscillations occurred during the last Glacial period (MIS 4-2). Dansgaard-
48 Oeschger (DO) cycles have been well identified in ice-core records (Bond et al., 1999; Dansgaard et al.,
49 1993; Johnsen et al., 1992; Rasmussen et al., 2014) and recognized in Atlantic sedimentary cores (e.g.
50 Bond et al., 1993, 1997; Roucoux et al., 2005; Sánchez Goñi et al., 2002; Shackleton et al., 2000,
51 Zumaque et al., 2025). Short periods of intense cold named Heinrich Stadials (HS) and linked with
52 intense iceberg discharges were also evidenced in Atlantic sediments (Bond et al., 1992; Heinrich,
53 1988; Hemming, 2004; Rasmussen et al., 2003; Ruddiman, 1977; Shackleton et al., 2004). Major cooling
54 events also occurred during MIS 5 and the penultimate deglaciation (e.g. Chapman & Shackleton, 1999;
55 Oppo et al., 2001). These high-frequency oscillations reflect major changes at global scale in the
56 oceanic circulation and the Atlantic Meridional Overturning Circulation (AMOC), that are important
57 features particularly during glacial terminations (Barker and Knorr, 2021). The Mediterranean region
58 has been very sensitive to the rapid climate oscillations of MIS 5 to MIS 1, with changes recorded in
59 both marine and continental environments (Cacho et al., 1999, 2006; Combourieu-Nebout et al., 2002,
60 2009; Fletcher et al., 2010; Martrat et al., 2007; Penaud et al., 2016; Sánchez Goñi et al., 2002, 2022).

61 The penultimate glacial (MIS 6) took place between ~185 and 130 ka BP and presented a
62 different ice-sheet and global climate configuration compared to the last glacial (MIS 4-2). It is
63 considered among the coldest glacial periods of the past 800 ka BP (Masson-Delmotte et al., 2010),
64 characterized by larger European Ice-Sheet and smaller Laurentide ice-sheet extension (Colleoni et al.,
65 2016; Ehlers et al., 2018; Ehlers & Gibbard, 2007; Rohling et al., 2017). In Europe, it corresponds to the
66 Riss glaciation in the Alpine area, and to the late Saalian glaciation complex in northern and central

67 Europe, with two major ice-sheet advances identified in Germany: the Drenthe advance (~170-155 ka
68 BP) characterized by the maximum ice extent in Europe, and the less extensive Warthe advance during
69 the younger stage of MIS 6 (Ehlers et al., 2011). The exact chronology of the Penultimate Glacial
70 Maximum (i.e. the maximum extension of the northern hemisphere ice-sheet) is still not well
71 constrained (Svendsen et al., 2004), but is usually considered around 140 ka BP (Colleoni et al., 2016).
72 Five marine isotopic substages were identified from MIS 6e to 6a, reflecting variations of global sea
73 temperatures : three cold substages (6e : ~180 ka BP, 6c : ~160 ka BP, 6a : ~136 ka BP) with increasing
74 cold intensity, and two warm substages (6d : ~170 ka BP and 6b : ~149 ka BP) (Railsback et al., 2015).
75 Different speleothem records revealed that MIS 6 glaciation in Europe, including the Mediterranean
76 region, was characterized by wetter conditions in comparison with the last glacial (Ayalon et al., 2002;
77 Koltai et al., 2017; Nehme et al., 2018; Regattieri et al., 2014). Furthermore, various studies highlighted
78 the apparent higher stability of the Laurentide ice-sheets during the penultimate glacial, leading to the
79 absence of typical “Heinrich layers” in the North Atlantic sediments, with the exception of the large
80 event recorded at the MIS 6 to MIS 5 transition, HS11 (~135-129 ka BP) (de Abreu et al., 2003;
81 McCarron et al., 2021; McManus et al., 1999; Obrochta et al., 2014; Ovsepyan and Murdmaa, 2017;
82 Shackleton et al., 2003).

83 Human Palaeolithic groups in Europe were likely affected by rapid climate changes
84 (Bradtmöller et al., 2012; Dennell et al., 2011; Raia et al., 2020; Willis et al., 2004). The South-Western
85 Mediterranean probably played a major role as one of the climate refugia areas around the
86 Mediterranean Basin during the most unfavourable climatic periods, permitting the persistence of
87 “source” population able to recolonize the northernmost areas during more favourable periods (Bailey
88 et al., 2008; Bicho & Carvalho, 2022). Neanderthal presence in very distinct ecotones in Eurasia proves
89 it could adapt to a very wide range of environments. However, recent niche modelling approaches
90 together with palaeoecological data from archaeological sites strengthened the view that warm
91 forested landscapes like the MIS 5e environments represented the most suitable habitats for
92 Neanderthals, where they could persist during colder periods (Carrión et al., 2026; Ochando et al.,
93 2019; Stewart et al., 2019; Trájer, 2023). This conception leads to the overlap of the notions of
94 refugium for vegetation and human populations, despite the greatest adaptability and niche extension
95 of humans.” Many studies focused on the potential impact of abrupt environmental changes on
96 Neanderthal populations, especially those associated with Heinrich Stadials during MIS 3 (e.g. Charton
97 et al., 2025; D’Errico & Sánchez Goñi, 2003; Finlayson & Carrión, 2007; Melchionna et al., 2018). During
98 the previous climatic cycles of the Middle Pleistocene, when Early to Middle Palaeolithic cultures
99 developed, repeated climate instability has been brought forward as an explanation for the large
100 variability in the lithic production (Dennell et al., 2011; Foerster et al., 2022; Sánchez-Yustos and Diez-

101 Martín, 2015), and the non-linearity of Neanderthal biological evolution (Bermúdez de Castro &
102 Martín-Torres, 2013; Hublin, 2009). Still, the short and long-term resilience of human populations
103 in a globally unstable environment is poorly understood, and partially hindered by our limited
104 knowledge of fast millennial-scale climate oscillations in older glaciations prior to MIS 4-2.

105 While the Greenland ice does not provide an adequate record for periods older than 123 ka BP
106 (Chappellaz et al., 1997), the description of a precise stratigraphy of climate events at sub millennial
107 scale for the previous glacial/interglacial cycles remains complex, and relies on the Antarctic isotope
108 record (Bazin et al., 2013; Jouzel et al., 2007), the study of marine sediments (de Abreu et al., 2003;
109 Lisiecki & Raymo, 2005; Margari et al., 2010, 2014; McManus et al., 1999; Obrochta et al., 2014) and
110 high-resolution continental archives such as speleothems (Burns et al., 2019; Held et al., 2024; Hodge
111 et al., 2008; Wainer et al., 2013; Wang et al., 2018; Wang et al., 2001). Benthic and planktonic isotopic
112 ratios together with Sea Surface Temperatures (SSTs) reconstructions in the North Atlantic and the
113 Western Mediterranean showcased the persistence of D-O-like events and interhemispheric bipolar
114 see-saw heat transport during MIS 6, in addition to important reorganization of the water circulation
115 during sapropel S6 deposition ~175 ka BP (Margari et al., 2010, 2014; Martrat et al., 2004, 2007, 2014;
116 Rousseau et al., 2020; Sierro & Andersen, 2022). Nevertheless, MIS 6 is much less well documented
117 than the last glacial in Mediterranean Europe. Few palynological sequences are available to document
118 the vegetation changes across this interval (Camuera et al., 2019, 2022; Follieri et al., 1988; Margari et
119 al., 2010; Okuda et al., 2001; Roucoux et al., 2011; Sadori et al., 2016; Sinopoli et al., 2019; Tzedakis et
120 al., 2006; Wilson et al., 2021). Among them, only one in SW Europe provides sufficient resolution to
121 document high-frequency changes (Margari et al., 2010, 2014). This record from the deep-sea core
122 MD01-2444 showed that several D-O like events impacted the vegetation during the lower part of MIS
123 6 (Margari et al., 2010). The core is located out of the Mediterranean Sea, along the Portuguese margin
124 in the Atlantic Ocean. Therefore, questions remain open concerning the impact of such rapid events
125 on the Western Mediterranean region, considered a Pleistocene refugium for human populations.

126 To fill this gap, our study provides high-resolution pollen data and quantitative climate
127 reconstructions from ODP site 976 in south-western Mediterranean focusing on MIS 6. We aim to (i)
128 reconstruct the vegetation and climate changes in the SW Mediterranean during the penultimate
129 glacial, (ii) identify abrupt climatic changes including potential Heinrich-like and D-O like events and
130 correlate them with other Atlantic and Mediterranean paleoenvironmental records, (iii) compare the
131 nature of millennial-scale climate and vegetation dynamics during the last glacial period and the
132 penultimate glacial using a single, continuous pollen record and (iv) explore the potential impact of
133 these climatic changes for Early Middle Palaeolithic human groups, with particular attention to the
134 presence of climate refugia during the most extreme glacial phases.

135 2. Study site

136 Ocean Drilling Program (ODP) Site 976 (36°12 N, 4°18W, 1108 m depth) core was retrieved in
137 1995 in the Alboran Sea (Zahn et al., 1999). The site is located about 110 km east of the Gibraltar Strait,
138 70 km south of the Spanish coast, and 100 km north of Morocco (Fig. 1).

139 The Alboran Sea is the westernmost extensional basin of the Mediterranean Sea, bordered to
140 the north by the Betic Cordillera and to the south by the Moroccan Rif mountains. Oceanic currents
141 result from the water masses exchanges between the Atlantic Ocean and the Mediterranean Sea
142 through the Gibraltar Strait. The surface currents are governed by the inflow of low-salinity Atlantic
143 waters (Atlantic Jet) forming two anticyclonic gyres named Western and Eastern Alboran Gyres (WAG
144 and EAG) (Renault et al., 2012) (Fig. 1). The Mediterranean high-salinity water masses flow out in the
145 Atlantic basin through the intermediate depth currents.

146 The modern climate in the Alboran Sea region is typically Mediterranean, defined by long, hot,
147 dry summers and mild and cool winters (Lionello et al., 2006; Sánchez-Laulhé et al., 2021). Atlantic
148 westerlies dominate during winter, while subtropical high pressure masses generate intense drought
149 during summer (Sumner et al., 2001). The current vegetation distribution on the Alboran borderlands
150 follows a strong altitudinal climatic gradient : dry steppe elements such as *Artemisia* and *Lygeum* grow
151 in the most arid lowlands along the coast, sclerophyllous evergreen taxa, including *Quercus ilex*, *Olea*
152 and *Pistacia* are the main representatives of the thermo-to meso-Mediterranean belts, while
153 temperate vegetation with deciduous trees constitutes the overlying supra-Mediterranean belt
154 (Quézel, 2000). Finally, coniferous forests of *Abies* and *Pinus* grow in the oro-Mediterranean belt
155 (above approximately 1200 m), with the presence of *Cedrus* in altitudinal vegetation of the Moroccan
156 Rif mountains.

157 The main sedimentation processes in the area originate from the strong erosion in the Betic
158 Cordillera (Alonso et al., 1999; Liqueste et al., 2005; Lobo et al., 2006) and the material transported by
159 the surface Atlantic waters (Auffret et al., 1974), although a significant but unknown proportion of
160 particles including pollen was transported by African winds as evidenced by the presence of Saharan
161 clay particles and *Cedrus* pollen across the Pleistocene (Bout-Roumazielles et al., 2007; Jiménez-
162 Moreno et al., 2020; Magri & Parra, 2002). Therefore, the pollen assemblage is interpreted as reflecting
163 the regional vegetation of the southern Iberian Peninsula, with smaller but variable contribution from
164 Northern Africa. Previous studies have shown that the Alboran Sea palynological record displays close
165 similarities with the Padul record in SE Spain (Camuera et al., 2019), indicating that ODP 976 is a valid
166 archive to reconstruct the southern Iberian Peninsula vegetation changes (Fletcher & Sánchez Goñi,
167 2008; Charton et al., 2025).

168 Two Organic-Rich Layers (ORLs) were identified in ODP 976 core during the MIS 6 interval, bed
 169 607 (50.43-49.93 m), and bed 606 (41.6-40.4 m) (Murat, 1999). The ages were recalculated based on
 170 the updated age model for MIS 6 presented here, giving 178.07-174.53 ka BP for bed 607, and 132.64-
 171 129.16 ka BP for bed 606. With a Total Organic Carbon (TOC) of 1.18% and 1.85% respectively, these
 172 layers have been described as “ghost sapropels”, as they present a lower organic matter content than
 173 the Eastern Mediterranean sapropels (Rogerson et al., 2008). Their relevance for hydrological and
 174 climatic inferences in the Alboran Sea will be discussed in the light of the vegetation dynamics.



Fig. 1. Map showing the location of ODP 976 core together with other paleoenvironmental and paleoclimate records covering part or all of MIS 6, as discussed in the text.

175

176 3. Methods

177 3.1. Age Model

178 The age model for the study interval uses three previously published tie-points between ODP
 179 976 Mg/Ca-derived SST (Jiménez-Amat and Zahn, 2015) and the speleothem temperature records from
 180 Dongge cave in China (Kelly et al., 2006, see Supplement Fig. S1). Several other marine records covering
 181 MIS 6 in the region are chronologically tuned to speleothems (e.g. Sierro & Anderson, 2022; Tzedakis
 182 et al., 2018). For the lower interval, the low resolution of planktonic isotopic data available for ODP
 183 976 did not allow direct correlation to global temperature stacks or orbital configuration (von
 184 Grafenstein et al., 1999). Instead, we chose to align the higher-resolution pollen record produced in
 185 this study with the one from MD01-2444 core on the Portuguese margin (Margari et al., 2010, 2014;
 186 Tzedakis et al., 2018). Previous studies highlighted the strong similarities between pollen records on
 187 the Atlantic margin and the Alboran Sea during the last glacial period (Fletcher et al., 2010; Fletcher &
 188 Sánchez Goñi, 2008; Sánchez Goñi et al., 2002), supporting this approach. MD01-2444 chronology is
 189 based on the alignment of benthic isotopic events with the Antarctic temperature record, on AICC2012
 190 timescale (Jouzel et al., 2007; Margari et al., 2010; Shin et al., 2020). The eleven tie-points between
 191 MD01-2444 core and Epica Dome C can be found in Supplement (Table S1). Five peaks of temperate
 192 forest in MD01-2444 were used as control-points for ODP 976 (Table 1). The main assumptions of these
 193 tuning approaches with Dongge cave speleothem and the Antarctic record are discussed in detail in
 194 Jiménez-Amat and Zahn (2015) and Margari et al. (2010) respectively. The obtained chronology for
 195 ODP 976 core for MIS 6 prevents any assessment of the southwestern Mediterranean vegetation
 196 response to global climatic events.

Event type	ODP 976 meters composite depth (mcd)	Age (ka BP)	References
Dongge cave speleothem D3	40.25	128.73	Jiménez-Amat and Zahn, 2015; Kelly et al., 2006
Dongge cave speleothem D2	42.61	135.57	Jiménez-Amat and Zahn, 2015; Kelly et al., 2006
Dongge cave speleothem D1	44.14	142.09	Jiménez-Amat and Zahn, 2015; Kelly et al., 2006
Temperate pollen peak in MD01-2444	46.4	149.43	(Margari et al., 2010; Shin et al., 2020)
Temperate pollen peak in MD01-2444	48.5	160.00	(Margari et al., 2010; Shin et al., 2020)
Temperate pollen peak in MD01-2444	49.3	170.07	(Margari et al., 2010; Shin et al., 2020)
Temperate pollen peak in MD01-2444	50.48	178.42	(Margari et al., 2010; Shin et al., 2020)
Temperate pollen peak in MD01-2444	53.2	193.758	(Margari et al., 2010; Shin et al., 2020)

197 **Table 1. List of control points used to calibrate the ODP 976 record for the MIS 6 interval.** The tie-
 198 points on MD01-2444 temperate pollen curve are on AICC2012 timescale.

199 A linear regression was applied to obtain a continuous age for the study interval, spanning from
200 126.4 to 196.6 ka BP, with a mean resolution of about 350 years for the record (Fig. 2).

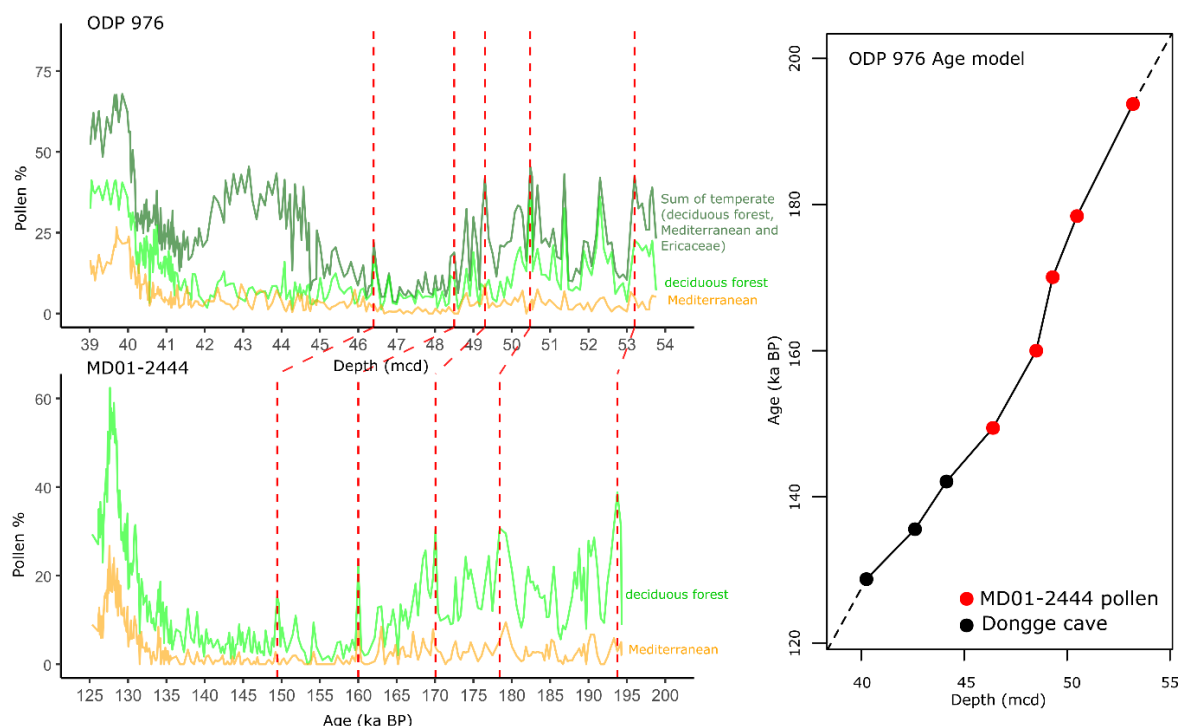


Fig. 2. Age versus depth model for the MIS 6 part of ODP 976 record, based on correlation between the Mg/Ca-based SST curve (Jiménez-Amat and Zahn, 2015) and the Dongge cave speleothem temperature record (Kelly et al., 2006) (black dots), and graphical correlation of the temperate pollen curve with the MD01-2444 palynological record (red dots and dotted lines) on AICC2012 timescale (Margari et al., 2010; Shin et al., 2020).

201

202 3.2. Pollen analyses

203 Two hundred samples have been analysed in this study, between 40 and 54 m (mcd) depth.
204 The sample processing followed the traditional steps used for pollen extraction (Faegri and Iversen,
205 1964) and previously applied to the ODP 976 core (Combourieu-Nebout et al., 2002; 2009; Sassoon et
206 al., 2023, Charton et al., 2025). It included sample weighing between 5 and 10 g of sediments, a 150
207 μm sieving for retrieving microfossils and macroparticles, followed by 10% HCl, 40% HF, 20% HCl and
208 a final 10 μm sieving.

209 A minimum of 150 pollen grains were counted for each sample, excluding *Pinus* as it is usually
210 overrepresented in marine sequences (e.g. Combourieu-Nebout et al., 2002; Fletcher et al., 2010b;
211 Mudie, 2011 and references therein), and represents often more than 50% of the total pollen sum in
212 the study interval (see Fig. 3).

213 Ecological groups of pollen taxa were defined following previous studies of the ODP 976 record
214 (Charton et al., 2025; Combourieu-Nebout et al., 2009; Sassoon et al., 2023). The percentage pollen

215 diagram was constructed using the *rioja* R package (Juggins, 2023). Constrained Incremental Sum-of-
216 Squares (CONISS) cluster analysis was applied for pollen zonation, using the *vegan* package on R
217 (Oksanen et al., 2024).

218 3.3. Pollen-inferred climate reconstructions: a multi-method approach

219 Four methods were applied to the ODP 976 record to reconstruct past climate changes during
220 MIS 6. This is the first time this approach is used for the entire MIS 6 interval (Sinopoli et al., 2019).
221 The multi-method approach allows for a more accurate climate reconstruction (trends and rapid
222 events) compared to the traditional single-method approach (Chevalier et al., 2020; Peyron et al.,
223 2011, 2013; Salonen et al., 2019; Sassoon et al., 2025). It also allows us to compare the reliability and
224 biases of the different methods, which are based on different ecological principles and mathematical
225 algorithms. Four methods were used in this study.

226 The Modern Analogue Technique (MAT) is the first “assemblage” method ever developed to
227 estimate climate parameters based on pollen assemblages, and is still the most widely used (Guiot,
228 1990). It is based on the calculation of a dissimilarity index between the fossil samples and samples
229 from a modern pollen dataset. The values of the closest modern analogues selected (here, 4) are
230 averaged to reconstruct the climate parameters for each fossil sample. Weighted-Averaging Partial
231 Least Squares (WA-PLS) (ter Braak and Juggins, 1993) is the second most widely used method, and is
232 based on a different mathematical approach using non-linear regression. Assuming that taxa are most
233 abundant where they find their optimum climatic conditions, WA-PLS models the plant/climate
234 relationships from the modern calibration dataset, weighing the climatic values based on the pollen
235 taxa percentage. These plant pollen abundance / climate transfer functions are then used to calculate
236 the climate parameters of the fossil samples. The last two methods, Random Forest (RF) and Boosted
237 Regression Trees (BRT), rely on a completely different approach using machine learning: they generate
238 a large set of regression trees based on a randomised pollen dataset by bootstrapping (with pollen
239 taxa selected randomly). Contrary to RF (Prasad et al., 2006), BRT (Salonen et al., 2012) assigns a higher
240 probability to select samples that have not been selected before (boosting), increasing the
241 performance of the model for elements that are less well predicted (Chevalier et al., 2020). The
242 application of these machine learning methodologies in paleoclimatology is very promising, especially
243 for BRT, and they have already been validated through different European and Mediterranean pollen
244 records, for different time periods (Charton et al, 2025; D’Oliveira et al., 2023; Robles et al., 2022,
245 2023; Salonen et al., 2019; Sassoon et al., 2025).

246 The four methods were run on R using the *Rioja* package for MAT and WA-PLS (Juggins, 2024),
247 *dismo* for BRT (Hijmans et al., 2023) and *randomForest* for RF (Liaw and Wiener, 2022).

248 We used the modern pollen dataset compiled by Peyron et al. (2013, 2017) and updated by
249 Dugerdil et al. (2021a) and Robles et al. (2023). Samples belonging to non-relevant biomes for this
250 study were excluded (Taiga, Tundra, Pioneer Forest, warm steppe and hot desert), resulting in 2373
251 samples for calibration dataset spanning Eurasia and NW Africa (see Supplement, Fig. S2). A total of
252 103 harmonized pollen taxa are included in the dataset, excluding *Pinus* and aquatic taxa.

253 Six climate variables were reconstructed: PANN (annual precipitation), MAAT (annual
254 temperatures), SUMMERPR (summer precipitation), WINTERPR (winter precipitation), MTWA (mean
255 temperature of the warmest month) and MTCO (mean temperature of the coldest month). The
256 climatic tolerance spectra of the ten most abundant pollen taxa in the ODP 976 record have been
257 reconstructed based on the modern dataset (Supplement, Fig. S3). They show that steppe and semi-
258 desert taxa display the highest tolerance to low winter temperature and precipitation, while
259 Mediterranean taxa (*Olea* and *Quercus ilex*-type) are the most tolerant taxa to high annual and summer
260 temperature, and *Cedrus* and Ericaceae to higher annual and seasonal precipitation. SUMMERPR was
261 poorly reconstructed according to the accuracy indicators (Table 2). This is in agreement with previous
262 studies showing the poor reliability of summer parameters (e.g. Camuera et al., 2022). Therefore, we
263 chose to represent seasonal parameters as contrast values for a better visualization: TCON
264 (temperature contrast) = MTCO - MTWA, and PCON (precipitation contrast) = WINTERPR -
265 SUMMERPR. The MTWA and SUMMERPR results can be found in Supplement (Fig. S4).

266 For comparison with the present-day climate, and the calculation of anomalies, the modern
267 values were extracted from ERA 5 reanalysis of the ECMWF (European Centre for Medium-Range
268 Weather Forecasts), based on data assimilation into meteorological modelling from 1960 to 2022
269 (Hersbach et al., 2020). Pollen dispersal is reduced beyond a radius of 175 km (Rojo et al., 2016).
270 However, other studies suggest that pollen can be transported up to distances of 200-300 km
271 (Fernández-Rodríguez et al., 2014) and even over distances greater than 500 km (Bayr et al., 2023;
272 Damialis et al., 2017). Sediments from marine cores such as ODP 976 can therefore include close and
273 long-distance pollen. To account for these observations, an averaged value of the climate parameters
274 on a 400 km radius around the ODP 976 site was extracted (Supplement, Fig. S5), giving MAP = 478
275 mm, MAAT = 16.78°C, MTCO = 13.78 °C, WINTERPR = 172 mm, TCON = -9.59, PCON = 141.5 mm. These
276 values for modern climate, averaged temporally and spatially, provide a better basis for understanding
277 the nature of the climate signal extracted from a marine palynological sequence at a regional pluri-
278 annual scale.

279 The reliability of the different methods and climate parameters reconstructed is evaluated with
280 bootstrapping cross-validation through two indicators: the correlation coefficient between the
281 variables (R^2) and the root mean square error (RMSE).

282 4. Results

283 4.1. Pollen record

284 The pollen diagram shows the vegetation dynamics between 196.6 and 127.5 ka BP, spanning
285 late MIS 7 to early MIS 5 (Fig. 3). Five pollen zones were separated by CONISS cluster analysis, with
286 zone 4 being divided in three subzones (Table 2).

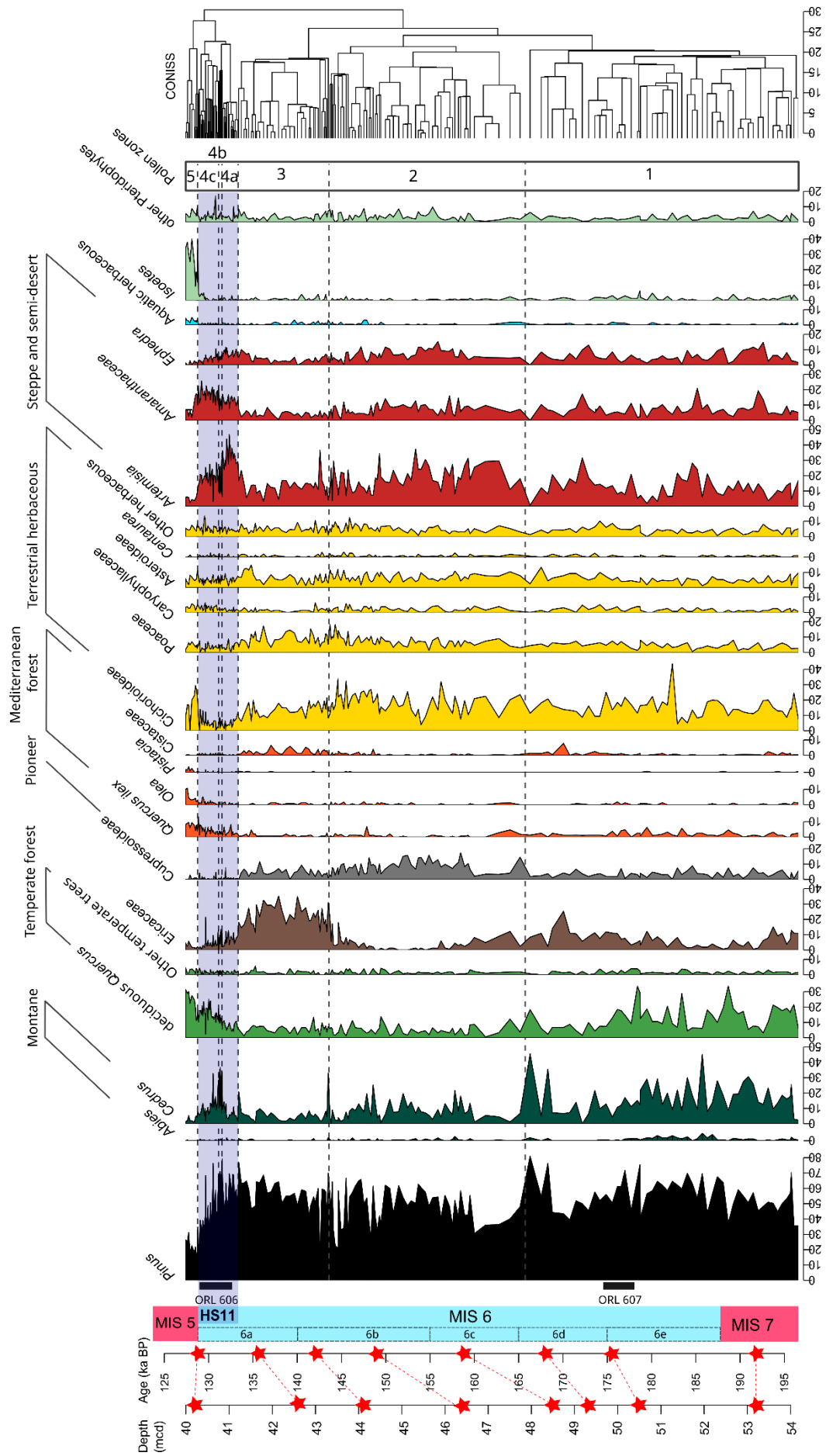


Fig. 3. Pollen diagram of selected taxa for MIS 6 interval in the ODP 976 record, plotted against age. Taxa are grouped by ecological groups (see Table 2). Red stars indicate control points used for the age calibration, and their correspondence with mcd (meters composite depth) (see Table 1). The blue bar indicates Heinrich Stadial 11. ORL : Organic Rich Layers from ODP 976 (Murat, 1999).

287

288 Zone 1 most represented taxa are deciduous *Quercus* and *Cedrus*, with important abundance
289 variability showing an unstable phase at the transition from MIS 7 to MIS 6e and 6d. Zone 2 displays
290 the maximum expansion of steppe and semi-desert vegetation together with other open vegetation
291 taxa and Cupressoideae during the MIS 6b and 6c. An additional noteworthy observation within this
292 interval is the presence of gastropod shells identified as *Limacina retroversa* (Jeanne Rampal, personal
293 communication, 2023), recovered during sieving of a sample at 46.4 m, corresponding to around
294 155.5 ka BP (Fig. 4). This species is usually most abundant in temperate to subpolar waters in the
295 North-Atlantic (Thabet et al., 2015). Zone 3 is mainly characterized by the abundance of Ericaceae at
296 the final stage of MIS 6 (6b and 6a). Zone 4, at the end of MIS 6a, is divided into 3 subzones which
297 display fast vegetation changes during the transition from MIS 6 to MIS 5 (Termination II), and Heinrich
298 Stadial 11. The fast expansion of steppe and semi-desert taxa (*Artemisia*, *Amaranthaceae*, *Ephedra*)
299 occurs simultaneously with the first increase of deciduous temperate and Mediterranean forest
300 indicative of the initialization of interglacial conditions (zone 4a). This episode of arid vegetation
301 dominance is interrupted in zone 4b by the fast expansion of montane vegetation mainly represented
302 by *Cedrus*. A new steppe and semi-desert vegetation increase is observed in zone 4c, while the
303 deciduous temperate forest and the Mediterranean vegetation continue to expand. Finally, zone 5 is
304 characterized by the maximum abundance of mesophilous and thermophilous elements, mainly
305 represented by deciduous *Quercus* and *Quercus ilex*, typical of the MIS 5 interglacial.

306

307

308

309

310

311

312

313

314

315

316

317

Pollen zone	Depth (mcd) and Age (ka BP)	Description of the pollen assemblage (Fig. 3)	Climate reconstructions (Fig. 5)
5	40.25-39.98 m 128.73-127.47 ka BP	Peak abundance of deciduous <i>Quercus</i> (up to 32%), <i>Quercus ilex</i> (4-10%), <i>Olea</i> (2-11%), <i>Pistacia</i> (up to 4%), aquatic herbaceous (up to 5%) and <i>Isoetes</i> (up to 38%). High values of Cichorioideae (up to 30%). Low percentages of <i>Pinus</i> (<35%), <i>Artemisia</i> (<11%), Amaranthaceae (<18%) and <i>Ephedra</i> (<3%).	Rapid increase of temperature, precipitation and seasonal contrast close to the modern value
4c	41.08-40.28 m 131.13-128.81 ka BP	New increase of <i>Artemisia</i> (up to 29%) and Amaranthaceae (up to 26%). High values of <i>Cedrus</i> (5-28%), and increasing percentages of deciduous <i>Quercus</i> (10-23%), Cichorioideae (0-14%) and <i>Quercus ilex</i> (1-13%). Decrease of Ericaceae (13-0%). Increasing percentages of <i>Isoetes</i> (0-5%) and Pteridophytes spores (0-17%).	First decrease, and then increase in temperatures and precipitation, with low PCON.
4b	41.21-41.09 m 131.51-131.16 ka BP	Peak abundance of <i>Cedrus</i> (up to 37%). Decrease of <i>Artemisia</i> (30-7%), Amaranthaceae (6-13%) and <i>Ephedra</i> (6-4%). Notable abundance of deciduous <i>Quercus</i> (6-15%) and <i>Quercus ilex</i> (1-3%).	Abrupt rise in precipitation contrast, but still cold conditions.
4a	41.82-41.22 m 133.28-131.54 ka BP	Peak abundance of <i>Artemisia</i> , (24-47%), Amaranthaceae (14-6%) and <i>Ephedra</i> (5-11%). Decreasing trend of Ericaceae percentages (12-2%), and progressive increasing of deciduous <i>Quercus</i> (4-11%) and <i>Quercus ilex</i> (1-8%). Decrease of Cichorioideae (<11%) and Cupressoideae (<8%).	Rapid decrease in temperature, precipitation and seasonal contrast.
3	44.57-41.85 m 143.49-133.37 ka BP	Peak abundance of Ericaceae (12-35 %), and high values of Cichorioideae (8-22%). Notable presence of Cupressoideae (2-11%). Peak abundance of <i>Artemisia</i> (37%) at 44.28 m / 142.54 ka BP and <i>Cedrus</i> (33%) at 44.57 m/143.49 ka BP.	Increase of temperatures (but still lower than present), and important precipitation rise until values higher-than-present. Seasonal contrast close to present-day.

2	48.91-44.63 m 165.16-143.68 ka BP	High percentages of Cichorioideae (11-34 %), Poaceae (4-18%), <i>Artemisia</i> (4-37%), Amaranthaceae (3-16%) and <i>Ephedra</i> (3-12%). Cupressoideae maximum between 150-160 ka BP (up to 17%), and abundant <i>Cedrus</i> (up to 25%). Very low values of deciduous <i>Quercus</i> (<10%), Mediterranean taxa (<4%) and Ericaceae (<12%), with minimum values between 150 and 158 ka BP.	Decline of temperatures and precipitation, both lower than the modern values, reaching a minimum between ~164-155 ka BP. Afterwards, progressive rise in temperature, precipitation and seasonal contrast.
1	53.76-49 m 196.15-166.29 ka BP	High percentages of <i>Cedrus</i> (8 to 45%) and deciduous <i>Quercus</i> (4 to 34%), with important variations. Abundant Cichorioideae (up to 43%) and Ericaceae (up to 25%), with notable presence of <i>Abies</i> (up to 5%), <i>Quercus ilex</i> (up to 6%) and <i>Isoetes</i> (up to 6%). Relatively low values of semi-desert elements (<i>Artemisia</i> , Amaranthaceae, <i>Ephedra</i>) but with two increases at 49.6 m / 172 ka BP and at 51.6 m / 185 ka BP.	Rather stable conditions expressed by the smoothed lines, but important and numerous rapid oscillations. In general, values of precipitation and seasonal contrast are close or higher than the modern value, while temperature is cooler than present.

320

321 **Table 2. Description of the pollen zones identified through CONISS cluster analysis, including the**
 322 **main characteristics of their pollen assemblage and associated climate reconstructions.**

323

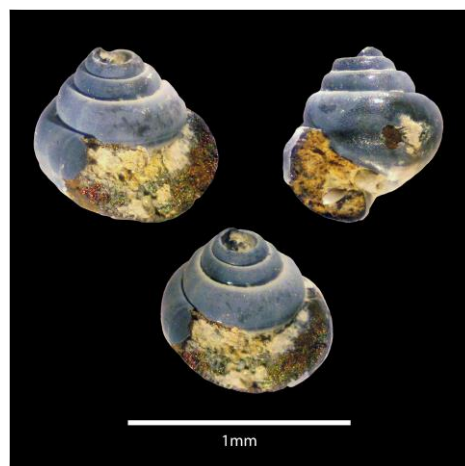


Fig. 4. *Limacina retroversa* specimen found in sample B6H4 130-132 (identification: Jeanne Rampal personal communication, 2023). Photo: Dael Sassoon.

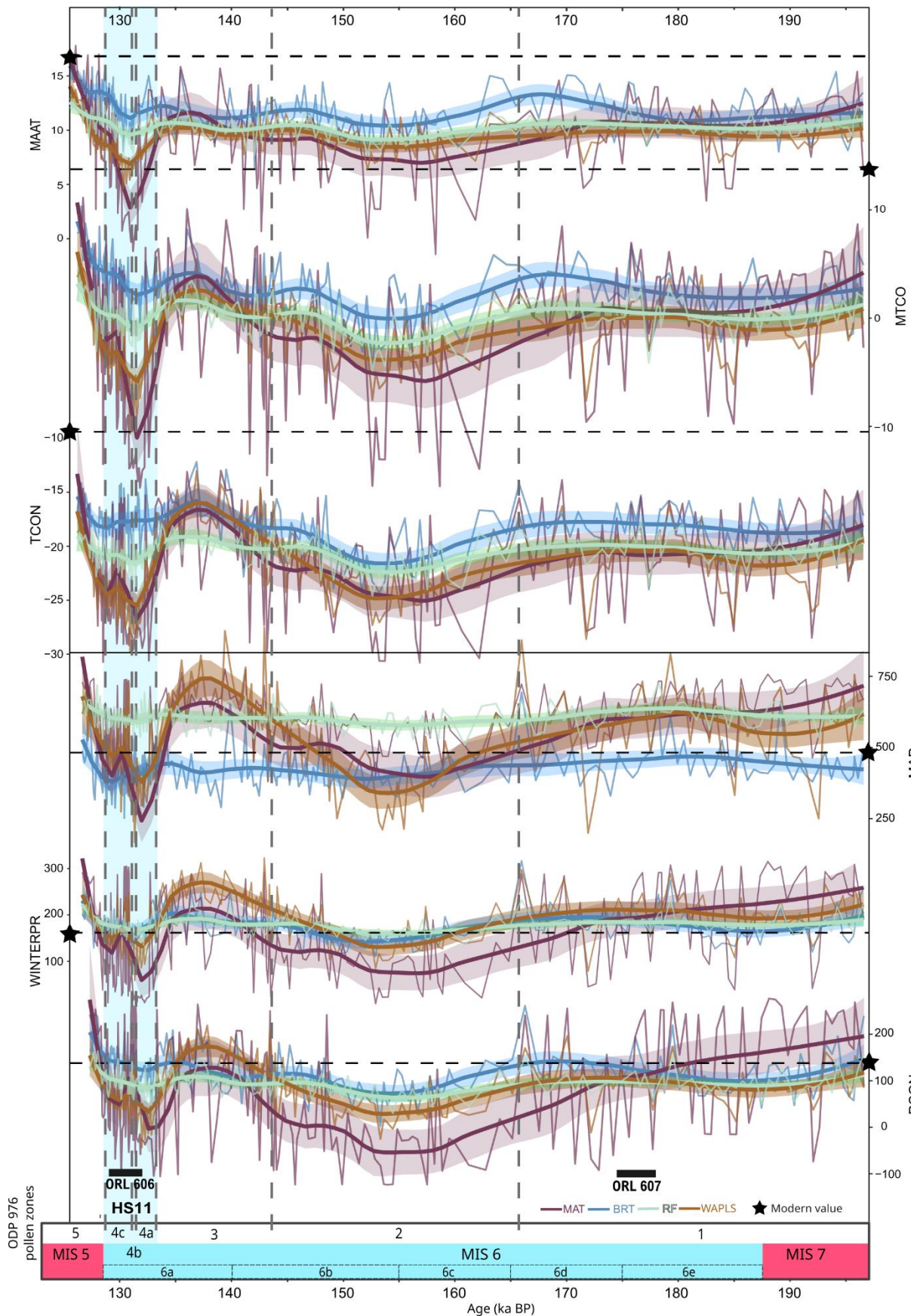
324

325 4.2. Pollen-inferred climate reconstructions

326 Results show significant temperatures and precipitation variations in connection with the
327 glacial / interglacial cyclicality and shorter-term variability (Fig. 5, Table 2). The most reliable methods
328 according to the two R^2 and RMSE indicators are MAT and BRT, and the most accurately reconstructed
329 parameters are MAAT and MTCO (Table 3). The four methods are in agreement for the general trends,
330 although MAT shows the widest amplitude of variations, and RF has the smoothest curve.

331 Temperatures are lower than the present during the complete MIS 6 interval, except at the
332 onset of MIS 5. A cooling trend is reconstructed during the final stage of MIS 7 (pollen zone 1, MIS 6e
333 and 6d), while MTCO and the seasonal temperature contrast (TCON) are stable. The methods do not
334 agree on the precipitation patterns during this phase, with MAT showing a trend toward aridity,
335 decreasing WINTERPR and seasonal precipitation contrast (PCON), while the three other methods
336 display a slight precipitation increase and stable PCON. From 166 ka BP onward (pollen zone 2, MIS 6c
337 and 6b), both temperatures and precipitation decrease, and the seasonal contrast between winter and
338 summer climate conditions reduced progressively. The MIS 6 minimum temperatures and precipitation
339 are reconstructed in pollen zone 2 between around 150 and 160 ka BP, corresponding to the transition
340 between MIS 6c and 6b. Subsequently, both temperatures and precipitation increase progressively in
341 the late pollen zone 2 and early pollen zone 3 (MIS 6b to 6a). Between 140-135 ka BP (early MIS 6a),
342 the four methods reconstruct temperatures similar to late MIS 7, a seasonal contrast close to the
343 present, and precipitation higher than the present (except for BRT). This climate optimum is abruptly
344 interrupted by the HS11 extreme arid event between ~134 and ~129 ka BP (pollen zone 4, late MIS 6a),
345 during which temperatures, precipitation and seasonal contrasts are significantly reduced, reaching
346 climate conditions similar to the MIS 6 glacial maxima ~155 ka BP. A short climate amelioration is
347 evidenced at ~132 ka BP (pollen zone 4b), where precipitation and seasonal contrasts increase
348 abruptly. Finally, after 130 ka BP the climate amelioration toward the MIS 5 interglacial conditions
349 happens very fast (pollen zone 5).

350



351 **Fig. 5. Pollen-based climate reconstructions for MIS 6 interval from the ODP 976 record.** MAAT (Mean
 352 Annual Temperature), MTCO (Mean Temperature of the Coldest Month), TCON (Temperature
 353 Contrast, see methods), MAP (Mean Annual Precipitation), WINTERPR (Winter Precipitation) and

354 PCON (Precipitation contrast, see methods) for the four different methods applied: MAT (Modern
 355 Analogue Technique), WA-PLS (Weighted Averaging Partial Least Square), BRT (Boosted Regression
 356 Trees) and RF (Random Forest). The light-coloured interval represents the 95% confidence window,
 357 and the bold curves the loess smoothed values (alpha = 0.25). Modern values (see methods) are
 358 indicated by the horizontal dashed line and the black star. Grey vertical dashed lines separate the
 359 pollen zones defined by CONISS cluster analysis.

360

	BRT		MAT		WA-PLS		RF	
	R ²	RMSE	R ²	RMSE	R ²	RMSE	R ²	RMSE
MTCO	0.87	2.96	0.88	3.19	0.71	4.44	0.77	3.88
MAAT	0.83	2.31	0.83	2.48	0.66	3.22	0.69	3.00
SUMMERPR	0.77	44.86	0.82	46.61	0.52	66.87	0.65	56.48
MAP	0.77	148.52	0.79	163.70	0.50	225.68	0.66	182.32
MTWA	0.76	2.25	0.79	2.33	0.53	3.16	0.61	2.81
WINTERPR	0.69	60.69	0.72	65.81	0.43	82.58	0.59	69.34

361

362 **Table 3. R² (coefficient of determination) and RMSE (Root Mean Square Error) values for the different**
 363 **climate parameters reconstructed with the four methods applied.** The lower the RMSE and the higher
 364 the R² (in bold), the more reliable the reconstruction.

365

366 5. Discussion

367 5.1. Paleoenvironment of MIS 6 and Termination II in the western Mediterranean

368 Important changes are recorded during MIS 6, that are consistent with orbital-scale variability
 369 during the different glacial substages.

370 Three phases can be discerned. The early phase (pollen zone 1) spans late MIS 7, MIS 6e and
 371 6d (~196-166 ka) and is characterized by high percentages of deciduous *Quercus*, *Cedrus* and
 372 Cichorioideae, with marked variability and several abrupt semi-desert and steppe increases under cool
 373 and humid climate conditions, with seasonal contrast similar to present-day. The middle phase (pollen
 374 zone 2) extends from MIS 6c to late 6b (~165-143 ka), and displays the maximum expansion of steppe
 375 and semi-desert taxa together with very low temperatures and precipitation between ~160 and ~150
 376 ka, a chronology compatible with the maximum Drenthe ice advance (Ehlers et al., 2011). Finally, the
 377 late phase (pollen zone 3), spanning late MIS 6b and 6a (~143-133 ka), is marked by a major expansion
 378 of Ericaceae vegetation associated with higher reconstructed precipitation and winter temperatures,
 379 as well as enhanced seasonal contrast during this phase.

380 Previous studies are consistent with a subdivision of MIS 6 into three phases characterized by
 381 different general trends and amplitude of millennial-scale oscillations (Margari et al., 2014; Nehme et

382 al., 2020). Margari et al. (2014) described an early phase between 185 and 160 ka BP, with warmer and
383 wetter conditions and important rapid climate variability, a middle transitional phase between 160
384 and 150 ka BP, and a late phase with stable glacial conditions between 150 and 135 ka BP. This three-
385 phasing for MIS 6 glaciation matches our interpretation of ODP 976 pollen zones 1, 2 and 3.

386 The final phase of MIS 6 is characterized by important changes in vegetation and climate,
387 indicating a rapid modification of vegetation communities and atmospheric configuration at the
388 transition between MIS 6 and MIS 5. Termination II (TII), defined as the period of fast reorganization
389 of the climate system from full glacial (MIS 6) to full interglacial (MIS 5) conditions, is indeed
390 characterized by extreme and fast internal dynamics including a major Heinrich Stadial, HS11 (Broecker
391 & Henderson, 1998; Gouzy et al., 2004; Martrat et al., 2014; Moseley et al., 2015; Ovsepyan &
392 Murdmaa, 2017). The timing for TII has been estimated based on the initialisation and termination of
393 Weak Asian Monsoon evidenced in the Dongge cave speleothems, lasting from ~136 to 129 ka BP (Bajo
394 et al., 2020; Kelly et al., 2006; Menviel et al., 2019). These boundaries for TII give a total duration of
395 about 7 ka. The timing of TII in the ODP 976 marine record is directly dependent on Dongge Cave
396 chronology (see methods, section 3.1). Approximately the same duration is observed in the vegetation
397 response to TII, but with ~1 ka delay: the imprint of HS11 on the vegetation in the Western
398 Mediterranean region is indeed recorded here between 133.3 – 128.8 ka BP (pollen zone 4). This delay
399 in marine and terrestrial proxies may reflect the vegetation response to the first cold pulse of HS11.
400 ODP 976 provides for the first time a very detailed record of vegetation successions during this arid
401 event (pollen zones 4a, 4b and 4c), in agreement with other SSTs and speleothem records that depict
402 a three-phases or “W” pattern for the event (see section 5.4). After the first rapid increase of steppe
403 and semi-desert taxa (pollen zone 4a), the middle phase shows an abrupt decrease of steppe and semi-
404 desert vegetation, and a fast increase of montane trees (mainly *Cedrus*) percentages (pollen zone 4b).
405 Climate reconstructions reflect this event through a fast increase of both precipitation and
406 temperatures. This pattern is fully compatible with the ODP 976 SSTs trend (Jiménez-Amat and Zahn,
407 2015; Martrat et al., 2014), although a delay of about 1 kyr is observed between the abrupt drop in
408 alkenone-based SSTs at the onset of HS11 and the expansion of steppe and semi-desert vegetation. In
409 the same way, the abrupt sea surface warming in the middle of HS11 (~133 ka BP) is shifted in the
410 pollen record, to around 131.5 ka BP (pollen zone 4b).

411 5.2. Hydroclimate connection with ORLs deposition during MIS 6

412 Pollen analyses help us to characterize the processes behind Organic Rich Layers (ORLs) deposition
413 in this western Mediterranean region. Like sapropels, ORLs reveal important changes in the water
414 stratification and circulation, with reduced bottom water ventilation and enhanced organic

415 productivity in direct connection with (i) increase in the freshwaters Atlantic inflow at times of
416 deglaciation and (ii) enhanced rivers runoff regionally linked with increased precipitation (Murat, 1999;
417 Pérez-Asensio et al., 2020; Rogerson et al., 2008). Although they are often considered as “ghost
418 sapropels”, their timing and the mechanism behind them may differ from those of Eastern
419 Mediterranean sapropels (Rogerson et al., 2008).

420 ORL bed 607 coincides with a period of enhanced precipitation around 176 ka reconstructed
421 through our pollen-based approach (Fig. 7). Its basis appears almost synchronous with the onset of
422 Sapropel S6 layer deposition in the Eastern Mediterranean (Emeis et al., 2003; Rohling et al., 2015;
423 Savannah et al., 2024). Its duration also appears shorter than Sapropel S6, possibly indicating an
424 interruption of favourable climate conditions in the Western Mediterranean region by a stadial event
425 occurring around 172 ka BP and marked by an abrupt decrease in precipitation (Fig. 7).

426 ORL bed 606 was deposited during the second half of Termination II, at a time of deglaciation and
427 directly following the first aridity pulse of HS11. Pollen-based reconstructions show enhanced
428 precipitation and seasonal contrast during this time, suggesting intense precipitation together with
429 deglacial freshwater input as combined causes for ORL deposition in the Western Mediterranean,
430 which finds no counterpart in the Eastern Mediterranean. The implications of such organic layer
431 deposition occurring at times of enhanced precipitation or deglaciation will be further discussed in
432 section 6.2.6.4.

433 5.3. Mediterranean vegetation changes during the penultimate glaciation: a 434 synthesis

435 The ODP 976 pollen record documents MIS 6 vegetation changes in the Western
436 Mediterranean with a temporal resolution comparable to the most detailed terrestrial palynological
437 sequences from the Eastern Mediterranean (Tenaghi Philippon and Ioannina). A W-E transect of
438 Mediterranean palynological records offers valuable insights on the spatial pattern of vegetation
439 changes during the penultimate glaciation (Fig. 6).

440 At the MIS 7-6 transition, no abrupt decline of temperate forest is recorded in the ODP 976 and
441 Padul records, in contrast with central and Eastern pollen records such as Tenaghi Philippon, Ioannina,
442 Ohrid and Castiglione where the transition is very abrupt (Follieri et al., 1988; Koutsodendris et al.,
443 2023; Roucoux et al., 2011; Sadori et al., 2016). At these sites, a higher contrast has been described
444 between interglacial periods with very high percentages of temperate deciduous forest taxa and glacial
445 periods with very reduced tree cover (Tzedakis, 1993; Tzedakis et al., 2006). The western
446 Mediterranean region, at the contrary, was generally characterized by a high proportion of herbaceous

447 taxa, even during interglacial periods, attenuating the vegetation contrasts during transitions to glacial
448 periods.

449 The first half of MIS 6 (~185-165 ka BP) is marked by relatively high percentages of arboreal
450 pollen across all records, especially deciduous forest (Roucoux et al., 2011; Margari et al., 2010, 2014).
451 The abundance of montane taxa (mainly *Cedrus*) is characteristic of ODP 976 record, and reflects the
452 development of altitudinal trees on the Moroccan mountains. Montane elements also increase during
453 early MIS 6 at Valle di Castiglione, mainly represented by *Fagus* and *Abies* (Follieri et al., 1988), and at
454 Ioannina, mainly represented by *Pinus* (Roucoux et al., 2011). No equivalent pattern is recorded in
455 Padul where herbaceous vegetation is largely dominant. The scarcity of palynological data from the
456 western Mediterranean, especially from North Africa, limits our understanding of the spatio-temporal
457 significance of *Cedrus* expansions during MIS 6, and past glaciations in general.

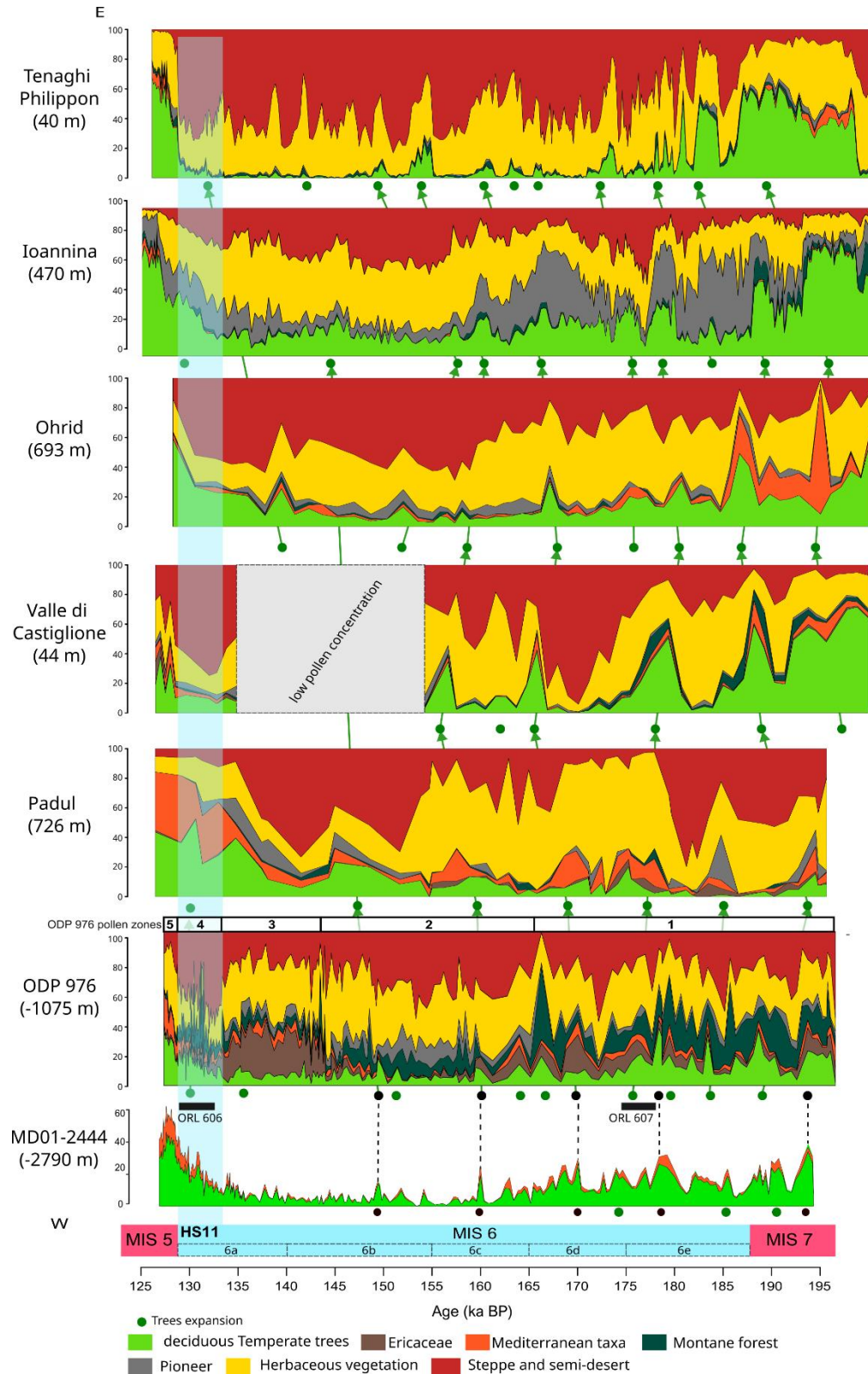


Fig. 6. Synthesis of vegetation changes in the Mediterranean during MIS 6 based on available palynological sequences, from west (bottom) to east (top): MD01-2444 (Margari et al., 2010; Tzedakis et al., 2018), ODP 976 (this study), Padul (Camuera et al., 2019), Valle di Castiglione (Follieri et al., 1988), Ohrid (Sadori et al., 2016), Ioannina (Roucoux et al., 2011), Tenaghi Philippon (Koutsodendris et al., 2023). Each synthetic pollen diagram is plotted according to its own age model. ODP 976 and Ioannina's chronologies are based on alignment with MD01-2444 temperate pollen curve on AICC2012 timescale. The ecological groups are the same as for ODP 976, except

Pinus was included in pioneer vegetation at Ioannina, as it is the only record where *Pinus* is not over-represented. Green dots indicate temperate vegetation increases, with tentative correlations between records. The two Organic Rich Layers (ORLs) identified in the ODP 976 core (Murat, 1999), were placed at the bottom.

458 The main phase of steppe and semi-arid vegetation is recorded between ~165-145 ka BP in the
459 Alboran Sea record, consistent with Ohrid and Ioannina pollen sequences (Fig. 6). In Padul, however,
460 the maximum expansion of steppe and semi-desert taxa occurs later, between ~155 and ~137 ka BP.
461 This time window corresponds to the glacial maximum recorded at Azzano X (northern Italy) between
462 148 and 135 ka BP (Pini et al., 2009), and to a period of low pollen concentration at Valle di Castiglione,
463 likely reflecting full glacial conditions. The ~10 ka lag in the vegetation glacial maxima between ODP
464 976 and Padul is probably the result of the low temporal resolution of the latter, in addition to
465 differences in the age models used. However, the presence of pioneer vegetation and to a lesser extent
466 of montane elements in Padul during the maximum glacial phase matches the ODP 976 pattern in
467 pollen zone 2, where Cupressaceae and *Cedrus* display high abundance.

468 A distinctive feature of the Western Mediterranean vegetation recorded during the final stage
469 of MIS 6 (pollen zone 3) is the marked increase in Ericaceae observed in the ODP 976 record, whereas
470 Ericaceae are almost absent in the rest of the Mediterranean region. A similar expansion is observed
471 in the Atlantic margin, where core MD01-2444 recorded patterns of Ericaceae expansion matching the
472 three insolation minima during MIS 6 (Margari et al., 2014). Ericaceae development during minimal
473 summer insolation is particularly favoured by reduced summer evaporation at times of low seasonal
474 contrast in precipitation, as already noted in the Alboran Sea during the last glacial (Fletcher and
475 Sánchez Goñi, 2008). Following the same interpretation, the expansion of heathland vegetation in the
476 Iberian Peninsula as recorded in ODP 976 during the final stage of MIS 6 may therefore mark the
477 renewed influence of westerlies and Atlantic moisture preceding the onset of the transition to MIS 5
478 interglacial (Margari et al., 2014). Supporting this state, an increase in temperate deciduous forest at
479 the end of MIS 6 is also seen in Padul, Ohrid and Ioannina records before the transition to MIS 5.

480 Despite some discrepancies due to the differences in age models and temporal resolutions, all
481 records display comparable variations in temperate pollen percentages during the penultimate glacial.
482 These variations support the persistent sensitivity of Mediterranean plant ecosystems to global-scale
483 millennial climate variability during the penultimate glaciation, with modulation of the vegetation
484 response depending on the local geography. Strong similarities can be observed between ODP 976 and
485 Padul, despite the lower temporal resolution of Padul record. In both sequences, temperate pollen
486 percentages reached ~30 % of total pollen as a maximum during the rapid forest expansion events in
487 the first half of MIS 6. This similarity supports the validity of the ODP 976 marine record to reconstruct

488 the SW Iberian Peninsula temperate forest history. However, ODP 976 sequence provides a more
489 regional image of the vegetation, including higher percentages of Ericaceae pollen coming from the
490 Atlantic coast, and *Cedrus* pollen from the Moroccan mountains (Jiménez-Moreno et al., 2020),
491 compared to Padul where percentages of Mediterranean taxa and hygrophyte herbaceous are higher
492 due to the local nature of the signal (Camuera et al., 2019). Looking further east, Valle di Castiglione
493 recorded various temperate trees expansions and contractions during the lower MIS 6, before the full
494 glacial conditions. In the Italian Peninsula, various interstadials have also been identified further north
495 at Azzano X (Pini et al., 2009). In the Balkans, Tenaghi Philippon shows the highest percentages of semi-
496 desert and herbaceous vegetation throughout MIS 6, with more abrupt changes than all the other
497 Mediterranean records, and more amplitude of the trees' contractions. This pattern was already
498 described during the last climatic cycle and reflects the exacerbated vegetation dynamics locally, with
499 episodes of rapid and enhanced colonization by tree vegetation (Koutsodendris et al., 2023; Tzedakis,
500 2005; Tzedakis et al., 2004). This has been mainly explained by the location of the site in a low
501 altitudinal plain characterized by a more continental climate with lower winter precipitation: tree
502 population at lower altitudinal location are closer to their ecological threshold in term of precipitation,
503 and are likely to be very affected even by minimal changes in the amount of rainfall. On the contrary,
504 the Ioannina record shows the highest deciduous forest percentages of all the records presented here,
505 supporting its character as a local trees refugium (Roucoux et al., 2011).

506 Termination II displays a particular pattern in vegetation records from the Mediterranean
507 region: while the expansion of trees and temperate vegetation is fast and continuous, HS11 represents
508 at the same time a remarkable episode of abrupt steppe and semi-desert expansion. Although this
509 event is visible in almost all the records, it is particularly prominent in ODP 976 record (pollen zone 4),
510 and appears less pronounced in the eastern Mediterranean sequences. This observation is compatible
511 with previous observations that Heinrich stadials during the last glacial had a minor impact on the
512 eastern Mediterranean vegetation compared to the western Mediterranean, likely due to the already
513 limited presence of tree vegetation in the eastern records during glacials (Tzedakis, 2005). A similar
514 interpretation can be proposed for the differential response of eastern and western Mediterranean
515 vegetation to HS11, supporting the major sensitivity of the southwestern Mediterranean vegetation
516 to North Atlantic cold events. In Padul, no major expansion of xerophyte vegetation is detected, but a
517 small decrease of temperate deciduous taxa was interpreted as the HS11 imprint (Camuera et al.,
518 2019), and the signal might be hindered by the low resolution of the record. A pattern of fast arid
519 vegetation increase contemporaneous to the temperate forest expansion is also found in central Italy
520 at Lago Grande di Monticchio, which was not presented in Fig. 6 as its record does not extend beyond
521 132 ka BP (Allen and Huntley, 2009; Brauer et al., 2007).

522 Finally, all palynological sequences reveal high-frequency oscillations of temperate and semi-
523 desert pollen, compatible at first look with DO-like variability based on their duration and intensity.
524 They represent a particularly distinctive feature of the lower part of MIS 6.

525 5.4. Rapid climate variability during MIS 6: a regional multiproxy comparison

526 In order to investigate the character of rapid climate variability during MIS 6, a comparison
527 with regional and global climatic archives is essential. The events of arboreal pollen increase observed
528 in the ODP 976 record show percentages and timing comparable to those from the Portuguese margin
529 core MD01-2444 (Margari et al., 2010, 2014; Tzedakis et al., 2018) (Fig. 7, m). However, the ODP 976
530 record generally presents lower values of temperate deciduous pollen percentages compared to the
531 Atlantic record, due to its more semiarid Mediterranean influence as previously evidenced for the last
532 glacial period (Charton et al., 2025; Fletcher et al., 2010b). To better capture temperate vegetation
533 dynamics, we added Ericaceae, a clear marker of Atlantic influence in the ODP 976 record, to the
534 deciduous temperate forest, to obtain a “total temperate pollen sum” which enhances the main
535 warming peaks and strengthens the correlation between the two marine cores on both sides of
536 Gibraltar Strait (Fig. 7, m and l). The ODP 976 pollen-inferred climate reconstructions show generally
537 consistent patterns with the SSTs trends based on alkenones (Martrat et al., 2004, 2007), and the
538 southern Iberian humidity recorded in the speleothem from Cueva Gitana (Hodge et al., 2008) (Fig. 7,
539 e and g). The ODP 976 pollen and climate record therefore appears to reflect well regional variations
540 in both temperature and humidity across MIS 6.

541 Warm events in the northern hemisphere are generally well-correlated to peaks in the ODP
542 976 temperate pollen curve (Fig. 7, c and l). An active bipolar seesaw dynamics was described during
543 the penultimate glacial Davtian & Bard, 2023; EPICA Community Members, 2006; Stocker, 1998), and
544 the Antarctic record was used to elaborate the Greenland GL_T-syn (Greenland temperature synthetic)
545 curve showing predicted $\delta^{18}\text{O}$ millennial-scale events for the past glacial eight climatic cycles, which
546 are not directly recorded in Greenland ice (Barker et al., 2011; Bazin et al., 2013; Jouzel et al., 2007).
547 Six Antarctic Isotopic maxima (AIM) events were recognized on the Deuterium curve during MIS 6 (6i
548 to 6vi), correlated with increases in CO₂ concentrations and benthic isotope minima in the North
549 Atlantic (Barker et al., 2011; Hodell et al., 2023; Margari et al., 2010, 2014; Shin et al., 2020) (Fig. 7, a-
550 c). These AIM and benthic minima in the Atlantic are not easily correlated with steppe expansions in
551 the ODP 976 record, indicating a limited response of vegetation in the Western Mediterranean to the
552 Antarctic warm events.

553 Barker et al. (2011) predicted the occurrence of eleven millennial-scale warming events during
554 MIS 6 (Fig. 7, c), while nine interstadials were recognized in the Alboran Sea from the alkenone record

555 (Fig. 7, e), (Martrat et al., 2004, 2007). In the loess record of Harletz in central Europe, ten interstadials
556 were described (Rousseau et al., 2020), strongly matching the Chinese speleothems records of stadial
557 and interstadial events related to the Asian Monsoon dynamics (Cheng et al., 2006; Li et al., 2014;
558 Wang et al., 2018; Wang et al., 2001; Xue et al., 2019). The global nature of fast climate oscillations in
559 the northern hemisphere thus appears controlled by the coupled influence of Atlantic cold events, and
560 tropical monsoon variations as evidenced by the eastern Mediterranean speleothems records from
561 Sofular, Soreq and Kanaan caves (Ayalon et al., 2002; Held et al., 2024; Matthews et al., 2021; Nehme
562 et al., 2018).

563

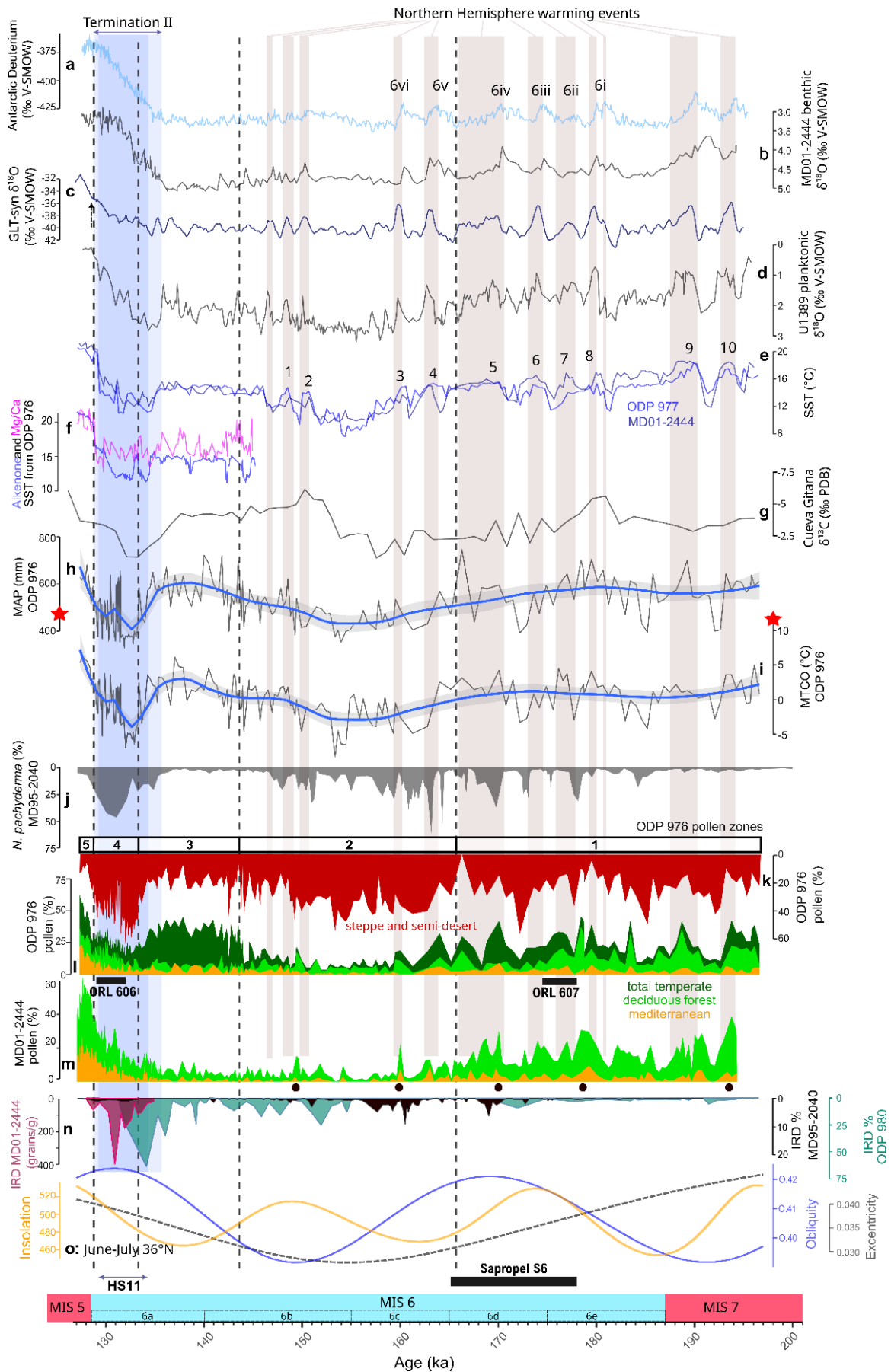


Fig. 7. Millennial climate changes during MIS 6. a) Antarctic Dome C δD (Bazin et al., 2013; Jouzel et al., 2007); **b)** Benthic $\delta^{18}O$ from MD01-2444 (Margari et al., 2010); **c)** Greenland synthetic $\delta^{18}O$

(Barker et al., 2011); **d**) Planktonic $\delta^{18}\text{O}$ from U1389 (Sierro & Andersen, 2022); **e**) alkenone-based SST from ODP 977 (darker blue) and MD01-2444 (lighter blue) (Martrat et al., 2004, 2007); **f**) Alkenone-based SST (Martrat et al., 2014) and Mg/Ca-based SST (Jiménez-Amat and Zahn, 2015) from ODP 976; **g**) $\delta^{13}\text{C}$ from Cueva Gitana (Hodge et al., 2008); **h**) Mean Annual Precipitation (MAP) reconstructed from ODP 976 pollen assemblage, mean of the four methods used in this study (MAT, WA-PLS, RF, BRT), with the red star showing the modern value ; **i**) Mean Temperature of the Coldest Month (MTCO) reconstructed from ODP 976 pollen assemblage, mean of the four methods used in this study (MAT, WA-PLS, RF, BRT), with the red star showing the modern value; **j**) *N. pachyderma* percentages from MD95-2040 (de Abreu et al., 2003; Voelker & de Abreu, 2011); **k**) ODP 976 pollen percentages of semi-desert and steppe taxa, with ODP 976 pollen zones (this study); **l**) ODP 976 pollen percentages of total temperate taxa including temperate deciduous forest + Ericaceae + Mediterranean (dark green), deciduous forest (light green), Mediterranean (orange) (this study); **m**) MD01-2444 pollen percentages of temperate tree (light green) and Mediterranean (orange) taxa (Margari et al., 2010; Tzedakis et al., 2018); **n**) Ice-Rafted Debris (IRD) percentages from MD01-2444, 37° N (pink) (Skinner & Shackleton, 2006) redrawn from Tzedakis et al. (2018), MD95-2040 (black), 40°N (de Abreu et al., 2003) and ODP 980 (blue), 55°N (McManus et al., 1999; Oppo et al., 2001, 2006); **o**) orbital parameters (Laskar et al., 2004) calculated for June-July at 36°N: Eccentricity (black), Obliquity (blue) and Insolation (yellow). The black rectangle indicates the interval of deposition of Sapropel layer S6 in the eastern Mediterranean (Ziegler et al., 2010). The marine substages MIS 6a-e follow (Railsback et al., 2015). All data are plotted on AICC2012 chronology (Bazin et al., 2013) following Sierro et al. (2020, 2022), except for the IRD records and Gitana Cave which is plotted on its own age model based on U-series absolute dating. The vertical grey bars indicate the Northern Atlantic interstadial events based on the planktonic isotope record and the predicted millennial-scale warming events from Greenland synthetic record, with the numbers of the Alboran interstadials (AI-1 to AI-10) from Martrat et al. (2004, 2007). Numbers 6i-6vi correspond to the Antarctic Isotope Maxima (AIM) from Margari et al. (2010). The vertical blue bar represents Heinrich Stadial 11 (HS11). Black dots and dotted lines show the five temperate pollen peaks in MD01-2444 used as control points for ODP 976 chronology.

564

565 The three phases identified during MIS 6 based on the ODP 976 vegetation and climate record
566 can be compared with regional and global records to be interpreted in a broader context, based on
567 general climatic trends and the expression of climatic instability:

568 5.4.1. *Early MIS 6 (187-166 ka BP): warm/wet conditions and instability.*

569 The first phase encompasses the two substages MIS 6e and 6d, and is characterized by humid
570 and rather warm climate conditions in the Mediterranean at the transition from MIS 7 to MIS 6. This
571 phase aligns well with the deposition of ORL bed 607 in the Alboran Sea, and the sapropel layer S6 in
572 the Eastern Mediterranean, associated with the maximum summer insolation and increased
573 intensification of the summer monsoonal system in the eastern Mediterranean between 178.5 to
574 165.5 ka (Emeis et al., 2003; Rohling et al., 2015; Ziegler et al., 2010). At the same time of S6 deposition,
575 Cheddadi and Rossignol-Strick (1995) described an increase in temperate pollen in the Nile region, and
576 Soreq cave speleothem records climatic conditions typical of an interglacial (Ayalon et al., 2002).
577 Sapropel depositions usually occur during interglacial periods as MIS 1 (Holocene), which makes
578 sapropel S6 an exceptional feature of early MIS 6. It reflects particularly warm and humid conditions,

579 and intense freshwater input in the Mediterranean which can result from various sources, including
580 increased rainfall and monsoon activity, Atlantic freshwater entrance, and enhanced river discharges
581 (Sierro & Andersen, 2022). The long speleothem records in China report a period of northern shift of
582 the Intertropical Convergence Zone associated with enhanced Asian Monsoon activity during this
583 phase (Wang et al., 2018). Higher pluviometry is also supported by foraminifera isotopic and SSTs signal
584 throughout the Mediterranean Sea, which were used to reconstruct past salinity and freshwater
585 budget regionally (Kallel et al., 2000). Enhanced rainfall in the Balkans is evidenced by the Ioannina
586 lake deepening (Wilson et al., 2021), and a more humid period is documented in speleothem records
587 from Argentarola cave in Italy (Bard et al., 2002) and Gitana cave in southern Spain (Hodge et al., 2008)
588 (Fig. 7, g). Therefore, humid conditions during this phase were not restricted to the eastern
589 Mediterranean where the sapropel deposition occurred. ODP 976 organic layer 607 together with the
590 pollen-based climate reconstructions support this view, with enhanced seasonal precipitation contrast
591 during this interval driven by enhanced winter precipitation (Fig. 5). Comparison with Padul pollen-
592 based hydroclimate reconstructions (Camuera et al., 2022) further strengthens this scenario: despite
593 the chronological delay between the two sequences, this early MIS 6 humid phase and ORL deposition
594 likely matches the Western Mediterranean Humid Period (WMHP 6) dated between 180-155 ka BP
595 (Fig. 8). The same study made the case for a co-occurrence of humid periods in the Western
596 Mediterranean and in West Africa (African Humid Periods) during periods of high precipitation
597 seasonality and enhanced West African Monsoon. Pollen-inferred climate reconstructions from lake
598 Ohrid have also shown the phase relationship between African Monsoons and periods of high winter
599 precipitation in the Mediterranean region (Wagner et al., 2019; Sinopoli et al., 2019).

600 Another characteristic of this early MIS 6 phase is the strong variations in pollen and isotopic
601 curves in the Atlantic and Western Mediterranean (Fig. 7, a-d and l-m). Variations in temperate
602 deciduous and Ericaceae percentages are observed in the ODP 976 record, in close correspondence
603 with the Atlantic record from MD01-2444. The largest interstadial peak in ODP 976 around 179 ka BP
604 is also identified in all the different records and marked by warmer conditions in the sea, and more
605 effective precipitation in SE Iberia (Hodge et al., 2008). It is well correlated with the stadial following
606 Antarctic event 6i (Margari et al., 2010), the associated predicted millennial-scale warming event in
607 Greenland synthetic curve, and the Alboran Sea SST interstadial event 8 (Martrat et al., 2004). In Padul
608 record, the temperate deciduous, Mediterranean and *Abies* percentages increase correlates well with
609 this event (Camuera et al., 2019). It could also match the WMHP 6.1 interstadial (Camuera et al., 2022)
610 (Fig. 8). This large interstadial was suggested to be at the origin of the initialisation of the sapropel S6
611 deposition (Sierro & Andersen, 2022), and could also have participated in the initialization of ORL 607
612 deposition in the Alboran Sea (Murat, 1999). On the other hand, the most important tree population

613 decline and semi-desert expansion in ODP 976 is recorded at ~ 172 ka BP, which could match Antarctic
 614 event 6iv, and is associated to a moderate increase of IRD deposition at the latitude of ODP 980 (Fig.
 615 7, n). A similar stadial can be observed in the Ioannina and Tenaghi Philippon records with a close
 616 chronology (Roucoux et al., 2011) (Fig. 6). Dry conditions at this time are also recorded in the eastern
 617 Mediterranean as shown in the Pentadactylos and Soreq speleothems (Ayalon et al., 2002; Nehme et
 618 al., 2018).

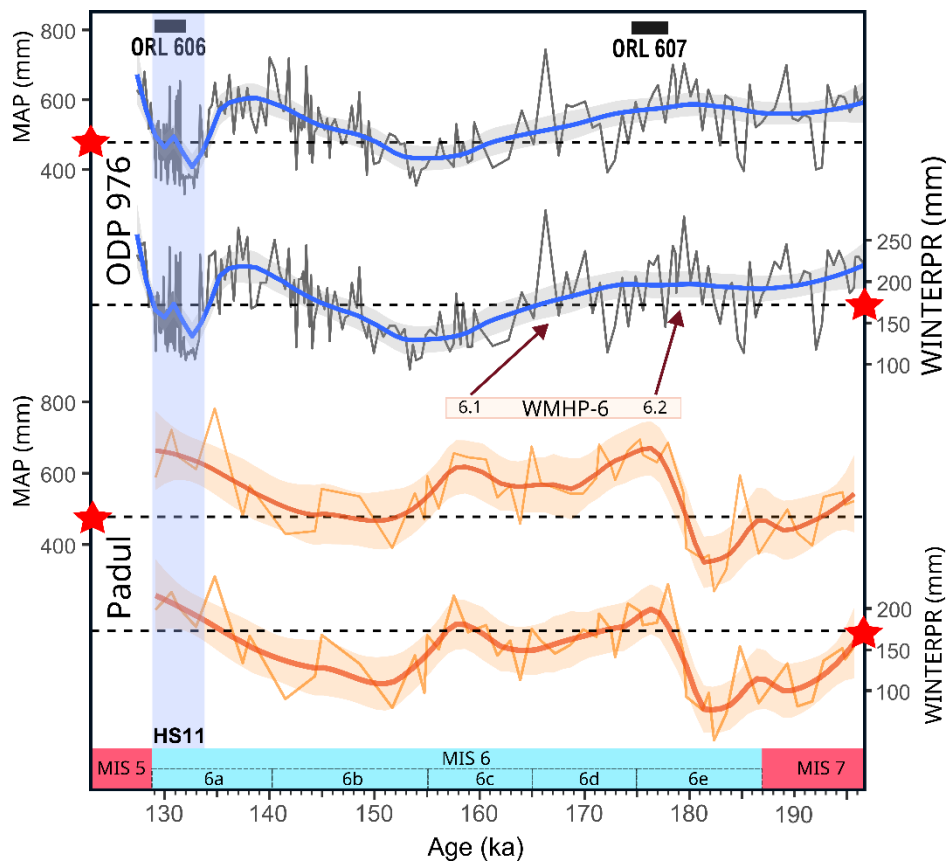


Fig. 8. Comparison between the precipitation pattern reconstructed from ODP 976 with our multi-method approach (mean) (this study) and from Padul with only the WA-PLS method (Camuera et al., 2022). Mean Annual Precipitation (MAP) and Winter Precipitation (WINTERPR) are represented, together with the two Organic Rich Layers (ORLs) identified in ODP 976 (Murat, 1999) and the Western Mediterranean Humid Period (WMHP) 6 defined by Camuera et al. (2022). Red arrows indicate tentative correlation between the two phases of WMHP 6, and the precipitation reconstructions from ODP 976. Red stars and dashed lines indicate the modern climate value (see methods).

619

5.4.2. Middle MIS 6 (165-144 ka BP): maximum glacial conditions and stability.

620

621 This phase is marked by the maximum expansion of semi-desert vegetation and the almost
 622 complete collapse of forest vegetation between ~ 163 and 150 ka BP, according to the ODP 976 pollen
 623 and MD01-2444 records, synchronous with the minimum in orbital eccentricity. This is in agreement
 624 with the lowest SSTs values reconstructed in the Alboran Sea from the alkenone record occurring

625 around 155 ka BP, and low SSTs in the Gulf of Lions too (Cortina et al., 2015). At the same time, high
626 percentages of the cold species *N. pachyderma*, together with important ice-detritus pulses, are
627 recorded on the Portuguese margin (de Abreu et al., 2003; Voelker & de Abreu, 2011) (Fig. 7, j and n).
628 The occurrence of the cold Atlantic species *Limacina retroversa* shells in the ODP 976 sediments at
629 ~155 ka BP is consistent with the enhanced entrance of cold subpolar water masses in the Alboran sea
630 at the time of full glacial conditions. In parallel, there is an intensification of “Fleuve Manche” paleo
631 river discharges evidenced in various sedimentary cores from the Bay of Biscay (Boswell et al., 2019;
632 Eynaud et al., 2007; Penaud et al., 2009, 2016; Toucanne et al., 2009), and a fluvial aggradation linked
633 with reduced vegetation cover in Spanish river basins (Macklin et al., 2002). A long-term aridification
634 is recorded in SE Spain in Gitana cave close to the ODP 976 location (Hodge et al., 2008). The glacial
635 maximum in Soreq cave speleothem is also recorded around 154 ka BP (Bard et al., 2002), and might
636 be responsible for the hiatus in the Pentadactylos speleothem in Cyprus (Nehme et al., 2020). In Italy,
637 the Tana che Urla cave also recorded cooling and aridification between 159-132 ka BP, indicated by
638 both the carbon and oxygen isotopic ratio (Regattieri et al., 2014). The coolest phase in Abaliget Cave
639 speleothem in central Europe is also recorded at that time (Koltai et al., 2017). Climate conditions
640 reconstructed at ODP 976 site during this phase show the maximum aridity and cold temperatures,
641 which are consistent and fall within the range of reconstructed temperatures and precipitation at the
642 same time at Ohrid (Sinopoli et al., 2019). This main phase of glaciation in Europe took place after 163
643 ka BP, corresponding to the Drenthe glacial advance (Ehlers et al., 2018; Margari et al., 2014). The
644 maximum ice expansion probably led to the almost complete collapse of temperate vegetation across
645 the Mediterranean region, except in specific climate refugia like Ioannina or Padul (Fig. 6). The
646 Mediterranean vegetation taxa were particularly affected and almost disappeared at this time in the
647 ODP 976 record.

648 Few interstadial events are observed during this cold and dry phase, probably due to the
649 extended ice volume reaching a critical threshold (McManus et al., 1999) and leading to higher climate
650 stability at time of glacial maximum expansion (Sierro and Andersen, 2022). One moderate interstadial
651 event around 150 ka BP is expressed in the ODP 976 and MD01-2444 records through an increase in
652 temperate deciduous tree taxa (Fig. 7, l and m). It may correspond to the interstadial recognized in
653 Gitana Cave speleothem approximately at the same time, and is compatible with the Alboran
654 Interstadial events 1 or 2 (Martrat et al., 2004), while a larger trees increase in Padul record is also
655 observed (Camuera et al., 2019) (Fig. 6). It is also compatible with interstadials recognized in other
656 speleothem records in eastern and central Mediterranean (Ayalon et al., 2002; Bard et al., 2002;
657 Regattieri et al., 2014). Sierro et al. (2022) described a major event of low Mediterranean overturning
658 and high freshwater entrance through the Gibraltar Strait at that time and contemporaneous to the

659 insolation maximum (Fig. 7, o). This configuration was similar to the one contemporaneous to sapropel
660 S6 and ORL 607 deposition during early MIS 6, but did not lead to any new sapropel deposition at 150
661 ka BP, probably because the climate conditions were more favourable but not enough for a sapropel
662 deposition.

663 *5.4.3. Late MIS 6 (144-129 ka BP): increased precipitation during the last glacial, and*
664 *arid conditions during HS11.*

665 Between 150 and 140 ka BP, warmer and wetter conditions are indicated by ODP 976 pollen
666 percentages of Ericaceae (pollen zone 3). Ericaceae expansions in the Iberian margin sediments were
667 found to be associated to insolation minima in core MD01-2444 (Margari et al., 2014). This pattern is
668 consistent with the ODP 976 Ericaceae curve (Fig. 7, l). The climate reconstructions evidenced high
669 precipitation and especially high WINTERPR values. These higher humidity and temperature values are
670 supported by the carbon isotope record from Gitana Cave (Hodge et al., 2008) and the Alboran Sea
671 SSTs (Martrat et al., 2007) (Fig. 7, e-g). In central Europe, Abaliget Cave speleothem also shows more
672 favourable climate conditions during this phase (Koltai et al., 2017). Climatic oscillations appear
673 subdued in the Western Mediterranean pollen records during this last phase. The high resolution ODP
674 976 record shows some SST variations (Jiménez-Amat and Zahn, 2015; Martrat et al., 2014) : Ericaceae
675 pollen contractions and semi-desert elements expansions could be correlated to three abrupt drops in
676 alkenone-based SSTs at 144, 142, and 139 ka BP (Fig. 7, f, k and l). Fifteen Chinese Interstadials (CIS)
677 were identified at Hulu Cave during late MIS 6, linked with Asian Monsoon dynamics (Wang et al.,
678 2018), and the ultra-high-resolution record of planktonic isotope ratio at U1389 by Sierro and
679 Andersen (2022) also expresses some variability. However, the vegetation response in the SW
680 Mediterranean was apparently limited.

681 Following the Ericaceae expansion, the most prominent feature of the late MIS 6 phase is the
682 large and fast expansion of steppe and semi-desert vegetation during HS11, between 133 and 129 ka
683 BP (pollen zone 4). It is characterized by a first large IRD peak at high latitude (ODP 980) around 134 ka
684 BP, and later at the MD01-2444 latitude, around 131 ka BP (Skinner & Shackleton, 2006; Tzedakis et
685 al., 2018). This event also corresponds to an increase in the oxygen isotopic ratio at the Portuguese
686 margin (especially planktonic, starting around 136 ka BP), also broadly synchronous to an important
687 decrease in SSTs of the Atlantic and the Mediterranean Sea (Jiménez-Amat and Zahn, 2015; Martrat et
688 al., 2004, 2007, 2014). A pronounced increase in *N. pachyderma* (sinistral) abundance is also recorded
689 on the Portuguese margin (Voelker & de Abreu, 2011). Climate reconstructions show particularly harsh
690 conditions in the Western Mediterranean region during this event, compatible with the
691 reconstructions from Lake Ohrid (Sinopoli et al., 2019) and from three French sites (Les Echets, la
692 Grande Pile and Le Bouchet) for the latest phase of MIS 6 (Guiot et al., 1989, 1993). An arid phase is

693 also evidenced at Gitana Cave (Hodge et al., 2008), which closely matches the trend of the ODP 976
694 precipitation curve (Fig. 8). Aridity is evidenced in other speleothem records in Europe like Villars
695 (Wainer et al., 2011), Sieben in the Alps (Moseley et al., 2015), and Abaliget cave in central Europe
696 (Koltai et al., 2017). Dryness over western Europe is also supported by an episode of intense loess
697 deposition in Rodderberg crater in northern Germany between 136-129 ka BP (Zhang et al., 2024). If
698 HS11 is also recorded in China speleothems (Wang et al., 2018), it appears subdued in the eastern
699 palynological Mediterranean records (Fig. 6), indicating that the Western Mediterranean region was
700 more severely impacted by the dry and cold pulse of HS11. The “double u” shape of HS11 described in
701 section 5.1 for the ODP 976 record matches well the Hulu cave record, where the particular event in
702 the middle of HS11 was linked with a strong Asian Monsoon episode that could represent an analogue
703 to the Bølling-Allerød during Termination I (Wang et al., 2018). The fast and multiphase vegetation and
704 climate dynamics evidenced in the ODP 976 record is in agreement with the description of a “HS11
705 complex” with multiple phases (Tzedakis et al., 2018), and will require more focused attention in the
706 future.

707 HS11 has been described as a “pause” in the glacial termination II (Gouzy et al., 2004; Hodge
708 et al., 2008). However, in the ODP 976 and MD01-2444 records, temperate vegetation keeps increasing
709 all along the event, despite the supposed cessation of the warming and moistening trend for almost
710 2000 years. Therefore, the trend toward increased temperate vegetation during Termination II did not
711 seem to be strongly affected by the abrupt arid event, following the continuous climate amelioration
712 described in various speleothem records from Italy covering Termination II, at Corchia cave, Tana che
713 Urla and Argentarola (Bard et al., 2002; Drysdale et al., 2005; Regattieri et al., 2014). On the contrary,
714 the Gitana Cave speleothem records a strong moisture deficit (Fig. 7, g), supporting a stronger impact
715 of HS11 in the SW Mediterranean compared to the Italian Peninsula.

716 Finally, it is to be pointed out that HS12, occurring around 140 ka BP (Lisiecki & Stern, 2016),
717 apparently did not have any imprint on the vegetation record of ODP 976, implying a subdued impact
718 of this event on Mediterranean vegetation compared to HS11.

719 5.5. Comparison of MIS 6 with the last glacial period (MIS 4-2)

720 Various studies have pointed out strong similarities between the millennial-scale oscillations
721 of the last glacial period and the penultimate glacial period, with the division between MIS 3 and MIS
722 2 being analogous to the early and mid-late phase of MIS 6 respectively (Held et al., 2024; Margari et
723 al., 2010, 2014; Roucoux et al., 2011; Rousseau et al., 2020; Shin et al., 2020; Sierro et al., 2020). The
724 same studies argued in favour of pervasive impact of stadial events on the continental climate and
725 vegetation in the Mediterranean region, even in absence of typical Heinrich layers (Roucoux et al.,

726 2011). The ODP 976 record shows a cooling and aridification trend during the first half of MIS 6 (Fig.
727 9), with decreasing intensity of interstadial events, that recalls the pattern of MIS 3 D-O cycles (Bond
728 et al., 1993).

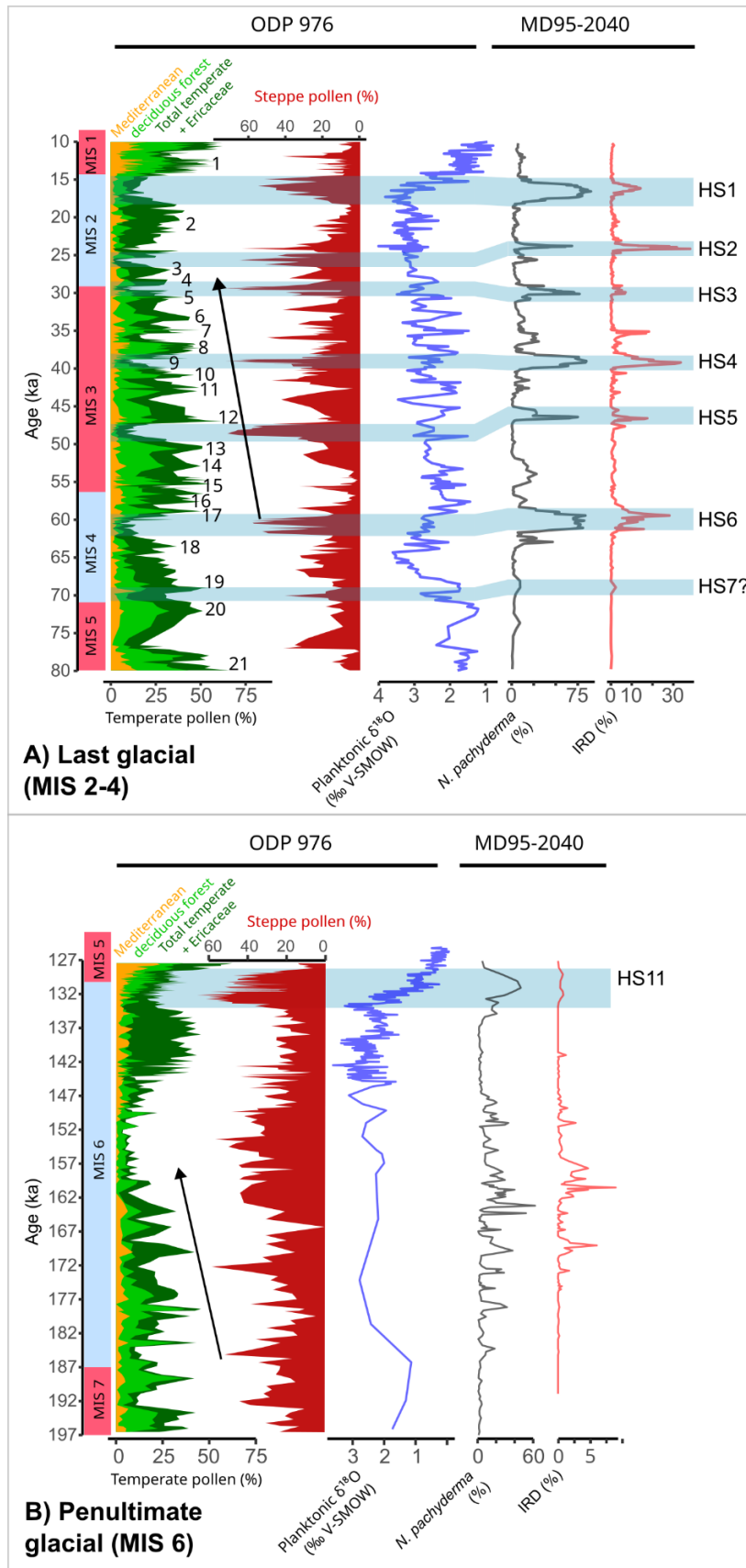


Fig. 9. Comparison of millennial changes during A) the last glacial (MIS 2-4) and B) the penultimate glacial (MIS 6), including the main pollen data from ODP 976 (Charton et al., 2025; Combourieu-

Nebout et al., 2002, 2009, and unpublished data for the last climatic cycle, and this study for MIS 6), the ODP 976 planktonic isotopic ratio from *G. bulloides* (Combourieu-Nebout et al., 2002; Jiménez-Amat & Zahn, 2015; von Grafenstein et al., 1999, and unpublished data), and the *N. pachyderma* and IRD record from core MD95-2040 (de Abreu et al., 2003; Voelker and de Abreu, 2011). Marine Isotope Stages follow the boundaries from Lisiecki & Raymo (2005). Numbers on the Last Glacial correspond to the Greenland D-O events chronology (Fletcher et al., 2010a; Rasmussen et al., 2014). Black arrows mark the aridification trend and decreasing interstadials intensity during MIS 3 and early MIS 6.

729

730 However, the absence of clear successions of stadial events and especially Heinrich stadials,
731 together with the more subdued expression of interstadials in the vegetation record, limits the
732 resemblance between the two glacial periods. The pacing of interstadial peaks also seems to be
733 reduced compared to the last glacial period high-frequency oscillations, as previously highlighted from
734 the high-resolution speleothem record from Sofular cave in Turkey (Held et al., 2024).

735 A comparison of millennial-scale changes during the past two glacial periods based on the ODP
736 976 and MD95-2040 records, on either side of the Gibraltar Strait, supports our view (Fig. 9). The last
737 glacial period (encompassing MIS 4 to MIS 2) was characterized in the Alboran Sea by high-intensity
738 oscillations in both temperate and semi-desert vegetation correlated with D-O cycles and intense ice-
739 rafting events HE1 to HE7 in MD95-2040. During interstadial events, temperate and Mediterranean
740 vegetation (deciduous forest + Mediterranean + Ericaceae) could reach values above 60 % of total
741 pollen; during stadial events, the semi-desert pollen values reached values as high as 70% of total
742 pollen (during HS3, HS4 and HS5). In comparison, the penultimate glacial (MIS 6) displays much lower
743 intensity events, with interstadials characterized by 45% as a maximum value for temperate
744 vegetation, and stadials with 65% for the steppe and semi-desert vegetation (during HS11). High-
745 intensity cold episodes during MIS 6 are limited to the HS11, and the ~172 ka BP event. This is
746 consistent with the multiproxy record of core MD95-2040 on the Portuguese margin, which evidenced
747 reduced variability in the *N. pachyderma* abundance and IRD deposition during the penultimate glacial
748 compared to the last glacial (de Abreu et al., 2003; Voelker & de Abreu, 2011). The ice rafting episodes
749 appear to be of different nature during MIS 6 (Hodell et al., 2008; Liu et al., 2018; McCarron et al.,
750 2021), with the main iceberg discharges originating from the European ice sheet, contrary to the typical
751 Hudson Strait origin of the last glacial Heinrich events. SST reconstructions in the western
752 Mediterranean also show less intense cooling during MIS 6 than during MIS 3 (Martrat et al., 2004,
753 2007), supporting limited incursions of polar waters in the Mediterranean during MIS 6 compared to
754 MIS 3 coldest stadials, and especially Heinrich stadials (Cacho et al., 1999).

755 Like ODP 976, Ioannina records lower intensity arboreal pollen oscillations during early MIS 6
756 compared to the last glacial (Roucoux et al., 2011). In comparison, the Atlantic pollen record from

757 MD01-2444 core displays similar amplitude of tree percentages during the last and the penultimate
758 glacial (Margari et al., 2010). This difference can be explained by the different climate conditions, and
759 the higher sensitivity to cold and aridity of sclerophyllous and deciduous forest vegetation on the
760 Mediterranean side, as recorded in the ODP 976 and Ioannina palynological sequence. It appears that
761 temperate vegetation in SW Mediterranean responded to millennial climate oscillations with higher
762 intensity during the last glacial compared to the penultimate, probably because the climate in Europe
763 was colder during MIS 6 compared to MIS 2. This is supported by larger European ice-sheet extension
764 during the penultimate glacial (Ehlers et al., 2011; Ehlers & Gibbard, 2007; Shackleton, 1987), favouring
765 the long-term establishment of open landscapes mainly composed by steppe and semi-desert plants.
766 The differences in humidity might not be as easily interpretable, with an early MIS 6 more humid, and
767 a MIS 6 glacial maximum more arid, compared to MIS 3 and MIS 2 as also suggested by the Ioannina
768 record (Roucoux et al., 2011). Future climate reconstructions applied to the complete last glacial cycle
769 in ODP 976 and other Mediterranean long pollen sequences will help understanding the different
770 climate configurations between the last two glacial periods.

771 5.6. Human occupation during MIS 6 in SW Europe

772 Only a limited number of sites in South-Western Europe has yielded archaeological layers
773 attributed to MIS 6, and even fewer of them have been radiometrically dated allowing for a robust
774 comparison with the environmental changes during MIS 6 (Fig. 10 and Supplements table S2). The
775 environmental proxies available in the archaeological layers (pollen, charcoal, macro and microfauna)
776 can help the chronological attribution, but are often insufficient to establish a precise correlation with
777 the high-resolution chrono-environmental framework of marine and glacial archives. Even when
778 absolute dates are available, their large uncertainty range and the poor resolution of the
779 archaeological record represent a major limitation and make it difficult to correlate the human
780 occupation phases with a specific substage of MIS 6.

781 It is generally accepted that the northern part of Europe was almost completely depopulated
782 during MIS 6, with very few sites identified compared to the southern European fringes, indicating
783 discontinuous occupation during more favourable climatic episodes (Hérisson et al., 2016) or total
784 abandonment like in the British lands (Scott, 2011; Shaw et al., 2016; White and Pettitt, 2011).
785 Southern France, Italy and the Iberian Peninsula could have represented climate refugia during the
786 most extreme ice-cap advances (Bicho and Carvalho, 2022). Notably, Italy is particularly deprived of
787 sites well-dated to MIS 6 including the isolated Neanderthal of Altamura, the short episode of elephant
788 scavenging at Poggetti Vecchi, and the long sequence of San Bernardino cave which chronological
789 range extends up to ~154 ka BP, a period marked by the most extensive glacial conditions of MIS 6.

790 Some other few archaeological layers have been attributed to MIS 6, but they lack a robust
 791 chronological attribution (Aureli & Ronchitelli, 2018; Fontana et al., 2010, Fig. 10). One can hypothesise
 792 that regional climate conditions in the peninsula were particularly harsh after 150 ka, and that
 793 potential refugia sites remain to be identified in Italy. Palaeoecological reconstructions at the Poggetti
 794 Vecchi site indicated cold and dry open environment (Aranguren et al., 2019; Benvenuti et al., 2017).
 795 Interestingly, the chronological range for the site could coincide with a major stadial event at 171 ka
 796 BP identified in the ODP 976 core, and particularly well expressed in the Valle di Castiglione record (Fig.
 797 6).

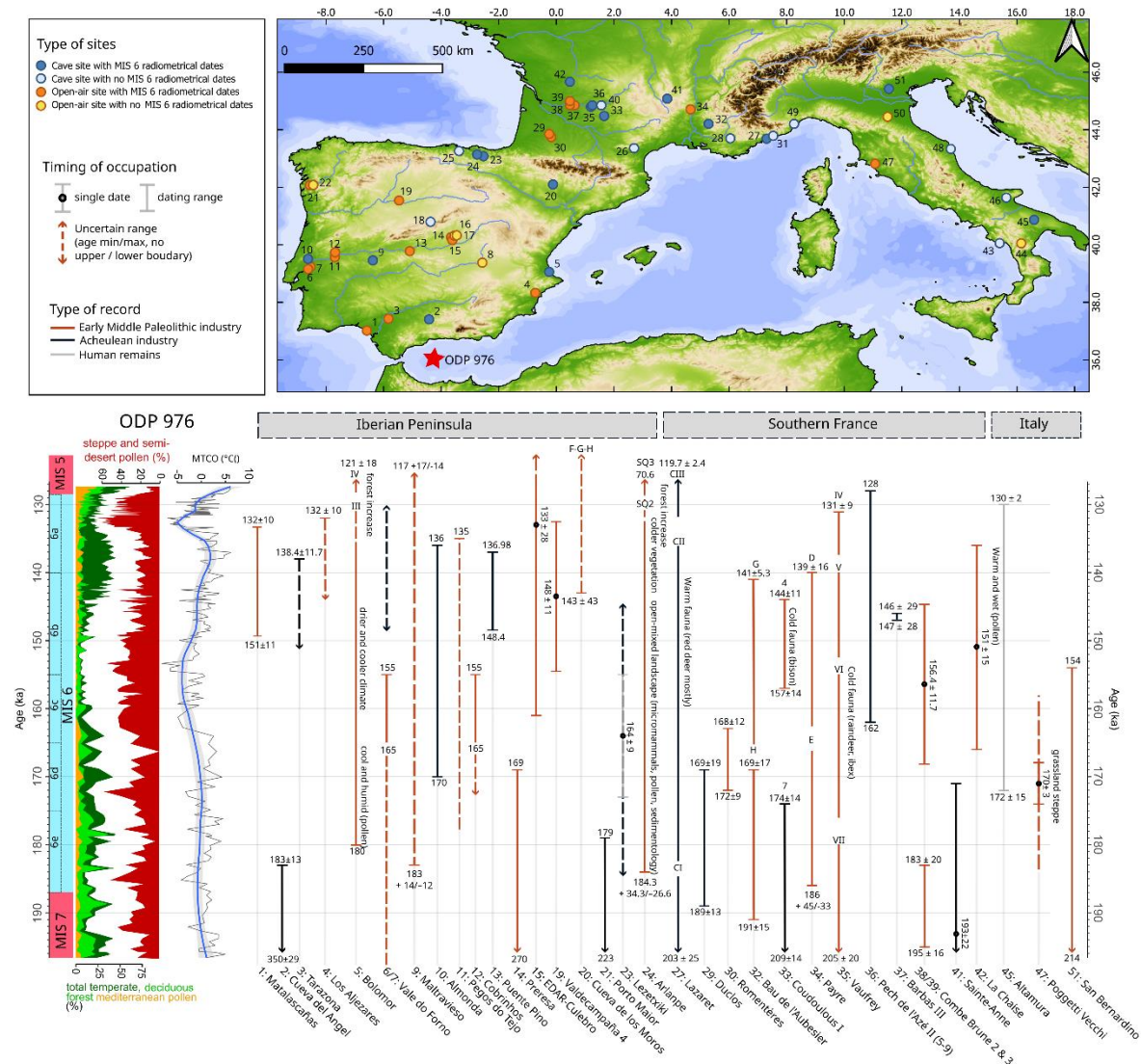


Fig. 10. Distribution of archaeological sites and radiometrically dated human occupation in western Mediterranean attributed to MIS 6, with some relevant palaeoecological information when available. The dates used and references can be found in Supplementary table S2. Sites on the map are numbered from south to north in each country: 1: Matalascañas ; 2: Cueva del Angel ; 3: Tarazona ; 4: Los Aljezares ; 5: Cueva del Bolomor ; 6: Vale do Forno ; 7: VF3 (Milharos) ; 8: El Provencio ; 9: Cueva de Maltravieso ; 10: Almonda ; 11: Pegos do Tejo ; 12: Cobrinhos ; 13: Puente Pino ; 14: Preresa ; 15: EDAR-Culebro 2 ; 16: Arriaga II/III ; 17: Arganda II (Valdocarros) ; 18: Villacastin

; **19**: Valdecampana ; **20**: Cueva de los Moros de Gabasa; **21**: Porto Maior; **22** : Arbo; **23**: Lezetxiki ; **24** : Arlanpe ; **25**: Ventalaperra ; **26**: Aldènes ; **27** : Grotte du Lazaret ; **28** : Baume Bonne ; **29** : Duclos ; **30**: Romenteres ; **31**: Grotte du Prince ; **32**: Bau de l'Aubesier; **33**: Coudoulous I ; **34**: Payre ; **35**: Grotte Vaufrey ; **36** : Pech de l'Aze II ; **37**: Barbas III ; **38**: Combe Brune 3 ; **39**: Combe Brune 2 ; **40**: Grotte Sirogne; **41**: Sainte -Anne ; **42**: La Chaise ; **43**: Riparo del Poggio; **44**: Rosaneto; **45**: Altamura; **46**: Riparo Paglicci; **47**: Poggetti Vecchi ; **48**: Monte Conero; **49**: Grotta del Colombo; **50**: Due Pozzi/Scornetta; **51**: Grotta di San Bernardino.

798 In Southern France and the Iberian Peninsula, according to available radiometric dates, human
799 occupation appears to have been continuous across MIS 6, even during the glacial maximum, with both
800 cave and open-air sites. France provides a comparable number of cave and open-air sites mainly
801 concentrated in the southwestern region. The Portuguese record is mainly constituted by open-air
802 sites in fluvial terrace systems of the lower Tagus, offering important insights into short-term
803 occupations during the full-glacial stage, but with complex chronological attribution (Cunha et al.,
804 2012, 2017; Pereira et al., 2019). The Spanish record includes various open-air settlements in the upper
805 Tagus valley (Panera et al., 2011, 2014; Yravedra et al., 2019), as well as the Duero (Diez-Martín, 2010)
806 and the Guadalquivir (Caro Gómez et al., 2011) valleys. Cave sites are fewer and are mainly located
807 closer to the coast (Cueva del Bolomor, Cueva del Angel, Lezetxiki, Arlanpe, Ventalaperra), with the
808 two exceptions of Cueva de Maltravieso and Villacastín. Key sites like Lazaret Cave (Late Acheulean,
809 France) and Cueva del Bolomor (Middle Palaeolithic, Spain) evidence the persistence of human groups
810 in possible climate refugia (Ochando et al., 2019; Valensi et al., 2005).

811 MIS 6 in Europe saw the final stage of the cultural transition from the Lower to the Middle
812 Palaeolithic industries (MIS 8-5), mainly characterized by the emergence of more complex core
813 technologies such as Levallois debitage and changes in subsistence strategies. No rupture is observed
814 between the technocomplexes, as cultural diversity and the permanence of Acheulean bifacial tools
815 associated to technological innovation mark these Early Middle Palaeolithic industries in Southern
816 Europe (Santonja et al., 2016; Terradillos-Bernal et al., 2023). The distribution of archaeological sites
817 and timing of human occupation in South-Western Mediterranean at that time reflect this pattern. A
818 mosaic of traditional and innovative behavioural traits can be observed, with late Acheulean and Early
819 Middle Palaeolithic coexisting continuously (Cueto et al., 2016; de Lumley, 2018; Mathias et al., 2020;
820 Moncel et al., 2025; Santonja et al., 2022; Torres et al., 2024; Valensi et al., 2013). Acheulean
821 technocomplexes are progressively abandoned during MIS 6 in Europe (Álvarez-Alonso, 2014; Key et
822 al., 2021), with the latest chronologies found possibly in the Manzanares basin in central Iberia at
823 Arriaga sites (Panera et al., 2014; Rubio-Jara et al., 2016; Rubio-Jara and Panera, 2019; Silva et al.,
824 2013), or at Lazaret cave (Michel et al., 2022), and dated to the beginning of MIS 5. No clear explanation
825 is accepted for the emergence and generalization of the Levallois debitage, and while cognition might
826 not be the only factor, some authors suggested that MIS 6 glaciation could have played a role in the

827 final abandonment of Acheulean industries (Moncel et al., 2020; Valensi et al., 2005). It is hard to claim
828 that specific environmental pressures favoured Levallois technology over bifacial production, as these
829 lithic technologies seem to have co-existed in Western Europe since MIS 12-11 over several
830 glacial/interglacial cycles (Baena et al., 2017; Moncel et al., 2020), including extremely cold stages (like
831 MIS 12 and 10). This “mosaic” pattern for the lower to middle palaeolithic transition, although at least
832 partly imputable to the large dating uncertainties, points toward more complex processes leading to
833 the generalization of Middle Palaeolithic industries from MIS 5. Interestingly, the end of the Lower to
834 Middle Palaeolithic transition is also associated with a shift in the morphology of human remains, from
835 “Early Neanderthals” (MIS 7-5) to “Classical Neanderthals” (MIS 5-3) (Di Vincenzo and Manzi, 2023).
836 Sites like La Chaise (Abri Suard), Lazaret and Altamura provide fossil evidence for these “Early
837 Neanderthals” which share characteristics with earlier Middle Pleistocene populations, and with later
838 Neanderthals (Buzi et al., 2025; Couture-Veschambre et al., 2021; de Lumley, 2018). Genetic data also
839 support an important population shift in western Europe sometimes around the transition from MIS 6
840 to MIS 5 (Peyrégne et al., 2019). Therefore, an important population reorganization seems to have
841 occurred at the time of the final Acheulean industries, leading to the onset of the so-called “Classical
842 neanderthal world” in western Eurasia, with generalized Middle Palaeolithic industries and established
843 Neanderthal morphological features. The role of environmental changes occurring during MIS 6 in this
844 population reorganization remains poorly understood.

845 Changes in land use and mobility pattern have been evidenced in north-central Iberia, and can
846 be viewed as adaptations to the severe climatic conditions of MIS 6 evidenced in the ODP 976 sequence
847 during pollen zone/phase 2: increasing mobility, more short-term occupations and reliance on more
848 local resources for subsistence strategies (Diez-Martín, 2010; Diez-Martín et al., 2008; Rios-Garaizar,
849 2016; Sánchez-Yustos, 2009). However, identifying cultural phases in the archaeological sequences
850 linked with specific climatic episodes is generally hindered by the poor resolution of the archaeological
851 record and chronological data. Among the sites identified in this synthesis, Lazaret and Bolomor caves
852 probably present the most informative and well-dated sequences with several archaeological layers
853 dated to MIS 6.

854 Cueva del Bolomor stands out in the Iberian Peninsula record as it provided an exceptionally
855 long and continuous record of human presence, and the oldest evidence of fire use in Spain during the
856 Middle Palaeolithic (Vidal-Matutano et al., 2019). Climate changes during MIS 6 documented in
857 Bolomor’s sediments through multiple proxies are consistent with the different phases identified in
858 the ODP 976 record, with a more humid and cool phase at the beginning of MIS 6, and the most arid
859 phase taking place at the middle of Phase III (layers X-VIII) (Arsuaga et al., 2012; Fernández Peris et al.,
860 2008). The site is described as a climatic refugium where Mediterranean vegetation persisted during

861 the colder phase of MIS 6 thanks to the coastal reservoir character of the site (Ochando et al., 2019).
862 No clear change in lithic production has been identified in the MIS 6 layers of Bolomor: according to
863 Fernández Peris et al. (2008), archaeological layers XII to VII (Phase III, MIS 6) are all dominated by
864 limestone flakes with few retouches, few recycling, and the presence non-Acheulean macro-lithic
865 elements. These layers are characterized by expeditive flaking (including Levallois *débitage*) relying on
866 local raw-material, pointing toward a high degree of mobility and search for immediate effectiveness.
867 It is thus hard to distinguish different techno-cultural tendencies during this phase. The most visible
868 change in the archaeological sequence occurs in layer VI (MIS 5) which shows an intensification of lithic
869 production dominated by flint, the production of more specialized tools including microlithic elements
870 and associated to more intense and stable occupation in the cave (Fernández Peris et al., 2008).
871 Therefore, a clear behavioural change in the technological and economical exploitation of raw
872 materials is identified at the beginning of MIS 5. Faunal remains show a large and constant diversity,
873 including abundant micro supporting both short-term and long-term not-specialized occupation, with
874 no clear change in the site's function across the sequence (Blasco et al., 2013).

875 Lazaret Cave, in south-eastern France, shows a very distinct scheme: the lower to middle
876 Palaeolithic transition is well documented in the archaeological sequence (Unit CII and CIII), with the
877 progressive replacement of large bifacial tools production by more standardized and smaller flakes
878 (Cauche, 2012). Levallois *débitage* is already present and well-mastered in the lower MIS 6 levels,
879 although rare, and becomes dominant in the upper levels (early MIS 5). Therefore, a subdivision of unit
880 CII can be made with a lower interval rich in handaxes, and an upper layer characterized as "final
881 Acheulean" with rare handaxes and more abundant flakes. Faunal assemblages are very constant
882 throughout MIS 6, with the large dominance of red deers and rare presence of cold species (*Rangifer*
883 *tarandus*, *Coelodonta antiquitatis*). Thus, the climatic oscillations of MIS 6 do not seem to have
884 influenced different hunting strategies or prey selection by human populations at Lazaret Cave, as large
885 game hunting of red deer prevailed (Valensi et al., 2013).

886 Therefore, Lazaret and Bolomor caves are examples of different strategies of site exploitation
887 and technological evolution during MIS 6: Lazaret Cave represents a specialized red-deer hunting camp
888 evidencing a progressive change from Lower to Middle Palaeolithic tools, while Cueva del Bolomor can
889 be characterized as a short-term camp with more generalized hunting and stable expeditive Middle
890 Palaeolithic industry. Despite these differences both sites provide evidence for a change in lithic
891 assemblages occurring at the end of MIS 6/ beginning of MIS 5: the disappearance of handaxes and
892 generalization of Levallois flakes in Lazaret, and the intensification and standardization of flint flakes
893 in Bolomor.

894 The fast climate dynamics during Termination II as evidenced in the ODP 976
895 paleoenvironmental record could have represented a critical period for human population. At the end
896 of MIS 6, more sites have been identified in the Iberian Peninsula than Southern France, showing the
897 latter could have represented a climate refugium at the time of maximum glacial expansion, with more
898 intense human occupation regionally. Many of these late MIS 6 sites present a chronological boundary
899 at the top of the sequence compatible with the onset of Termination II around 136 ka BP, and with
900 HS11, within the dating uncertainty: Matalascañas, Tarrazona, Los Aljezares, Bolomor Unit III,
901 Almonda, Pegos do Tejo, Puente Pino, Arlanpe Unit SQ2, Lazaret Unit CII, Payre layer D, Vauffrey unit
902 IV, and Pech de l'Azé II layer 5. The extreme character of this event in the South-Western
903 Mediterranean as expressed in the ODP 976 sequence could have put further environmental pressure
904 on hominin groups already diminished. A niche modelling approach based on 41 sites of Western
905 Eurasia since 145 ka BP has shown that the projected potential niche space for Neanderthals at the
906 end of MIS 6 (~145ka BP) was very reduced and concentrated in Western Europe (Yaworsky et al.,
907 2024). This coincides with the end of pollen zone/phase 2 in the ODP 976 record, the most cold and
908 arid phase of the penultimate Glacial before HS11. Then, the authors reconstruct a progressive
909 expansion of Neanderthal potential niche space between 145 and 130 ka, compatible with the climatic
910 warming and moistening during pollen zone/phase 3 in the ODP 976 record (Yaworsky et al., 2024).
911 The temporal resolution of the model (1000 years) does not allow to detect the impact of HS11 on the
912 niche projection, and only a small slowdown and decline of the projected niche is visible at ~130 ka BP,
913 before the MIS 5e optimum (Yaworsky et al., 2024, Fig. 5). A regional study focused on North-Western
914 Spain argued in favour of a demographic vacuum at the end of MIS 6, compatible with HS11 and leading
915 to a population reorganization implying contraction or micro-extinction, before the generalization of
916 Middle Palaeolithic industries during MIS 5 (Sánchez-Yustos and Díez-Martín, 2015). According to the
917 same authors, following this crisis, Neanderthal population entered a "reorganisation phase" leading
918 to demographical stability and more technological standardization, visible in the explosion of the
919 number of sites in Europe in general, especially after the MIS 5e climatic optimum (Bringmans, 2007;
920 Lewis et al., 2011; Wenzel, 2007). This statement is supported by niche modelling which shows a peak
921 in projected potential niche space of Neanderthal during MIS 5e (Yaworsky et al., 2024), and by recent
922 genetic data which provided evidence for at least two radiation events linked with the environmental
923 conditions of the last interglacial (Vernot et al., 2021), and Neanderthal population continuity since
924 ~120 ka BP (Peyrégne et al., 2019). Thus, HS11 did not lead to complete extinction of hominin groups
925 but might have induced deep demographical and technological reorganization, representing the first
926 and one of the most intense abrupt changes that Neanderthal population had to face in South-Western
927 Europe before the Last Glacial largest oscillations (HS6-4). According to this view, the emergence of
928 the "classical Neanderthal" world in Europe after the MIS 6/5 transition corresponds to the

929 initialization of dynamics of repeated population contraction and expansion in response to the Upper
930 Pleistocene instability, especially during MIS 4-2 (Sánchez-Yustos, 2009). In that sense, the subdued
931 environmental instability during MIS 6 evidenced in the OD P976 record compared to the last glacial
932 period (Section 5.5 and Fig. 9) could also have implications for human populations, with less
933 fragmented (although harsh) habitats and more stable (although reduced) population during MIS 6.
934 This hypothesis remains however hard to test based on the very different nature and quality of
935 preservation of the archaeological record during MIS 6 compared to MIS 4-2 (e.g. Charton et al., 2025).

936 6. Conclusion

937 The ODP 976 record sheds light on the environmental and climate changes during MIS 6 in the
938 SW Mediterranean. The sequence is characterized by the high representation of *Cedrus* and Ericaceae
939 pollen, resulting from the combined influence of African and Atlantic input respectively. ODP 976
940 position, at the confluence of Mediterranean versus Atlantic, and Eurasian versus African climatic
941 areas, is ideal to decipher the processes behind orbital and sub-orbital climate dynamics during past
942 glaciations. Three main phases have been distinguished during MIS 6 with different trends in
943 vegetation and climate changes. Millennial-scale oscillations are recorded especially during the early
944 part of MIS 6 (~187-166 ka BP) through the rapid increases of temperate and Mediterranean pollen,
945 some of which are similar to millennial-scale warming events identified in the ice-core and marine
946 temperature records, as well as other palynological sequences in the Mediterranean region. This Early
947 MIS 6 phase is characterized by overall warmer and wetter climate conditions, in agreement with other
948 paleoclimate archives in the Mediterranean showing enhanced moisture availability at the beginning
949 of MIS 6. This phase of enhanced moisture availability was likely connected with enhanced Asian and
950 African monsoon activity and was probably at the origin of the deposition of the Organic Rich Layer
951 607 in the Alboran Sea and sapropel S6 in the eastern Mediterranean. The second phase (165-144 ka
952 BP) shows the establishment of full glacial conditions in the Mediterranean, with the maximum spread
953 of steppe and semi-desert vegetation associated to cold and arid climate conditions and limited rapid
954 oscillations. Finally, the final stages of MIS 6 are marked by increased humidity and the development
955 of Ericaceae, with moderate millennial-scale oscillations seen in the vegetation record. Termination II
956 is very particular in the ODP 976 record, with the continuous increase of temperate and Mediterranean
957 vegetation being contemporaneous to a major episode of steppe expansion and aridity increase
958 identified as HS11. This event shows a particular three phases or “W” shape, in agreement with other
959 records, and had a major impact on the SW Mediterranean environments. A comparison with the
960 changes occurring during the last glacial period (MIS 4-2) inferred from the same core highlighted the
961 limited duration, frequency and intensity of MIS 6 millennial climate events compared to the last
962 Glacial D-O cycles and Heinrich Events (MIS 4-2). These results support a subdued impact of the

963 millennial-scale climate oscillations on the continental vegetation in the Mediterranean region during
964 the Penultimate glaciation compared to the Last Glacial. The only exception is HS11, which stands out
965 by its notable intensity and duration and is of particular interest to understand the mechanisms behind
966 Termination II.

967 Human populations continuously inhabited the SW Mediterranean territory during MIS 6.
968 While few sites are available and robustly dated to MIS 6 in Italy, Southern France and the Iberian
969 Peninsula appear to have been intensely populated, supporting their nature of Pleistocene Climate
970 refugia. More ecological data from well-dated archaeological sites during MIS 6 would be needed to
971 increase the quality of human-environmental dynamics comparison. However, the synthesis drawn in
972 the present study highlights the extreme nature of events characterizing Termination II, and
973 particularly HS11, which could have represented an important environmental crisis for human
974 population at that time, catalysing the end of the Lower to Middle Palaeolithic Transition and the onset
975 of the “classical” Neanderthal world through a drastic population bottleneck.

976 7. Data availability

977 Pollen counts and climate reconstruction results from ODP 976 will soon be submitted to PANGAEA
978 data repository (<https://www.pangaea.de/>).

979 8. Supplements

980

981 The supplementary figures and tables related to this study can be downloaded at the following
982 link:

983 9. Author contribution

984

985 LC, NC, AB and VL designed the project. LC and NC carried out the palynological analyses. LC, OP
986 and MR applied the four methods of pollen-based climate reconstruction to the ODP 976 record. LC
987 and MHM led the archaeological synthesis. LC made the figures and wrote the text. All authors
988 contributed to improve the manuscript by their expertise.

989 10. Competing interests

990

991 Odile Peyron is a member of the editorial board of CP.

992

993 11. Acknowledgments

994

995 We want to thank the three anonymous reviewers and the editor for their very helpful
996 comments on this manuscript. We acknowledge the International Ocean Drilling Project and the
997 MARUM Bremen Core Repository for making available the ODP 976 samples. The sample processing
998 was funded by the CNRS and the MNHN. We thank the European Research Council (ERC) under the
999 European Union's HORIZON1.1 research program (LATEUROPE project, grant agreement ID
1000 101052653) for funding this publication. L. Charton doctoral contract was funded by the French
1001 Ministère de l'Enseignement Supérieur et de la Recherche at the doctoral school ED 227 of the
1002 Muséum National d'Histoire Naturelle, Paris. The international cotutorship with the University of
1003 Florence is supported by the Ecole Franco-Italienne Vinci grant (project C2-166). We thank Lionel
1004 Dubost for assistance in laboratory treatment of samples to HF. We are grateful to Francisco Sierra for
1005 sharing the isotopic data on AICC2012 timescale, to Jon Camuera for the pollen data from Padul and
1006 to Katherine Roucoux for the pollen data from Ioannina. This is an ISEM contribution.

1007

1008 12. References

1009

1010 de Abreu, L., Shackleton, N. J., Schönfeld, J., Hall, M., and Chapman, M.: Millennial-scale oceanic
1011 climate variability off the Western Iberian margin during the last two glacial periods, *Marine Geology*,
1012 196, 1–20, [https://doi.org/10.1016/S0025-3227\(03\)00046-X](https://doi.org/10.1016/S0025-3227(03)00046-X), 2003.

1013 Allen, J. R. M. and Huntley, B.: Last Interglacial palaeovegetation, palaeoenvironments and chronology:
1014 a new record from Lago Grande di Monticchio, southern Italy, *Quaternary Science Reviews*, 28, 1521–
1015 1538, <https://doi.org/10.1016/j.quascirev.2009.02.013>, 2009.

1016 Álvarez-Alonso, D.: First Neanderthal settlements in northern Iberia: The Acheulean and the
1017 emergence of Mousterian technology in the Cantabrian region, *Quaternary International*, 326–327,
1018 288–306, <https://doi.org/10.1016/j.quaint.2012.12.023>, 2014.

1019 Aranguren, B., Grimaldi, S., Benvenuti, M., Capalbo, C., Cavanna, F., Cavulli, F., Ciani, F., Comencini, G.,
1020 Giuliani, C., Grandinetti, G., Mariotti Lippi, M., Masini, F., Mazza, P. P. A., Pallecchi, P., Santaniello, F.,
1021 Savorelli, A., and Revedin, A.: Poggetti Vecchi (Tuscany, Italy): A late Middle Pleistocene case of
1022 human–elephant interaction, *Journal of Human Evolution*, 133, 32–60,
1023 <https://doi.org/10.1016/j.jhevol.2019.05.013>, 2019.

1024 Arsuaga, J. L., Fernández Peris, J., Gracia-Téllez, A., Quam, R., Carretero, J. M., Barciela González, V.,
1025 Blasco, R., Cuartero, F., and Sañudo, P.: Fossil human remains from Bolomor Cave (Valencia, Spain),
1026 *Journal of Human Evolution*, 62, 629–639, <https://doi.org/10.1016/j.jhevol.2012.02.002>, 2012.

1027 Auffret, G.-A., Pastouret, L., Chamley, H., and Lanoix, F.: Influence of the prevailing current regime on
1028 sedimentation in the Alboran Sea, *Deep Sea Research and Oceanographic Abstracts*, 21, 839–849,
1029 [https://doi.org/10.1016/0011-7471\(74\)90003-5](https://doi.org/10.1016/0011-7471(74)90003-5), 1974.

1030 Aureli, D. and Ronchitelli, A.: The Lower Tyrrhenian Versant: was it a techno-cultural area during the
1031 Middle Palaeolithic? Evolution of the lithic industries of the Riparo del Molare sequence in the frame
1032 of Neanderthal peopling dynamics in Italy, 59–94, 2018.

- 1033 Ayalon, A., Bar-Matthews, M., and Kaufman, A.: Climatic conditions during marine oxygen isotope
1034 stage 6 in the eastern Mediterranean region from the isotopic composition of speleothems of Soreq
1035 Cave, Israel, *Geology*, 30, [https://doi.org/10.1130/0091-7613\(2002\)030<0303:CCDMOI>2.0.CO;2](https://doi.org/10.1130/0091-7613(2002)030<0303:CCDMOI>2.0.CO;2),
1036 2002a.
- 1037 Ayalon, A., Bar-Matthews, M., and Kaufman, A.: Climatic conditions during marine oxygen isotope
1038 stage 6 in the eastern Mediterranean region from the isotopic composition of speleothems of Soreq
1039 Cave, Israel, *Geol*, 30, 303, [https://doi.org/10.1130/0091-7613\(2002\)030<0303:CCDMOI>2.0.CO;2](https://doi.org/10.1130/0091-7613(2002)030<0303:CCDMOI>2.0.CO;2),
1040 2002b.
- 1041 Baena, J., Moncel, M.-H., Cuartero, F., Chacón Navarro, M. G., and Rubio, D.: Late Middle Pleistocene
1042 genesis of Neanderthal technology in Western Europe: The case of Payre site (south-east France),
1043 *Quaternary International*, 436, 212–238, <https://doi.org/10.1016/j.quaint.2014.08.031>, 2017.
- 1044 Bailey, G., Carrión, J., Fa, D., Finlayson, C., Finlayson, G., and Vidal, J.: The coastal shelf of the
1045 Mediterranean and beyond: Corridor and refugium for human populations in the Pleistocene
1046 Introduction, *Quaternary Science Reviews*, 27, 2095–2099,
1047 <https://doi.org/10.1016/j.quascirev.2008.08.005>, 2008.
- 1048 Bajo, P., Drysdale, R. N., Woodhead, J. D., Hellstrom, J. C., Hodell, D., Ferretti, P., Voelker, A. H. L.,
1049 Zanchetta, G., Rodrigues, T., Wolff, E., Tyler, J., Frisia, S., Spötl, C., and Fallick, A. E.: Persistent influence
1050 of obliquity on ice age terminations since the Middle Pleistocene transition, *Science*, 367, 1235–1239,
1051 <https://doi.org/10.1126/science.aaw1114>, 2020.
- 1052 Barbante, C., Barnola, J.-M., Becagli, S., Beer, J., Bigler, M., Boutron, C., Blunier, T., Castellano, E.,
1053 Cattani, O., Chappellaz, J., Dahl-Jensen, D., Debret, M., Delmonte, B., Dick, D., Falourd, S., Faria, S.,
1054 Federer, U., Fischer, H., Freitag, J., Frenzel, A., Fritzsche, D., Fundel, F., Gabrielli, P., Gaspari, V.,
1055 Gersonde, R., Graf, W., Grigoriev, D., Hamann, I., Hansson, M., Hoffmann, G., Hutterli, M. A.,
1056 Huybrechts, P., Isaksson, E., Johnsen, S., Jouzel, J., Kaczmarek, M., Karlin, T., Kaufmann, P., Kipfstuhl,
1057 S., Kohno, M., Lambert, F., Lambrecht, A., Lambrecht, A., Landais, A., Lawer, G., Leuenberger, M., Littot,
1058 G., Loulergue, L., Lüthi, D., Maggi, V., Marino, F., Masson-Delmotte, V., Meyer, H., Miller, H., Mulvaney,
1059 R., Narcisi, B., Oerlemans, J., Oerter, H., Parrenin, F., Petit, J.-R., Raisbeck, G., Raynaud, D.,
1060 Röthlisberger, R., Ruth, U., Rybak, O., Severi, M., Schmitt, J., Schwander, J., Siegenthaler, U., Siggaard-
1061 Andersen, M.-L., Spahni, R., Steffensen, J. P., Stenni, B., Stocker, T. F., Tison, J.-L., Traversi, R., Udisti,
1062 R., Valero-Delgado, F., van den Broeke, M. R., van de Wal, R. S. W., Wagenbach, D., Wegner, A., Weiler,
1063 K., Wilhelms, F., Winther, J.-G., Wolff, E., and EPICA Community Members: One-to-one coupling of
1064 glacial climate variability in Greenland and Antarctica, *Nature*, 444, 195–198,
1065 <https://doi.org/10.1038/nature05301>, 2006.
- 1066 Bard, E., Delaygue, G., Rostek, F., Antonioli, F., Silenzi, S., and Schrag, D. P.: Hydrological conditions
1067 over the western Mediterranean basin during the deposition of the cold Sapropel 6 (ca. 175 kyr BP),
1068 *Earth and Planetary Science Letters*, 202, 481–494, [https://doi.org/10.1016/S0012-821X\(02\)00788-4](https://doi.org/10.1016/S0012-821X(02)00788-4),
1069 2002a.
- 1070 Bard, E., Antonioli, F., and Silenzi, S.: Sea-level during the penultimate interglacial period based on a
1071 submerged stalagmite from Argentarola Cave (Italy), *Earth and Planetary Science Letters*, 196, 135–
1072 146, [https://doi.org/10.1016/S0012-821X\(01\)00600-8](https://doi.org/10.1016/S0012-821X(01)00600-8), 2002b.
- 1073 Barker, S. and Knorr, G.: Millennial scale feedbacks determine the shape and rapidity of glacial
1074 termination, *Nat Commun*, 12, 2273, <https://doi.org/10.1038/s41467-021-22388-6>, 2021.

- 1075 Barker, S., Knorr, G., Edwards, R. L., Parrenin, F., Putnam, A. E., Skinner, L. C., Wolff, E., and Ziegler, M.:
1076 800,000 Years of Abrupt Climate Variability, *Science*, 334, 347–351,
1077 <https://doi.org/10.1126/science.1203580>, 2011.
- 1078 Bayr, D., Plaza, M. P., Gilles, S., Kolek, F., Leier-Wirtz, V., Traidl-Hoffmann, C., and Damialis, A.: Pollen
1079 long-distance transport associated with symptoms in pollen allergics on the German Alps: An old story
1080 with a new ending?, *Sci Total Environ*, 881, 163310, <https://doi.org/10.1016/j.scitotenv.2023.163310>,
1081 2023.
- 1082 Bazin, L., Landais, A., Lemieux-Dudon, B., Toyé Mahamadou Kele, H., Veres, D., Parrenin, F., Martinerie,
1083 P., Ritz, C., Capron, E., Lipenkov, V., Loutre, M.-F., Raynaud, D., Vinther, B., Svensson, A., Rasmussen,
1084 S. O., Severi, M., Blunier, T., Leuenberger, M., Fischer, H., Masson-Delmotte, V., Chappellaz, J., and
1085 Wolff, E.: An optimized multi-proxy, multi-site Antarctic ice and gas orbital chronology (AICC2012):
1086 120–800 ka, *Climate of the Past*, 9, 1715–1731, <https://doi.org/10.5194/cp-9-1715-2013>, 2013.
- 1087 Benvenuti, M., Bahain, J.-J., Capalbo, C., Capretti, C., Ciani, F., D’Amico, C., Esu, D., Giachi, Gi., Giuliani,
1088 C., Gliozzi, E., Lazzeri, S., Macchioni, N., Lippi, M. M., Masini, F., Mazza, P. P. A., Pallecchi, P., Revedin,
1089 A., Savorelli, A., Spadi, M., Sozzi, L., Vietti, A., Voltaggio, M., and Aranguren, B.: Paleoenvironmental
1090 context of the early Neanderthals of Poggetti Vecchi for the late middle Pleistocene of Central Italy,
1091 *Quat. res.*, 88, 327–344, <https://doi.org/10.1017/qua.2017.51>, 2017.
- 1092 Bermúdez de Castro, J. M. and Martínón-Torres, M.: A new model for the evolution of the human
1093 Pleistocene populations of Europe, *Quaternary International*, 295, 102–112,
1094 <https://doi.org/10.1016/j.quaint.2012.02.036>, 2013.
- 1095 Bicho, N. and Carvalho, M.: Peninsular southern Europe refugia during the Middle Palaeolithic: an
1096 introduction, *J Quaternary Science*, 37, 133–135, <https://doi.org/10.1002/jqs.3410>, 2022.
- 1097 Bisschop, K., Mortier, F., Etienne, R. S., and Bonte, D.: Transient local adaptation and source–sink
1098 dynamics in experimental populations experiencing spatially heterogeneous environments,
1099 *Proceedings of the Royal Society B: Biological Sciences*, 286, 20190738,
1100 <https://doi.org/10.1098/rspb.2019.0738>, 2019.
- 1101 Blasco, R., Rosell, J., Fernández Peris, J., Arsuaga, J. L., Bermúdez de Castro, J. M., and Carbonell, E.:
1102 Environmental availability, behavioural diversity and diet: a zooarchaeological approach from the
1103 TD10-1 sublevel of Gran Dolina (Sierra de Atapuerca, Burgos, Spain) and Bolomor Cave (Valencia,
1104 Spain), *Quaternary Science Reviews*, 70, 124–144, <https://doi.org/10.1016/j.quascirev.2013.03.008>,
1105 2013.
- 1106 Bond, G., Heinrich, H., Broecker, W., Labeyrie, L., McManus, J., Andrews, J., Huon, S., Jantschik, R.,
1107 Clasen, S., Simet, C., Tedesco, K., Klas, M., Bonani, G., and Ivy, S.: Evidence for massive discharges of
1108 icebergs into the North Atlantic ocean during the last glacial period, *Nature*, 360, 245–249,
1109 <https://doi.org/10.1038/360245a0>, 1992.
- 1110 Bond, G., Broecker, W., Johnsen, S., McManus, J., Labeyrie, L., Jouzel, J., and Bonani, G.: Correlations
1111 between climate records from North Atlantic sediments and Greenland ice, *Nature*, 365, 143–147,
1112 <https://doi.org/10.1038/365143a0>, 1993.
- 1113 Bond, G., Showers, W., Cheseby, M., Lotti, R., Almasi, P., Demenocal, P., Priore, P., Cullen, H., Hajdas,
1114 I., and Bonani, G.: A pervasive millennial-scale cycle in the North Atlantic Holocene and glacial climates,
1115 *sci*, 278, 1257, <https://doi.org/10.1126/science.278.5341.1257>, 1997.

- 1116 Bond, G. C., Showers, W., Elliot, M., Evans, M., Lotti, R., Hajdas, I., Bonani, G., and Johnson, S.: The
1117 North Atlantic's 1-2 kyr climate rhythm: Relation to Heinrich events, Dansgaard/Oeschger cycles and
1118 the Little Ice Age, Washington DC American Geophysical Union Geophysical Monograph Series, 112,
1119 35–58, <https://doi.org/10.1029/GM112p0035>, 1999.
- 1120 Boswell, S. M., Toucanne, S., Pitel-Roudaut, M., Creyts, T. T., Eynaud, F., and Bayon, G.: Enhanced
1121 surface melting of the Fennoscandian Ice Sheet during periods of North Atlantic cooling, *Geology*, 47,
1122 664–668, <https://doi.org/10.1130/G46370.1>, 2019.
- 1123 Bout-Roumazelles, V., Combourieu Nebout, N., Peyron, O., Cortijo, E., Landais, A., and Masson-
1124 Delmotte, V.: Connection between South Mediterranean climate and North African atmospheric
1125 circulation during the last 50,000yrBP North Atlantic cold events, *Quaternary Science Reviews*, 26,
1126 3197–3215, <https://doi.org/10.1016/j.quascirev.2007.07.015>, 2007.
- 1127 ter Braak, C. and Juggins, S.: Weighted Averaging Partial Least Squares Regression (WA-PLS): An
1128 Improved Method for Reconstructing Environmental Variables from Species Assemblages,
1129 *Hydrobiologia*, 269–270, 485–502, <https://doi.org/10.1007/BF00028046>, 1993.
- 1130 Bradtmöller, M., Pastoors, A., Weninger, B., and Weniger, G.-C.: The repeated replacement model –
1131 Rapid climate change and population dynamics in Late Pleistocene Europe, *Quaternary International*,
1132 247, 38–49, <https://doi.org/10.1016/j.quaint.2010.10.015>, 2012.
- 1133 Brauer, A., Allen, J. R. M., Mingram, J., Dulski, P., Wulf, S., and Huntley, B.: Evidence for last interglacial
1134 chronology and environmental change from Southern Europe, *Proceedings of the National Academy
1135 of Sciences*, 104, 450–455, <https://doi.org/10.1073/pnas.0603321104>, 2007.
- 1136 Bringmans, P.: First Evidence of Neanderthal Presence in Northwest Europe during the Late Saalian
1137 “Zeifen Interstadial” (MIS 6.01) found at the VLL and VLB Sites at Veldwezelt-Hezerwater, Belgium,
1138 *Journal of Archaeology of Northwest Europe*, 1, 2007.
- 1139 Broecker, W. S. and Henderson, G. M.: The sequence of events surrounding Termination II and their
1140 implications for the cause of glacial-interglacial CO₂ changes, *Paleoceanography*, 13, 352–364, 1998.
- 1141 Burns, S. J., Welsh, L. K., Scroxton, N., Cheng, H., and Edwards, R. L.: Millennial and orbital scale
1142 variability of the South American Monsoon during the penultimate glacial period, *Sci Rep*, 9, 1234,
1143 <https://doi.org/10.1038/s41598-018-37854-3>, 2019.
- 1144 Buzi, C., Profico, A., Lorenzo, C., and Manzi, G.: The first preserved nasal cavity in the human fossil
1145 record: The Neanderthal from Altamura, *Proceedings of the National Academy of Sciences*, 122,
1146 e2426309122, <https://doi.org/10.1073/pnas.2426309122>, 2025.
- 1147 Cacho, I., Grimalt, J. O., Pelejero, C., Canals, M., Sierro, F. J., Flores, J. A., and Shackleton, N.: Dansgaard-
1148 Oeschger and Heinrich event imprints in Alboran Sea paleotemperatures, *Paleoceanography*, 14, 698–
1149 705, <https://doi.org/10.1029/1999PA900044>, 1999.
- 1150 Cacho, I., Shackleton, N., Elderfield, H., Sierro, F. J., and Grimalt, J. O.: Glacial rapid variability in deep-
1151 water temperature and $\delta^{18}\text{O}$ from the Western Mediterranean Sea, *Quaternary Science Reviews*, 25,
1152 3294–3311, <https://doi.org/10.1016/j.quascirev.2006.10.004>, 2006.
- 1153 Camuera, J., Jiménez-Moreno, G., Ramos-Román, M. J., García-Alix, A., Toney, J. L., Anderson, R. S.,
1154 Jiménez-Espejo, F., Bright, J., Webster, C., Yanes, Y., and Carrión, J. S.: Vegetation and climate changes
1155 during the last two glacial-interglacial cycles in the western Mediterranean: A new long pollen record

- 1156 from Padul (southern Iberian Peninsula), *Quaternary Science Reviews*, 205, 86–105,
1157 <https://doi.org/10.1016/j.quascirev.2018.12.013>, 2019.
- 1158 Camuera, J., Ramos-Román, M. J., Jiménez-Moreno, G., García-Alix, A., Ilvonen, L., Ruha, L., Gil-Romera,
1159 G., González-Sampériz, P., and Seppä, H.: Past 200 kyr hydroclimate variability in the western
1160 Mediterranean and its connection to the African Humid Periods, *Sci Rep*, 12, 9050,
1161 <https://doi.org/10.1038/s41598-022-12047-1>, 2022.
- 1162 Caro Gómez, J. A., Díaz Del Olmo, F., Artigas, R. C., Recio Espejo, J. M., and Barrera, C. B.:
1163 Geoarchaeological alluvial terrace system in Tarazona: Chronostratigraphical transition of Mode 2 to
1164 Mode 3 during the middle-upper pleistocene in the Guadalquivir River valley (Seville, Spain),
1165 *Quaternary International*, 243, 143–160, <https://doi.org/10.1016/j.quaint.2011.04.022>, 2011.
- 1166 Chapman, M. R. and Shackleton, N. J.: Global ice-volume fluctuations, North Atlantic ice-rafting events,
1167 and deep-ocean circulation changes between 130 and 70 ka, *Geology*, 27, 795,
1168 [https://doi.org/10.1130/0091-7613\(1999\)027<0795:GIVFNA>2.3.CO;2](https://doi.org/10.1130/0091-7613(1999)027<0795:GIVFNA>2.3.CO;2), 1999.
- 1169 Chappellaz, J., Brook, E., Blunier, T., and Malaizé, B.: CH₄ and δ¹⁸O of O₂ records from Antarctic and
1170 Greenland ice: A clue for stratigraphic disturbance in the bottom part of the Greenland Ice Core Project
1171 and the Greenland Ice Sheet Project 2 ice cores, *J. Geophys. Res.*, 102, 26547–26557,
1172 <https://doi.org/10.1029/97JC00164>, 1997.
- 1173 Charton, L.: Vegetation and climate changes during the Middle to Upper Palaeolithic transition in the
1174 southwestern Mediterranean: What happened to the last Neanderthals during Heinrich stadial 4?,
1175 *Quaternary Science Reviews*, 2025.
- 1176 Charton, L., Combourieu-Nebout, N., Bertini, A., Lebreton, V., Peyron, O., Robles, M., Sasso, D., and
1177 Moncel, M.-H.: Vegetation and climate changes during the Middle to Upper Palaeolithic transition in
1178 the southwestern Mediterranean: What happened to the last Neanderthals during Heinrich stadial 4?,
1179 2025.
- 1180 Cheddadi, R. and Rossignol-Strick, M.: Eastern Mediterranean Quaternary paleoclimates from pollen
1181 and isotope records of marine cores in the Nile Cone Area, *Paleoceanography*, 10, 291–300,
1182 <https://doi.org/10.1029/94PA02672>, 1995.
- 1183 Cheng, H., Edwards, R. L., Wang, Y., Kong, X., Ming, Y., Kelly, M. J., Wang, X., Gallup, C. D., and Liu, W.:
1184 A penultimate glacial monsoon record from Hulu Cave and two-phase glacial terminations, *Geology*,
1185 34, 217–220, <https://doi.org/10.1130/G22289.1>, 2006.
- 1186 Chevalier, M., Davis, B. A. S., Heiri, O., Seppä, H., Chase, B. M., Gajewski, K., Lacourse, T., Telford, R. J.,
1187 Finsinger, W., Guiot, J., Kühl, N., Maezumi, S. Y., Tipton, J. R., Carter, V. A., Brussel, T., Phelps, L. N.,
1188 Dawson, A., Zanon, M., Vallé, F., Nolan, C., Mauri, A., de Vernal, A., Izumi, K., Holmström, L., Marsicek,
1189 J., Goring, S., Sommer, P. S., Chaput, M., and Kupriyanov, D.: Pollen-based climate reconstruction
1190 techniques for late Quaternary studies, *Earth-Science Reviews*, 210,
1191 <https://doi.org/10.1016/j.earscirev.2020.103384>, 2020.
- 1192 Colleoni, F., Wekerle, C., Näslund, J.-O., Brandefelt, J., and Masina, S.: Constraint on the penultimate
1193 glacial maximum Northern Hemisphere ice topography (≈140 kyrs BP), *Quaternary Science Reviews*,
1194 137, 97–112, <https://doi.org/10.1016/j.quascirev.2016.01.024>, 2016.
- 1195 Combourieu-Nebout, N., Turon, J. L., Zahn, R., Capotondi, L., Londeix, L., and Pahnke, K.: Enhanced
1196 aridity and atmospheric high-pressure stability over the western Mediterranean during the North

- 1197 Atlantic cold events of the past 50 k.y., *Geol*, 30, 863, [https://doi.org/10.1130/0091-7613\(2002\)030<0863:EAAAHP>2.0.CO;2](https://doi.org/10.1130/0091-7613(2002)030<0863:EAAAHP>2.0.CO;2), 2002.
- 1199 Combourieu-Nebout, N., Peyron, O., Dormoy, I., Desprat, S., Célia, B., Kotthoff, U., and Marret, F.:
1200 Rapid climatic variability in the west Mediterranean during the last 25 000 years from high resolution
1201 pollen data, *Climate of the Past*, 5, <https://doi.org/10.5194/cpd-5-671-2009>, 2009.
- 1202 Cortina, A., Sierro, F. J., Flores, J. A., Martrat, B., and Grimalt, J. O.: The response of SST to insolation
1203 and ice sheet variability from MIS 3 to MIS 11 in the northwestern Mediterranean Sea (Gulf of Lions),
1204 *Geophysical Research Letters*, 42, 10,366-10,374, <https://doi.org/10.1002/2015GL065539>, 2015.
- 1205 Couture-Veschambre, C., López-Onaindia, D., Sala, N., Arlegi, M., Balzeau, A., Crevecoeur, I., Maureille,
1206 B., Tournepiche, J.-F., and Gómez-Olivencia, A.: Reassessment of the Neandertal fossil collection from
1207 Abri Suard (La Chaise de Vouthon, Charente, France), *Bulletins et mémoires de la Société*
1208 *d'Anthropologie de Paris. BMSAP*, 33, <https://doi.org/10.4000/bmsap.6982>, 2021.
- 1209 Cueto, S., Preysler, J., Pérez-González, A., Torres, C., Pérez, I., and Miguel, J.: Acheulian flint quarries in
1210 the Madrid Tertiary basin, central Iberian Peninsula: First data obtained from geoarchaeological
1211 studies, *Quaternary International*, 411, <https://doi.org/10.1016/j.quaint.2016.01.041>, 2016.
- 1212 Cunha, P. P., Almeida, N. A. C., Aubry, T., Martins, A. A., Murray, A. S., Buylaert, J.-P., Sohbaty, R.,
1213 Raposo, L., and Rocha, L.: Records of human occupation from Pleistocene river terrace and aeolian
1214 sediments in the Arneiro depression (Lower Tejo River, central eastern Portugal), *Geomorphology*,
1215 165–166, 78–90, <https://doi.org/10.1016/j.geomorph.2012.02.017>, 2012.
- 1216 Cunha, P. P., Martins, A. A., Buylaert, J.-P., Murray, A. S., Raposo, L., Mozzi, P., and Stokes, M.: New
1217 data on the chronology of the Vale do Forno sedimentary sequence (Lower Tejo River terrace staircase)
1218 and its relevance as a fluvial archive of the Middle Pleistocene in western Iberia, *Quaternary Science*
1219 *Reviews*, 166, 204–226, <https://doi.org/10.1016/j.quascirev.2016.11.001>, 2017.
- 1220 Damialis, A., Kaimakamis, E., Konoglou, M., Akritidis, I., Traidl-Hoffmann, C., and Gioulekas, D.:
1221 Estimating the abundance of airborne pollen and fungal spores at variable elevations using an aircraft:
1222 how high can they fly?, *Sci Rep*, 7, 44535, <https://doi.org/10.1038/srep44535>, 2017.
- 1223 Dansgaard, W., Johnsen, S. J., Clausen, H. B., Dahl-Jensen, D., Gundestrup, N. S., Hammer, C. U.,
1224 Hvidberg, C. S., Steffensen, J. P., Sveinbjörnsdóttir, A. E., and Jouzel, J.: Evidence for general instability
1225 of past climate from a 250-kyr ice-core record, *Nature*, 364, 218–220, 1993.
- 1226 Davtian, N. and Bard, E.: A new view on abrupt climate changes and the bipolar seesaw based on
1227 paleotemperatures from Iberian Margin sediments, *Proceedings of the National Academy of Sciences*,
1228 120, e2209558120, <https://doi.org/10.1073/pnas.2209558120>, 2023.
- 1229 Dennell, R. W., Martínón-Torres, M., and Bermúdez de Castro, J. M.: Hominin variability, climatic
1230 instability and population demography in Middle Pleistocene Europe, *Quaternary Science Reviews*, 30,
1231 1511–1524, <https://doi.org/10.1016/j.quascirev.2009.11.027>, 2011.
- 1232 D'Errico, F. and Sánchez Goñi, M. F. S.: Neandertal extinction and the millennial scale climatic variability
1233 of OIS 3, *Quaternary Science Reviews*, 22, 769–788, [https://doi.org/10.1016/S0277-3791\(03\)00009-X](https://doi.org/10.1016/S0277-3791(03)00009-X),
1234 2003.
- 1235 Di Vincenzo, F. and Manzi, G.: *Homo heidelbergensis* as the Middle Pleistocene common ancestor of
1236 Denisovans, Neanderthals and modern humans, *Journal of Mediterranean Earth Sciences*, Vol. 15
1237 (2023): In progress, <https://doi.org/10.13133/2280-6148/18074>, 2023.

- 1238 Diez-Martín, F.: Evaluating the effect of plowing on the archaeological record: The early middle
1239 palaeolithic in the river Duero basin plateaus (north-central Spain), *Quaternary International*, 214, 30–
1240 43, <https://doi.org/10.1016/j.quaint.2009.10.024>, 2010.
- 1241 Diez-Martín, F., Sánchez-Yustos, P., Gómez-González, J. Á., and Gómez De La Rúa, D.: Earlier
1242 Palaeolithic Settlement Patterns: Landscape Archaeology on the River Duero Basin Plateaus (Castilla y
1243 León, Spain), *J World Prehist*, 21, 103–137, <https://doi.org/10.1007/s10963-008-9012-0>, 2008.
- 1244 D’Oliveira, L., Dugerdil, L., Ménot, G., Evin, A., Muller, S., Ansanay-Alex, S., Azuara, J., Bonnet, C.,
1245 Bremond, L., Shah, M., and Peyron, O.: Reconstructing 15 000 years of southern France temperatures
1246 from coupled pollen and molecular (branched glycerol dialkyl glycerol tetraether) markers (Canroute,
1247 Massif Central), *Climate of the Past*, 19, 2127–2156, <https://doi.org/10.5194/cp-19-2127-2023>, 2023.
- 1248 Drysdale, R. N., Zanchetta, G., Hellstrom, J. C., Fallick, A. E., and Zhao, J.: Stalagmite evidence for the
1249 onset of the Last Interglacial in southern Europe at 129 ± 1 ka, *Geophysical Research Letters*, 32,
1250 <https://doi.org/10.1029/2005GL024658>, 2005.
- 1251 Ehlers, J. and Gibbard, P. L.: The extent and chronology of Cenozoic Global Glaciation, *Quaternary*
1252 *International*, 164–165, 6–20, <https://doi.org/10.1016/j.quaint.2006.10.008>, 2007a.
- 1253 Ehlers, J. and Gibbard, P. L.: The extent and chronology of Cenozoic Global Glaciation, *Quaternary*
1254 *International*, 164–165, 6–20, <https://doi.org/10.1016/j.quaint.2006.10.008>, 2007b.
- 1255 Ehlers, J., Grube, A., Stephan, H.-J., and Wansa, S.: Pleistocene Glaciations of North Germany—New
1256 Results, in: *Developments in Quaternary Sciences*, vol. 15, Elsevier, 149–162,
1257 <https://doi.org/10.1016/B978-0-444-53447-7.00013-1>, 2011.
- 1258 Ehlers, J., Gibbard, P. L., and Hughes, P. D.: Chapter 4 - Quaternary Glaciations and Chronology, in: *Past*
1259 *Glacial Environments (Second Edition)*, edited by: Menzies, J. and van der Meer, J. J. M., Elsevier, 77–
1260 101, <https://doi.org/10.1016/B978-0-08-100524-8.00003-8>, 2018.
- 1261 Emeis, K., Schulz, H., Struck, U., Rossignol-Strick, M., Erlenkeuser, H., Howell, M., Kroon, D.,
1262 Mackensen, A., Ishizuka, S., Oba, T., Sakamoto, T., and Koizumi, I.: Eastern Mediterranean surface
1263 water temperatures and $\delta^{18}O$ composition during deposition of sapropels in the late Quaternary,
1264 *Paleoceanography*, 18, 1005, <https://doi.org/10.1029/2000PA000617>, 2003a.
- 1265 Emeis, K.-C., Schulz, H., Struck, U., Rossignol-Strick, M., Erlenkeuser, H., Howell, M. W., Kroon, D.,
1266 Mackensen, A., Ishizuka, S., Oba, T., Sakamoto, T., and Koizumi, I.: Eastern Mediterranean surface
1267 water temperatures and $\delta^{18}O$ composition during deposition of sapropels in the late Quaternary,
1268 *Paleoceanography*, 18, <https://doi.org/10.1029/2000PA000617>, 2003b.
- 1269 Eynaud, F., Zaragosi, S., Scourse, J. D., Mojtahid, M., Bourillet, J. F., Hall, I. R., Penaud, A., Locascio, M.,
1270 and Reijonen, A.: Deglacial laminated facies on the NW European continental margin: The
1271 hydrographic significance of British-Irish Ice Sheet deglaciation and Fleuve Manche paleoriver
1272 discharges, *Geochemistry, Geophysics, Geosystems*, 8, <https://doi.org/10.1029/2006GC001496>, 2007.
- 1273 Faegri, K. and Iversen, J.: *Textbook of Pollen Analysis*, 4th Edition., John Wiley and Sons, Chichester,
1274 UK, 338 pp., 1964.
- 1275 Fernández Peris, J., Barciela, V., Blasco, R., Cuartero, F., and Sañudo, P.: El Paleolítico Medio en el
1276 territorio valenciano y la variabilidad tecno-económica de la Cova del Bolomor, *Treballs d’Arqueologia*,
1277 141–169, 2008.

- 1278 Fernández-Rodríguez, S., Skjøth, C. A., Tormo-Molina, R., Brandao, R., Caeiro, E., Silva-Palacios, I.,
 1279 Gonzalo-Garijo, A., and Smith, M.: Identification of potential sources of airborne *Olea* pollen in the
 1280 Southwest Iberian Peninsula, *Int J Biometeorol*, 58, 337–348, [https://doi.org/10.1007/s00484-012-](https://doi.org/10.1007/s00484-012-0629-4)
 1281 0629-4, 2014.
- 1282 Finlayson, C. and Carrión, J. S.: Rapid ecological turnover and its impact on Neanderthal and other
 1283 human populations, *Trends in Ecology & Evolution*, 22, 213–222,
 1284 <https://doi.org/10.1016/j.tree.2007.02.001>, 2007.
- 1285 Fletcher, W. J. and Sánchez Goñi, M. F.: Orbital- and sub-orbital-scale climate impacts on vegetation of
 1286 the western Mediterranean basin over the last 48,000 yr, *Quaternary Research*, 70, 451–464,
 1287 <https://doi.org/10.1016/j.yqres.2008.07.002>, 2008.
- 1288 Fletcher, W. J., Sánchez Goñi, M. F., Allen, J. R. M., Cheddadi, R., Combourieu-Nebout, N., Huntley, B.,
 1289 Lawson, I., Londeix, L., Magri, D., Margari, V., Müller, U. C., Naughton, F., Novenko, E., Roucoux, K., and
 1290 Tzedakis, P. C.: Millennial-scale variability during the last glacial in vegetation records from Europe,
 1291 *Quaternary Science Reviews*, 29, 2839–2864, <https://doi.org/10.1016/j.quascirev.2009.11.015>, 2010.
- 1292 Foerster, V., Asrat, A., Bronk Ramsey, C., Brown, E. T., Chapot, M. S., Deino, A., Duesing, W., Grove, M.,
 1293 Hahn, A., Junginger, A., Kaboth-Bahr, S., Lane, C. S., Opitz, S., Noren, A., Roberts, H. M., Stockhecke,
 1294 M., Tiedemann, R., Vidal, C. M., Vogelsang, R., Cohen, A. S., Lamb, H. F., Schaebitz, F., and Trauth, M.
 1295 H.: Pleistocene climate variability in eastern Africa influenced hominin evolution, *Nat Geosci*, 15, 805–
 1296 811, <https://doi.org/10.1038/s41561-022-01032-y>, 2022.
- 1297 Follieri, M., Magri, D., and Sadori, L.: A 250 000-years pollen record from Valle di Castiglione (Roma),
 1298 *Pollen et Spores*, 30, 329–356, 1988.
- 1299 Fontana, F., Nenzioni, G., and Peretto, C.: The southern Po plain area (Italy) in the mid-late Pleistocene:
 1300 Human occupation and technical behaviours, *Quaternary International*, 223, 465–471,
 1301 <https://doi.org/10.1016/j.quaint.2010.02.013>, 2010.
- 1302 Gouzy, A., Malaizé, B., Pujol, C., and Charlier, K.: Climatic “pause” during Termination II identified in
 1303 shallow and intermediate waters off the Iberian margin, *Quaternary Science Reviews*, 23, 1523–1528,
 1304 <https://doi.org/10.1016/j.quascirev.2004.03.002>, 2004.
- 1305 von Grafenstein, R., Zahn, R., and Tiedemann, R.: Planktonic $\delta^{18}O$ records at Sites 976 and 977,
 1306 Alboran Sea: stratigraphy, forcing, and paleoceanographic implications. In Curry, W.B., Shackleton,
 1307 N.J., and Richter, C, *Proceedings Ocean Drilling Program Scientific Results*, 154, 299–318, 1999.
- 1308 Guiot, J.: Methodology of the last climatic cycle reconstruction in France from pollen data,
 1309 *Palaeogeography, Palaeoclimatology, Palaeoecology*, 80, 49–69, [https://doi.org/10.1016/0031-](https://doi.org/10.1016/0031-0182(90)90033-4)
 1310 0182(90)90033-4, 1990.
- 1311 Guiot, J., Pons, A., De Beaulieu, J. L., and Reille, M.: A 140,000-year continental climate reconstruction
 1312 from two European pollen records, *Nature*, 338, 309–313, <https://doi.org/10.1038/338309a0>, 1989.
- 1313 Guiot, J., De Beaulieu, J. L., Cheddadi, R., David, F., Ponel, P., and Reille, M.: The climate in Western
 1314 Europe during the last Glacial/Interglacial cycle derived from pollen and insect remains,
 1315 *Palaeogeography, Palaeoclimatology, Palaeoecology*, 103, 73–93, [https://doi.org/10.1016/0031-](https://doi.org/10.1016/0031-0182(93)90053-L)
 1316 0182(93)90053-L, 1993.

- 1317 Heinrich, H.: Origin and Consequences of Cyclic Ice Rafting in the Northeast Atlantic Ocean During the
1318 Past 130,000 Years, *Quaternary Research*, 29, 142–152, [https://doi.org/10.1016/0033-5894\(88\)90057-9](https://doi.org/10.1016/0033-5894(88)90057-9), 1988.
- 1320 Held, F., Cheng, H., Edwards, R. L., Tüysüz, O., Koç, K., and Fleitmann, D.: Dansgaard-Oeschger cycles
1321 of the penultimate and last glacial period recorded in stalagmites from Türkiye, *Nat Commun*, 15, 1183,
1322 <https://doi.org/10.1038/s41467-024-45507-5>, 2024.
- 1323 Hemming, S. R.: Heinrich events: Massive late Pleistocene detritus layers of the North Atlantic and
1324 their global climate imprint, *Reviews of Geophysics*, 42, <https://doi.org/10.1029/2003RG000128>,
1325 2004.
- 1326 Hérissou, D., Brenet, M., Cliquet, D., Moncel, M.-H., Richter, J., Scott, B., Van Baelen, A., Di Modica, K.,
1327 Loecker, D., Ashton, N., Bourguignon, L., Delagnes, A., Faivre, J.-P., Folgado-Lopez, M., Locht, J.-L.,
1328 Pope, M., Raynal, J.-P., Roebroeks, W., Santagata, C., and Peer, P.: The emergence of the Middle
1329 Palaeolithic in north-western Europe and its southern fringes, *Quaternary International*, 411,
1330 <https://doi.org/10.1016/j.quaint.2016.02.049>, 2016.
- 1331 Hersbach, H., Bell, B., Berrisford, P., Hirahara, S., Horányi, A., Muñoz-Sabater, J., Nicolas, J., Peubey, C.,
1332 Radu, R., Schepers, D., Simmons, A., Soci, C., Abdalla, S., Abellan, X., Balsamo, G., Bechtold, P., Biavati,
1333 G., Bidlot, J., Bonavita, M., De Chiara, G., Dahlgren, P., Dee, D., Diamantakis, M., Dragani, R., Flemming,
1334 J., Forbes, R., Fuentes, M., Geer, A., Haimberger, L., Healy, S., Hogan, R. J., Hólm, E., Janisková, M.,
1335 Keeley, S., Laloyaux, P., Lopez, P., Lupu, C., Radnoti, G., de Rosnay, P., Rozum, I., Vamborg, F., Villaume,
1336 S., and Thépaut, J.-N.: The ERA5 global reanalysis, *Quarterly Journal of the Royal Meteorological
1337 Society*, 146, 1999–2049, <https://doi.org/10.1002/qj.3803>, 2020.
- 1338 Hodell, D. A., Channell, J. E. T., Curtis, J. H., Romero, O. E., and Röhl, U.: Onset of “Hudson Strait”
1339 Heinrich events in the eastern North Atlantic at the end of the middle Pleistocene transition (~640
1340 ka)?, *Paleoceanography*, 23, 2008PA001591, <https://doi.org/10.1029/2008PA001591>, 2008.
- 1341 Hodell, D. A., Crowhurst, S. J., Lourens, L., Margari, V., Nicolson, J., Rolfe, J. E., Skinner, L. C., Thomas,
1342 N. C., Tzedakis, P. C., Mleneck-Vautravers, M. J., and Wolff, E. W.: A 1.5-million-year record of orbital
1343 and millennial climate variability in the North Atlantic, *Clim. Past*, 19, 607–636,
1344 <https://doi.org/10.5194/cp-19-607-2023>, 2023.
- 1345 Hodge, E., Richards, D., Smart, P., Andreo, B., Hoffmann, D., Matthey, D., and González-Ramón, A.:
1346 Effective precipitation in southern Spain (~ 266 to 46 ka) based on a speleothem stable carbon isotope
1347 record, *Quaternary Research*, 69, 447–457, <https://doi.org/10.1016/j.yqres.2008.02.013>, 2008.
- 1348 Hublin, J. J.: The origin of Neandertals, *Proceedings of the National Academy of Sciences*, 106, 16022–
1349 16027, <https://doi.org/10.1073/pnas.0904119106>, 2009.
- 1350 Jiménez-Amat, P. and Zahn, R.: Offset timing of climate oscillations during the last two glacial-
1351 interglacial transitions connected with large-scale freshwater perturbation, *Paleoceanography*, 30,
1352 768–788, <https://doi.org/10.1002/2014PA002710>, 2015.
- 1353 Jiménez-Moreno, G., Anderson, R. S., Ramos-Román, M. J., Camuera, J., Mesa-Fernández, J. M., García-
1354 Alix, A., Jiménez-Espejo, F. J., Carrión, J. S., and López-Avilés, A.: The Holocene Cedrus pollen record
1355 from Sierra Nevada (S Spain), a proxy for climate change in N Africa, *Quaternary Science Reviews*, 242,
1356 106468, <https://doi.org/10.1016/j.quascirev.2020.106468>, 2020.

- 1357 Johnsen, S. J., Clausen, H. B., Dansgaard, W., Fuhrer, K., Gundestrup, N., Hammer, C. U., Iversen, P.,
1358 Jouzel, J., Stauffer, B., and Steffensen, J. P.: Irregular glacial interstadials recorded in a new Greenland
1359 record, *Nature*, 359, 311–313, 1992.
- 1360 Jouzel, J., Masson-Delmotte, V., Cattani, O., Dreyfus, G., Falourd, S., Hoffmann, G., Minster, B., Nouet,
1361 J., Barnola, J. M., Chappellaz, J., Fischer, H., Gallet, J. C., Johnsen, S., Leuenberger, M., Loulergue, L.,
1362 Luethi, D., Oerter, H., Parrenin, F., Raisbeck, G., Raynaud, D., Schilt, A., Schwander, J., Selmo, E.,
1363 Souchez, R., Spahni, R., Stauffer, B., Steffensen, J. P., Stenni, B., Stocker, T. F., Tison, J. L., Werner, M.,
1364 and Wolff, E. W.: Orbital and millennial Antarctic climate variability over the past 800,000 years,
1365 *Science*, 317, 793–796, <https://doi.org/10.1126/science.1141038>, 2007.
- 1366 Kallel, N., Duplessy, J.-C., Labeyrie, L., Fontugne, M., Paterne, M., and Montacer, M.: Mediterranean
1367 pluvial periods and sapropel formation over the last 200 000 years, *Palaeogeography,*
1368 *Palaeoclimatology, Palaeoecology*, 157, 45–58, [https://doi.org/10.1016/S0031-0182\(99\)00149-2](https://doi.org/10.1016/S0031-0182(99)00149-2),
1369 2000.
- 1370 Kelly, M., Edwards, R., Cheng, H., Yuan, D., Cai, Y., Zhang, M., Lin, Y., and An, Z.: High resolution
1371 characterization of the Asian Monsoon between 146,000 and 99,000 years B.P. from Dongge Cave,
1372 China and global correlation of events surrounding Termination II, *Palaeogeography,*
1373 *Palaeoclimatology, Palaeoecology*, 236, 20–38, <https://doi.org/10.1016/j.palaeo.2005.11.042>, 2006.
- 1374 Key, A. J. M., Jarić, I., and Roberts, D. L.: Modelling the end of the Acheulean at global and continental
1375 levels suggests widespread persistence into the Middle Palaeolithic, *Humanit Soc Sci Commun*, 8, 55,
1376 <https://doi.org/10.1057/s41599-021-00735-8>, 2021.
- 1377 Koltai, G., Spötl, C., Shen, C.-C., Wu, C.-C., Rao, Z., Palcsu, L., Kele, S., Surányi, G., and Bárányi-Kevei, I.:
1378 A penultimate glacial climate record from southern Hungary, *Journal of Quaternary Science*, 32, 946–
1379 956, <https://doi.org/10.1002/jqs.2968>, 2017.
- 1380 Koutsodendris, A., Dakos, V., Fletcher, W. J., Knipping, M., Kotthoff, U., Milner, A. M., Müller, U. C.,
1381 Kaboth-Bahr, S., Kern, O. A., Kolb, L., Vakhrameeva, P., Wulf, S., Christanis, K., Schmiedl, G., and Pross,
1382 J.: Atmospheric CO₂ forcing on Mediterranean biomes during the past 500 kyrs, *Nat Commun*, 14,
1383 1664, <https://doi.org/10.1038/s41467-023-37388-x>, 2023.
- 1384 Laskar, J., Robutel, P., Joutel, F., Gastineau, M., Correia, A. C. M., and Levrard, B.: A long-term numerical
1385 solution for the insolation quantities of the Earth, *A&A*, 428, 261–285, <https://doi.org/10.1051/0004-6361:20041335>, 2004.
- 1387 Lewis, S., Ashton, N., and Jacobi, R.: 9 - Testing Human Presence During the Last Interglacial (MIS 5e):
1388 A Review of the British Evidence, in: *Developments in Quaternary Sciences*, vol. 14, edited by: Ashton,
1389 N., Lewis, S. G., and Stringer, C., Elsevier, 125–164, <https://doi.org/10.1016/B978-0-444-53597-9.00009-1>, 2011.
- 1391 Li, T.-Y., Shen, C.-C., Huang, L.-J., Jiang, X.-Y., Yang, X.-L., Mii, H.-S., Lee, S.-Y., and Lo, L.: Stalagmite-
1392 inferred variability of the Asian summer monsoon during the penultimate glacial–interglacial period,
1393 *Climate of the Past*, 10, 1211–1219, <https://doi.org/10.5194/cp-10-1211-2014>, 2014.
- 1394 Lionello, P., Malanotte-Rizzoli, P., Boscolo, R., Alpert, P., Artale, V., Li, L., Luterbacher, J., May, W., Trigo,
1395 R., Tsimplis, M., Ulbrich, U., and Xoplaki, E.: The Mediterranean climate: An overview of the main
1396 characteristics and issues, in: *Developments in Earth and Environmental Sciences*, vol. 4, edited by:
1397 Lionello, P., Malanotte-Rizzoli, P., and Boscolo, R., Elsevier, 1–26, [https://doi.org/10.1016/S1571-9197\(06\)80003-0](https://doi.org/10.1016/S1571-9197(06)80003-0), 2006.

- 1399 Lisiecki, L. and Raymo, M.: Pliocene-Pleistocene stack of 57 globally distributed benthic $\delta^{18}\text{O}$ records.,
1400 *Paleoceanography*, 20, <https://doi.org/10.1029/2004PA001071>, 2005.
- 1401 Lisiecki, L. E. and Stern, J. V.: Regional and global benthic $\delta^{18}\text{O}$ stacks for the last glacial cycle,
1402 *Paleoceanography*, 31, 1368–1394, <https://doi.org/10.1002/2016PA003002>, 2016.
- 1403 Liu, J., Fang, N., Wang, F., Yang, F., and Ding, X.: Features of ice-rafted debris (IRD) at IODP site U1312
1404 and their palaeoenvironmental implications during the last 2.6 Myr, *Palaeogeography,*
1405 *Palaeoclimatology, Palaeoecology*, 511, 364–378, <https://doi.org/10.1016/j.palaeo.2018.09.002>,
1406 2018.
- 1407 de Lumley, M. A.: Les restes humains fossiles de la grotte du Lazaret. Généralités, approche
1408 démographique., in: *Les restes humains fossiles de la grotte du Lazaret, Nice, Alpes-Maritimes. Des*
1409 *Homo erectus européens évolués en voie de néandertalisation*, CNRS Editions, 217–220, 2018.
- 1410 Macklin, M. G., Fuller, I. C., Lewin, J., Maas, G. S., Passmore, D. G., Rose, J., Woodward, J. C., Black, S.,
1411 Hamlin, R. H. B., and Rowan, J. S.: Correlation of fluvial sequences in the Mediterranean basin over the
1412 last 200 ka and their relationship to climate change, *Quaternary Science Reviews*, 21, 1633–1641,
1413 [https://doi.org/10.1016/S0277-3791\(01\)00147-0](https://doi.org/10.1016/S0277-3791(01)00147-0), 2002.
- 1414 Magri, D. and Parra, I.: Late Quaternary western Mediterranean pollen records and African winds,
1415 *Earth and Planetary Science Letters*, 200, 401–408, [https://doi.org/10.1016/S0012-821X\(02\)00619-2](https://doi.org/10.1016/S0012-821X(02)00619-2),
1416 2002.
- 1417 Margari, V., Skinner, L. C., Tzedakis, P. C., Ganopolski, A., Vautravers, M., and Shackleton, N. J.: The
1418 nature of millennial-scale climate variability during the past two glacial periods, *Nature Geosci*, 3, 127–
1419 131, <https://doi.org/10.1038/ngeo740>, 2010.
- 1420 Margari, V., Skinner, L., Hodell, D., Martrat, B., Toucanne, S., Gibbard, P., Lunkka, J., and Tzedakis, C.:
1421 Land-ocean changes on orbital and millennial time scales and the penultimate glaciation, *Geology*,
1422 <https://doi.org/10.1130/G35070.1>, 2014.
- 1423 Martrat, B., Grimalt, J. O., Lopez-Martinez, C., Cacho, I., Sierro, F. J., Flores, J. A., Zahn, R., Canals, M.,
1424 Curtis, J. H., and Hodell, D. A.: Abrupt Temperature Changes in the Western Mediterranean over the
1425 Past 250,000 Years, *Science*, 306, 1762–1765, <https://doi.org/10.1126/science.1101706>, 2004.
- 1426 Martrat, B., Grimalt, J. O., Shackleton, N. J., de Abreu, L., Hutterli, M. A., and Stocker, T. F.: Four Climate
1427 Cycles of Recurring Deep and Surface Water Destabilizations on the Iberian Margin, *Science*, 317, 502–
1428 507, <https://doi.org/10.1126/science.1139994>, 2007.
- 1429 Martrat, B., Jimenez-Amat, P., Zahn, R., and Grimalt, J. O.: Similarities and dissimilarities between the
1430 last two deglaciations and interglaciations in the North Atlantic region, *Quaternary Science Reviews*,
1431 99, 122–134, <https://doi.org/10.1016/j.quascirev.2014.06.016>, 2014.
- 1432 Masson-Delmotte, V., Stenni, B., Pol, K., Braconnot, P., Cattani, O., Falourd, S., Kageyama, M., Jouzel,
1433 J., Landais, A., Minster, B., Barnola, J. M., Chappellaz, J., Krinner, G., Johnsen, S., Röthlisberger, R.,
1434 Hansen, J., Mikolajewicz, U., and Otto-Bliesner, B.: EPICA Dome C record of glacial and interglacial
1435 intensities, *Quaternary Science Reviews*, 29, 113–128,
1436 <https://doi.org/10.1016/j.quascirev.2009.09.030>, 2010.
- 1437 Mathias, C., Bourguignon, L., Brenet, M., Grégoire, S., and Moncel, M.-H.: Between new and inherited
1438 technical behaviours: a case study from the Early Middle Palaeolithic of Southern France, *Archaeol*
1439 *Anthropol Sci*, 12, 146, <https://doi.org/10.1007/s12520-020-01114-1>, 2020.

- 1440 Matthews, A., Affek, H. P., Ayalon, A., Vonhof, H. B., and Bar-Matthews, M.: Eastern Mediterranean
1441 climate change deduced from the Soreq Cave fluid inclusion stable isotopes and carbonate clumped
1442 isotopes record of the last 160 ka, *Quaternary Science Reviews*, 272, 107223,
1443 <https://doi.org/10.1016/j.quascirev.2021.107223>, 2021.
- 1444 McCarron, A. P., Bigg, G. R., Brooks, H., Leng, M. J., Marshall, J. D., Ponomareva, V., Portnyagin, M.,
1445 Reimer, P. J., and Rogerson, M.: Northwest Pacific ice-rafted debris at 38°N reveals episodic ice-sheet
1446 change in late Quaternary Northeast Siberia, *Earth and Planetary Science Letters*, 553, 116650,
1447 <https://doi.org/10.1016/j.epsl.2020.116650>, 2021.
- 1448 McManus, J. F., Oppo, D. W., and Cullen, J. L.: A 0.5-Million-Year Record of Millennial-Scale Climate
1449 Variability in the North Atlantic, *Science*, 283, 971–975,
1450 <https://doi.org/10.1126/science.283.5404.971>, 1999.
- 1451 Melchionna, M., Di Febbraro, M., Carotenuto, F., Rook, L., Mondanaro, A., Castiglione, S., Serio, C.,
1452 Vero, V. A., Tesone, G., Piccolo, M., Diniz-Filho, J. A. F., and Raia, P.: Fragmentation of Neanderthals'
1453 pre-extinction distribution by climate change, *Palaeogeography, Palaeoclimatology, Palaeoecology*,
1454 496, 146–154, <https://doi.org/10.1016/j.palaeo.2018.01.031>, 2018.
- 1455 Menviel, L., Capron, E., Govin, A., Dutton, A., Tarasov, L., Abe-Ouchi, A., Drysdale, R. N., Gibbard, P. L.,
1456 Gregoire, L., He, F., Ivanovic, R. F., Kageyama, M., Kawamura, K., Landais, A., Otto-Bliesner, B. L., Oyabu,
1457 I., Tzedakis, P. C., Wolff, E., and Zhang, X.: The penultimate deglaciation: protocol for Paleoclimate
1458 Modelling Intercomparison Project (PMIP) phase 4 transient numerical simulations between 140 and
1459 127 ka, version 1.0, *Geoscientific Model Development*, 12, 3649–3685,
1460 <https://doi.org/10.5194/gmd-12-3649-2019>, 2019.
- 1461 Michel, V., Shen, G., Shen, C.-C., Duval, M., Woodhead, J., Chou, Y.-M., Hu, H.-M., Wu, C.-C., Kan, Y.-C.,
1462 Yang, H., Yu, T.-L., Gallet, S., and Valensi, P.: Datations radioisotopiques (U-Th, U-Pb) et
1463 paléodosimétriques (ESR) des plus anciens sites préhistoriques des Alpes-Maritimes: la grotte du
1464 Vallonnet, le site de plein air de Terra Amata et la grotte du Lazaret, in: *Bulletin du Musée*
1465 *d'Anthropologie préhistorique de Monaco*, vol. 61, 65–80, 2022.
- 1466 Moncel, M., Vaissié, E., Marin, J., Fernandes, P., Abrunhosa, A., Hardy, B., Richard, M., Torres, C., and
1467 Baena, J.: Early Middle Palaeolithic Occupations Dated to MIS 7 at the Abri du Maras (Ardèche,
1468 Southeast France), *Journal of Paleolithic Archaeology*, 2025.
- 1469 Moncel, M.-H., Ashton, N., Arzarello, M., Fontana, F., Lamotte, A., Scott, B., Muttillio, B., Berruti, G.,
1470 Nenzioni, G., Tuffreau, A., and Peretto, C.: Early Levallois core technology between Marine Isotope
1471 Stage 12 and 9 in Western Europe, *Journal of Human Evolution*, 139, 102735,
1472 <https://doi.org/10.1016/j.jhevol.2019.102735>, 2020.
- 1473 Moseley, G. E., Spötl, C., Cheng, H., Boch, R., Min, A., and Edwards, R. L.: Termination-II
1474 interstadial/stadial climate change recorded in two stalagmites from the north European Alps,
1475 *Quaternary Science Reviews*, 127, 229–239, <https://doi.org/10.1016/j.quascirev.2015.07.012>, 2015.
- 1476 Mudie, P.: Pollen distribution in recent marine sediments, eastern Canada, *Canadian Journal of Earth*
1477 *Sciences*, 19, 729–747, <https://doi.org/10.1139/e82-062>, 2011.
- 1478 Murat, A. (Ed.): Chapitre 41 : Pliocene–pleistocene occurrence of sapropels in the western
1479 mediterranean sea and their relation to eastern mediterranean sapropels, in: *Proceedings of the*
1480 *Ocean Drilling Program*, 161 *Scientific Results*, vol. 161, *Ocean Drilling Program*,
1481 <https://doi.org/10.2973/odp.proc.sr.161.1999>, 1999.

- 1482 Nehme, C., Verheyden, S., Breitenbach, S. F. M., Gillikin, D. P., Verheyden, A., Cheng, H., Edwards, R.
 1483 L., Hellstrom, J., Noble, S. R., Farrant, A. R., Sahy, D., Goovaerts, T., Salem, G., and Claeys, P.: Climate
 1484 dynamics during the penultimate glacial period recorded in a speleothem from Kanaan Cave, Lebanon
 1485 (central Levant), *Quaternary Research*, 90, 10–25, <https://doi.org/10.1017/qua.2018.18>, 2018.
- 1486 Nehme, C., Kluge, T., Verheyden, S., Nader, F., Charalambidou, I., Weissbach, T., Gucel, S., Cheng, H.,
 1487 Edwards, R. L., Satterfield, L., Eiche, E., and Claeys, P.: Speleothem record from Pentadactylos cave
 1488 (Cyprus): new insights into climatic variations during MIS 6 and MIS 5 in the Eastern Mediterranean,
 1489 *Quaternary Science Reviews*, 250, 106663, <https://doi.org/10.1016/j.quascirev.2020.106663>, 2020.
- 1490 Obrochta, S. P., Crowley, T. J., Channell, J. E. T., Hodell, D. A., Baker, P. A., Seki, A., and Yokoyama, Y.:
 1491 Climate variability and ice-sheet dynamics during the last three glaciations, *Earth and Planetary Science*
 1492 *Letters*, 406, 198–212, <https://doi.org/10.1016/j.epsl.2014.09.004>, 2014.
- 1493 Ochando, J., Carrión, J. S., Blasco, R., Fernández, S., Amorós, G., Munuera, M., Sañudo, P., and
 1494 Fernández Peris, J.: Silvicolous Neanderthals in the far West: the mid-Pleistocene palaeoecological
 1495 sequence of Bolomor Cave (Valencia, Spain), *Quaternary Science Reviews*, 217, 247–267,
 1496 <https://doi.org/10.1016/j.quascirev.2019.03.015>, 2019.
- 1497 Okuda, M., Yasuda, Y., and Setoguchi, T.: Middle to Late Pleistocene vegetation history and climatic
 1498 changes at Lake Kopais, Southeast Greece, *Boreas*, 30, 73–82, <https://doi.org/10.1111/j.1502-3885.2001.tb00990.x>, 2001.
- 1500 Oppo, D. W., Keigwin, L. D., McManus, J. F., and Cullen, J. L.: Persistent suborbital climate variability in
 1501 marine isotope stage 5 and termination II, *Paleoceanography*, 16, 280–292,
 1502 <https://doi.org/10.1029/2000PA000527>, 2001.
- 1503 Oppo, D. W., McManus, J. F., and Cullen, J. L.: Evolution and demise of the Last Interglacial warmth in
 1504 the subpolar North Atlantic, *Quaternary Science Reviews*, 25, 3268–3277,
 1505 <https://doi.org/10.1016/j.quascirev.2006.07.006>, 2006.
- 1506 Ovsepyan, E. A. and Murdmaa, I. O.: Response of the bering sea to Heinrich Event 11, *Lithol Miner*
 1507 *Resour*, 52, 442–446, <https://doi.org/10.1134/S0024490217060062>, 2017.
- 1508 Panera, J., Torres, T., Pérez-González, A., Ortiz, J. E., Rubio-Jara, S., and Val, D. U. del: Geocronología
 1509 de la Terraza Compleja de Arganda en el valle del río Jarama (Madrid, España), *Estudios Geológicos*,
 1510 67, 495–504, <https://doi.org/10.3989/egeol.40550.204>, 2011.
- 1511 Panera, J., Rubio-Jara, S., Yravedra, J., Blain, H.-A., Sesé, C., and Pérez-González, A.: Manzanares Valley
 1512 (Madrid, Spain): A good country for Proboscideans and Neanderthals, *Quaternary International*, 326–
 1513 327, 329–343, <https://doi.org/10.1016/j.quaint.2013.09.009>, 2014.
- 1514 Penaud, A., Eynaud, F., Turon, J. L., Zaragosi, S., Malaizé, B., Toucanne, S., and Bourillet, J. F.: What
 1515 forced the collapse of European ice sheets during the last two glacial periods (150 ka B.P. and 18 ka
 1516 cal B.P.)? Palynological evidence, *Palaeogeography, Palaeoclimatology, Palaeoecology*, 281, 66–78,
 1517 <https://doi.org/10.1016/j.palaeo.2009.07.012>, 2009.
- 1518 Penaud, A., Eynaud, F., Voelker, A. H. L., and Turon, J.-L.: Palaeohydrological changes over the last 50
 1519 ky in the central Gulf of Cadiz: complex forcing mechanisms mixing multi-scale processes,
 1520 *Biogeosciences*, 13, 5357–5377, <https://doi.org/10.5194/bg-13-5357-2016>, 2016.
- 1521 Pereira, T., Cunha, P. P., Martins, A. A., Nora, D., Paixão, E., Figueiredo, O., Raposo, L., Henriques, F.,
 1522 Caninas, J., Moura, D., and Bridgland, D. R.: Geoarchaeology of the Cobrinhos site (Vila Velha de Ródão,

- 1523 Portugal) - a record of the earliest Mousterian in western Iberia, *Journal of Archaeological Science: Reports*, 24, 640–654, <https://doi.org/10.1016/j.jasrep.2018.11.026>, 2019.
- 1525 Pérez-Asensio, J. N., Frigola, J., Pena, L. D., Sierro, F. J., Reguera, M. I., Rodríguez-Tovar, F. J., Dorador, J., Asioli, A., Kuhlmann, J., Huhn, K., and Cacho, I.: Changes in western Mediterranean thermohaline circulation in association with a deglacial Organic Rich Layer formation in the Alboran Sea, *Quaternary Science Reviews*, 228, 106075, <https://doi.org/10.1016/j.quascirev.2019.106075>, 2020.
- 1529 Peyrégne, S., Slon, V., Mafessoni, F., de Filippo, C., Hajdinjak, M., Nagel, S., Nickel, B., Essel, E., Le Cabec, A., Wehrberger, K., Conard, N. J., Kind, C. J., Posth, C., Krause, J., Abrams, G., Bonjean, D., Di Modica, K., Toussaint, M., Kelso, J., Meyer, M., Pääbo, S., and Prüfer, K.: Nuclear DNA from two early Neandertals reveals 80,000 years of genetic continuity in Europe, *Science Advances*, 5, eaaw5873, <https://doi.org/10.1126/sciadv.aaw5873>, 2019.
- 1534 Pini, R., Ravazzi, C., and Donegana, M.: Pollen stratigraphy, vegetation and climate history of the last 215 ka in the Azzano Decimo core (plain of Friuli, north-eastern Italy), *Quaternary Science Reviews*, 28, 1268–1290, <https://doi.org/10.1016/j.quascirev.2008.12.017>, 2009.
- 1537 Prasad, A. M., Iverson, L. R., and Liaw, A.: Newer Classification and Regression Tree Techniques: Bagging and Random Forests for Ecological Prediction, *Ecosystems*, 9, 181–199, <https://doi.org/10.1007/s10021-005-0054-1>, 2006.
- 1540 Quézel, P.: *Réflexions sur l'évolution de la flore et de la végétation au Maghreb Méditerranéen*, Ibis Press., Paris, 117 pp., 2000.
- 1542 Raia, P., Mondanaro, A., Melchionna, M., Di Febbraro, M., Diniz-Filho, J. A., Rangel, T., Holden, P., Carotenuto, F., Edwards, N., Lima-Ribeiro, M., Profico, A., Maiorano, L., Castiglione, S., Serio, C., and Rook, L.: Past Extinctions of Homo Species Coincided with Increased Vulnerability to Climatic Change, *One Earth*, 3, 480–490, <https://doi.org/10.1016/j.oneear.2020.09.007>, 2020.
- 1546 Railsback, L. B., Gibbard, P. L., Head, M. J., Voarintsoa, N. R. G., and Toucanne, S.: An optimized scheme of lettered marine isotope substages for the last 1.0 million years, and the climatostratigraphic nature of isotope stages and substages, *Quaternary Science Reviews*, 111, 94–106, <https://doi.org/10.1016/j.quascirev.2015.01.012>, 2015.
- 1550 Rasmussen, S. O., Bigler, M., Blockley, S. P., Blunier, T., Buchardt, S. L., Clausen, H. B., Cvijanovic, I., Dahl-Jensen, D., Johnsen, S. J., Fischer, H., Gkinis, V., Guillevic, M., Hoek, W. Z., Lowe, J. J., Pedro, J. B., Popp, T., Seierstad, I. K., Steffensen, J. P., Svensson, A. M., Vallelonga, P., Vinther, B. M., Walker, M. J. C., Wheatley, J. J., and Winstrup, M.: A stratigraphic framework for abrupt climatic changes during the Last Glacial period based on three synchronized Greenland ice-core records: refining and extending the INTIMATE event stratigraphy, *Quaternary Science Reviews*, 106, 14–28, <https://doi.org/10.1016/j.quascirev.2014.09.007>, 2014.
- 1557 Rasmussen, T. L., Oppo, D. W., Thomsen, E., and Lehman, S. J.: Deep sea records from the southeast Labrador Sea: Ocean circulation changes and ice-rafting events during the last 160,000 years, *Paleoceanography*, 18, <https://doi.org/10.1029/2001PA000736>, 2003.
- 1560 Regattieri, E., Zanchetta, G., Drysdale, R. N., Isola, I., Hellstrom, J. C., and Roncioni, A.: A continuous stable isotope record from the penultimate glacial maximum to the Last Interglacial (159–121 ka) from Tana Che Urla Cave (Apuan Alps, central Italy), *Quaternary Research*, 82, 450, 2014.

- 1563 Renault, L., Oguz, T., Pascual, A., Vizoso, G., and Tintore, J.: Surface circulation in the Alborán Sea
 1564 (western Mediterranean) inferred from remotely sensed data, *J. Geophys. Res.*, 117, 2011JC007659,
 1565 <https://doi.org/10.1029/2011JC007659>, 2012.
- 1566 Rios-Garaizar, J.: Early Middle Palaeolithic occupations at Ventalaperra cave (Cantabrian Region,
 1567 Northern Iberian Peninsula), *Journal of Lithic Studies*, 3, <https://doi.org/10.2218/jls.v3i1.1287>, 2016.
- 1568 Robles, M., Peyron, O., Ménot, G., Brugiapaglia, E., Wulf, S., Appelt, O., Blache, M., Vannièrè, B.,
 1569 Dugerdil, L., Paura, B., Ansanay-Alex, S., Cromartie, A., Charlet, L., Guédron, S., De Beaulieu, J.-L., and
 1570 Joannin, S.: Climate changes during the Lateglacial in South Europe: new insights based on pollen and
 1571 brGDGTs of Lake Matese in Italy, <https://doi.org/10.5194/cp-2022-54>, 2022.
- 1572 Robles, M., Peyron, O., Ménot, G., Elisabetta, B., Wulf, S., Appelt, O., Blache, M., Vannièrè, B., Dugerdil,
 1573 L., Paura, B., Ansanay-Alex, S., Cromartie, A., Charlet, L., Guedron, S., de Beaulieu, jacques-L., and
 1574 Joannin, S.: Climate changes during the Late Glacial in southern Europe: new insights based on pollen
 1575 and brGDGTs of Lake Matese in Italy, 19, 493–515, <https://doi.org/10.5194/cp-19-493-2023>, 2023.
- 1576 Rogerson, M., Cacho, I., Jimenez-Espejo, F., Reguera, M. I., Sierro, F. J., Martinez-Ruiz, F., Frigola, J.,
 1577 and Canals, M.: A dynamic explanation for the origin of the western Mediterranean organic-rich layers,
 1578 *Geochemistry, Geophysics, Geosystems*, 9, <https://doi.org/10.1029/2007GC001936>, 2008.
- 1579 Rohling, E. J., Marino, G., and Grant, K. M.: Mediterranean climate and oceanography, and the periodic
 1580 development of anoxic events (sapropels), *Earth-Science Reviews*, 143, 62–97,
 1581 <https://doi.org/10.1016/j.earscirev.2015.01.008>, 2015.
- 1582 Rohling, E. J., Hibbert, F. D., Williams, F. H., Grant, K. M., Marino, G., Foster, G. L., Hennekam, R., de
 1583 Lange, G. J., Roberts, A. P., Yu, J., Webster, J. M., and Yokoyama, Y.: Differences between the last two
 1584 glacial maxima and implications for ice-sheet, $\delta^{18}O$, and sea-level reconstructions, *Quaternary Science*
 1585 *Reviews*, 176, 1–28, <https://doi.org/10.1016/j.quascirev.2017.09.009>, 2017.
- 1586 Rojo, J., Orlandi, F., Pérez-Badia, R., Aguilera, F., Ben Dhiab, A., Bouziane, H., Díaz de la Guardia, C.,
 1587 Galán, C., Gutiérrez-Bustillo, A. M., Moreno-Grau, S., Msallem, M., Trigo, M. M., and Fornaciari, M.:
 1588 Modeling olive pollen intensity in the Mediterranean region through analysis of emission sources,
 1589 *Science of The Total Environment*, 551–552, 73–82, <https://doi.org/10.1016/j.scitotenv.2016.01.193>,
 1590 2016.
- 1591 Roucoux, K. H., de Abreu, L., Shackleton, N. J., and Tzedakis, P. C.: The response of NW Iberian
 1592 vegetation to North Atlantic climate oscillations during the last 65kyr, *Quaternary Science Reviews*, 24,
 1593 1637–1653, <https://doi.org/10.1016/j.quascirev.2004.08.022>, 2005.
- 1594 Roucoux, K. H., Tzedakis, P. C., Lawson, I. T., and Margari, V.: Vegetation history of the penultimate
 1595 glacial period (Marine isotope stage 6) at Ioannina, north-west Greece, *Journal of Quaternary Science*,
 1596 26, 616–626, <https://doi.org/10.1002/jqs.1483>, 2011.
- 1597 Rousseau, D.-D., Antoine, P., Boers, N., Lagroix, F., Ghil, M., Lomax, J., Fuchs, M., Debret, M., Christine,
 1598 H., Moine, O., Gauthier, C., Jordanova, D., and Jordanova, N.: Dansgaard-Oeschger-like events of the
 1599 penultimate climate cycle: the loess point of view, *Climate of the Past*, 16, 713–727,
 1600 <https://doi.org/10.5194/cp-16-713-2020>, 2020.
- 1601 Rubio-Jara, S. and Panera, J.: Unravelling an essential archive for the European Pleistocene. The human
 1602 occupation in the Manzanares valley (Madrid, Spain) throughout nearly 800,000 years, *Quaternary*
 1603 *International*, 520, 5–22, <https://doi.org/10.1016/j.quaint.2018.08.007>, 2019.

- 1604 Rubio-Jara, S., Panera, J., Rodríguez-de-Tembleque, J., Santonja, M., and Pérez-González, A.: Large
1605 flake Acheulean in the middle of Tagus basin (Spain): Middle stretch of the river Tagus valley and lower
1606 stretches of the rivers Jarama and Manzanares valleys, *Quaternary International*, 411, 349–366,
1607 <https://doi.org/10.1016/j.quaint.2015.12.023>, 2016.
- 1608 Ruddiman, W. F.: Late Quaternary deposition of ice-rafted sand in the subpolar North Atlantic (lat 40°
1609 to 65°N), *Geol Soc America Bull*, 88, 1813, [https://doi.org/10.1130/0016-7606\(1977\)88<1813:LQDOIS>2.0.CO;2](https://doi.org/10.1130/0016-7606(1977)88<1813:LQDOIS>2.0.CO;2), 1977.
- 1611 Sadori, L., Koutsodendris, A., Panagiotopoulos, K., Masi, A., Bertini, A., Combourieu-Nebout, N.,
1612 Francke, A., Kouli, K., Joannin, S., Mercuri, A. M., Peyron, O., Torri, P., Wagner, B., Zanchetta, G.,
1613 Sinopoli, G., and Donders, T. H.: Pollen-based paleoenvironmental and paleoclimatic change at Lake
1614 Ohrid (south-eastern Europe) during the past 500 ka, *Biogeosciences*, 13, 1423–1437,
1615 <https://doi.org/10.5194/bg-13-1423-2016>, 2016.
- 1616 Salonen, J. S., Korpela, M., Williams, J. W., and Luoto, M.: Machine-learning based reconstructions of
1617 primary and secondary climate variables from North American and European fossil pollen data, *Sci*
1618 *Rep*, 9, 15805, <https://doi.org/10.1038/s41598-019-52293-4>, 2019.
- 1619 Sánchez Goñi, M.: The climatic and environmental context of the Late Pleistocene, in: *Updating*
1620 *Neanderthals. Understanding Behavioural Complexity in the Late Middle Palaeolithic.*,
1621 Elsevier/Academic Press, London, 165–169, <https://doi.org/10.1016/B978-0-12-823498-3.00012-1>,
1622 2022.
- 1623 Sánchez Goñi, M. F.: Millennial-scale variability during the last glacial in vegetation records from
1624 Europe, *Quaternary Science Reviews*, 2010.
- 1625 Sánchez Goñi, M. S., I, C., J, T., J, G., F, S., J, P., J, G., and N, S.: Synchronicity between marine and
1626 terrestrial responses to millennial scale climatic variability during the last glacial period in the
1627 Mediterranean region, *Climate Dynamics*, 19, 95, 2002.
- 1628 Sánchez-Laulhé, J. M., Jansa, A., and Jiménez, C.: Alboran Sea Area Climate and Weather, in: *Alboran*
1629 *Sea - Ecosystems and Marine Resources*, edited by: Báez, J. C., Vázquez, J.-T., Camiñas, J. A., and
1630 Malouli Idrissi, M., Springer International Publishing, Cham, 31–83, https://doi.org/10.1007/978-3-030-65516-7_3, 2021.
- 1632 Sánchez-Yustos, P.: El paleolítico antiguo en la cuenca del Duero. Instrumentos teóricos para la
1633 construcción de un modelo interpretativo de arqueología económica, 2009.
- 1634 Sánchez-Yustos, P. and Diez-Martín, F.: Dancing to the rhythms of the Pleistocene? Early Middle
1635 Paleolithic population dynamics in NW Iberia (Duero Basin and Cantabrian Region), *Quaternary Science*
1636 *Reviews*, 121, <https://doi.org/10.1016/j.quascirev.2015.05.005>, 2015.
- 1637 Santonja, M., Pérez-González, A., Panera, J., Rubio-Jara, S., and Méndez-Quintas, E.: The coexistence
1638 of Acheulean and Ancient Middle Palaeolithic techno-complexes in the Middle Pleistocene of the
1639 Iberian Peninsula, *Quaternary International*, 411, 367–377,
1640 <https://doi.org/10.1016/j.quaint.2015.04.056>, 2016.
- 1641 Santonja, M., Pérez-González, A., Baena, J., Panera, J., Méndez-Quintas, E., Uribelarrea, D., Demuro,
1642 M., Arnold, L., Abrunhosa, A., and Rubio-Jara, S.: The Acheulean of the Upper Guadiana River Basin
1643 (Central Spain). Morphostratigraphic Context and Chronology, *Front. Earth Sci.*, 10,
1644 <https://doi.org/10.3389/feart.2022.912007>, 2022.

- 1645 Sassoon, D., Lebreton, V., Combourieu-Nebout, N., Peyron, O., and Moncel, M.-H.:
 1646 Palaeoenvironmental changes in the southwestern Mediterranean (ODP site 976, Alboran sea) during
 1647 the MIS 12/11 transition and the MIS 11 interglacial and implications for hominin populations,
 1648 *Quaternary Science Reviews*, 304, 108010, <https://doi.org/10.1016/j.quascirev.2023.108010>, 2023.
- 1649 Sassoon, D., Combourieu-Nebout, N., Peyron, O., Bertini, A., Toti, F., Lebreton, V., and Moncel, M.-H.:
 1650 Pollen-based climatic reconstructions for the interglacial analogues of MIS 1 (MIS 19, 11, and 5) in the
 1651 southwestern Mediterranean: insights from ODP Site 976, *Clim. Past*, 21, 489–515,
 1652 <https://doi.org/10.5194/cp-21-489-2025>, 2025.
- 1653 Savannah, M., Eelco, R., Timme, D., Katharine, G., Jörg, K., Gianluca, M., Francesca, S., Francesca, C.,
 1654 Caterina, M., Anna, S., and Alessandra, N.: The “glacial” sapropel S6 (172 ka; MIS 6): A multiproxy
 1655 approach to solve a Mediterranean “cold case,” *Palaeogeography, Palaeoclimatology, Palaeoecology*,
 1656 650, 112384, <https://doi.org/10.1016/j.palaeo.2024.112384>, 2024.
- 1657 Scott, B.: *Becoming Neanderthals: the earlier British middle palaeolithic*, Oxbow books, Oxford, 2011.
- 1658 Shackleton, N. J.: Oxygen isotopes, ice volume and sea level, *Quaternary Science Reviews*, 6, 183–190,
 1659 [https://doi.org/10.1016/0277-3791\(87\)90003-5](https://doi.org/10.1016/0277-3791(87)90003-5), 1987.
- 1660 Shackleton, N. J., Hall, M. A., and Vincent, E.: Phase relationships between millennial-scale events
 1661 64,000–24,000 years ago, *Paleoceanography*, 15, 565–569, <https://doi.org/10.1029/2000PA000513>,
 1662 2000.
- 1663 Shackleton, N. J., Sánchez-Goñi, M. F., Pailler, D., and Lancelot, Y.: Marine Isotope Substage 5e and the
 1664 Eemian Interglacial, *Global and Planetary Change*, 36, 151–155, [https://doi.org/10.1016/S0921-8181\(02\)00181-9](https://doi.org/10.1016/S0921-8181(02)00181-9), 2003.
- 1666 Shackleton, N. J., Fairbanks, R. G., Chiu, T., and Parrenin, F.: Absolute calibration of the Greenland time
 1667 scale: implications for Antarctic time scales and for $\Delta 14C$, *Quaternary Science Reviews*, 23, 1513–1522,
 1668 <https://doi.org/10.1016/j.quascirev.2004.03.006>, 2004.
- 1669 Shaw, A., Bates, M., Conneller, C., Gamble, C., Julien, M.-A., McNabb, J., Pope, M., and Scott, B.: The
 1670 archaeology of persistent places: the Palaeolithic case of La Cotte de St Brelade, Jersey, *Antiquity*, 90,
 1671 1437–1453, <https://doi.org/10.15184/aqy.2016.212>, 2016.
- 1672 Shin, J., Nehrbass-Ahles, C., Grilli, R., Chowdhry Beeman, J., Parrenin, F., Teste, G., Landais, A.,
 1673 Schmidely, L., Silva, L., Schmitt, J., Bereiter, B., Stocker, T. F., Fischer, H., and Chappellaz, J.: Millennial-
 1674 scale atmospheric CO₂ variations during the Marine Isotope Stage 6 period (190–135 ka),
 1675 *Climate of the Past*, 16, 2203–2219, <https://doi.org/10.5194/cp-16-2203-2020>, 2020.
- 1676 Sierro, F. J. and Andersen, N.: An exceptional record of millennial-scale climate variability in the
 1677 southern Iberian Margin during MIS 6: Impact on the formation of sapropel S6, *Quaternary Science*
 1678 *Reviews*, 286, 107527, <https://doi.org/10.1016/j.quascirev.2022.107527>, 2022.
- 1679 Sierro, F. J., Hodell, D. A., Andersen, N., Azibeiro, L. A., Jimenez-Espejo, F. J., Bahr, A., Flores, J. A., Ausin,
 1680 B., Rogerson, M., Lozano-Luz, R., Lebreiro, S. M., and Hernandez-Molina, F. J.: Mediterranean Overflow
 1681 Over the Last 250 kyr: Freshwater Forcing From the Tropics to the Ice Sheets, *Paleoceanography and*
 1682 *Paleoclimatology*, 35, e2020PA003931, <https://doi.org/10.1029/2020PA003931>, 2020.
- 1683 Silva, P. G., López-Recio, M., Tapias, F., Roquero, E., Morín, J., Rus, I., Carrasco-García, P., Giner-Robles,
 1684 J. L., Rodríguez-Pascua, M. A., and Pérez-López, R.: Stratigraphy of the Arriaga Palaeolithic sites.
 1685 Implications for the geomorphological evolution recorded by thickened fluvial sequences within the

- 1686 Manzanares River valley (Madrid Neogene Basin, Central Spain), *Geomorphology*, 196, 138–161,
1687 <https://doi.org/10.1016/j.geomorph.2012.10.019>, 2013.
- 1688 Sinopoli, G., Peyron, O., Masi, A., Holtvoeth, J., Francke, A., Wagner, B., and Sadori, L.: Pollen-based
1689 temperature and precipitation changes in the Ohrid Basin (western Balkans) between 160 and 70 ka,
1690 *Climate of the Past*, 15, 53–71, <https://doi.org/10.5194/cp-15-53-2019>, 2019.
- 1691 Skinner, L. C. and Shackleton, N. J.: Deconstructing Terminations I and II: revisiting the glacioeustatic
1692 paradigm based on deep-water temperature estimates, *Quaternary Science Reviews*, 25, 3312–3321,
1693 <https://doi.org/10.1016/j.quascirev.2006.07.005>, 2006a.
- 1694 Skinner, L. C. and Shackleton, N. J.: Deconstructing Terminations I and II: revisiting the glacioeustatic
1695 paradigm based on deep-water temperature estimates, *Quaternary Science Reviews*, 25, 3312–3321,
1696 <https://doi.org/10.1016/j.quascirev.2006.07.005>, 2006b.
- 1697 Stocker, T. F.: The Seesaw Effect, *Science*, 282, 61–62, <https://doi.org/10.1126/science.282.5386.61>,
1698 1998.
- 1699 Sumner, G., Homar, V., and Ramis, C.: Precipitation seasonality in eastern and southern coastal Spain,
1700 *Intl Journal of Climatology*, 21, 219–247, <https://doi.org/10.1002/joc.600>, 2001.
- 1701 Svendsen, J. I., Alexanderson, H., Astakhov, V. I., Demidov, I., Dowdeswell, J. A., Funder, S., Gataullin,
1702 V., Henriksen, M., Hjort, C., Houmark-Nielsen, M., Hubberten, H. W., Ingólfsson, Ó., Jakobsson, M.,
1703 Kjær, K. H., Larsen, E., Lokrantz, H., Lunkka, J. P., Lyså, A., Mangerud, J., Matiouchkov, A., Murray, A.,
1704 Möller, P., Niessen, F., Nikolskaya, O., Polyak, L., Saarnisto, M., Siegert, C., Siegert, M. J., Spielhagen, R.
1705 F., and Stein, R.: Late Quaternary ice sheet history of northern Eurasia, *Quaternary Science Reviews*,
1706 23, 1229–1271, <https://doi.org/10.1016/j.quascirev.2003.12.008>, 2004.
- 1707 Terradillos-Bernal, M., Demuro, M., Arnold, L. J., Jordá-Pardo, J. F., Clemente-Conte, I., Benito-Calvo,
1708 A., and Díez Fernández-Lomana, J. C.: San Quirce (Palencia, Spain): new chronologies for the Lower to
1709 Middle Palaeolithic transition of south-west Europe, *Journal of Quaternary Science*, 38, 21–37,
1710 <https://doi.org/10.1002/jqs.3460>, 2023.
- 1711 Thabet, A. A., Maas, A. E., Lawson, G. L., and Tarrant, A. M.: Life cycle and early development of the
1712 thecosomatous pteropod *Limacina retroversa* in the Gulf of Maine, including the effect of elevated
1713 CO₂ levels, *Mar Biol*, 162, 2235–2249, <https://doi.org/10.1007/s00227-015-2754-1>, 2015.
- 1714 Torres, C., Tapias, F., Demuro, M., Arnold, L., Arriolabengoa, M., Pérez, S., and Preysler, J.: The
1715 Acheulian site of Cantera Vieja (Madrid, Spain) and the Lower to Middle Palaeolithic transition in
1716 central Spain, <https://doi.org/10.21203/rs.3.rs-4195503/v1>, 2024.
- 1717 Toucanne, S., Zaragosi, S., Bourillet, J. F., Cremer, M., Eynaud, F., Van Vliet-Lanoë, B., Penaud, A.,
1718 Fontanier, C., Turon, J. L., Cortijo, E., and Gibbard, P. L.: Timing of massive ‘Fleuve Manche’ discharges
1719 over the last 350 kyr: insights into the European ice-sheet oscillations and the European drainage
1720 network from MIS 10 to 2, *Quaternary Science Reviews*, 28, 1238–1256,
1721 <https://doi.org/10.1016/j.quascirev.2009.01.006>, 2009.
- 1722 Tzedakis, P. C.: Long-term tree populations in northwest Greece through multiple Quaternary climatic
1723 cycles, *Nature*, 364, 437–440, <https://doi.org/10.1038/364437a0>, 1993.
- 1724 Tzedakis, P. C.: Towards an understanding of the response of southern European vegetation to orbital
1725 and suborbital climate variability, *Quaternary Science Reviews*, 24, 1585–1599,
1726 <https://doi.org/10.1016/j.quascirev.2004.11.012>, 2005.

- 1727 Tzedakis, P. C., Frogley, M. R., Lawson, I. T., Preece, R. C., Cacho, I., and de Abreu, L.: Ecological
1728 thresholds and patterns of millennial-scale climate variability: The response of vegetation in Greece
1729 during the last glacial period, *Geology*, 32, 109, <https://doi.org/10.1130/G20118.1>, 2004.
- 1730 Tzedakis, P. C., Hooghiemstra, H., and Pälike, H.: The last 1.35 million years at Tenaghi Philippon:
1731 revised chronostratigraphy and long-term vegetation trends, *Quaternary Science Reviews*, 25, 3416–
1732 3430, <https://doi.org/10.1016/j.quascirev.2006.09.002>, 2006.
- 1733 Tzedakis, P. C., Drysdale, R. N., Margari, V., Skinner, L. C., Menviel, L., Rhodes, R. H., Taschetto, A. S.,
1734 Hodell, D. A., Crowhurst, S. J., Hellstrom, J. C., Fallick, A. E., Grimalt, J. O., McManus, J. F., Martrat, B.,
1735 Mokeddem, Z., Parrenin, F., Regattieri, E., Roe, K., and Zanchetta, G.: Enhanced climate instability in
1736 the North Atlantic and southern Europe during the Last Interglacial, *Nat Commun*, 9, 4235,
1737 <https://doi.org/10.1038/s41467-018-06683-3>, 2018.
- 1738 Valensi, P., Aouraghe, H., Bailon, S., Cauche, D., Combiér, J., Desclaux, E., Gagnepain, J., Gaillard, C.,
1739 Khatib, S., Lumley, H., Moigne, A.-M., Moncel, M.-H., and Notter, O.: Les peuplements préhistoriques
1740 dans le sud-est de la France à la fin du Pléistocène moyen : 400 - 120 000 ans. *Terra Amata*, Orgnac 3,
1741 Baume Bonne, Lazaret. Cadre géochronologique et biostratigraphique, paléoenvironnements et
1742 évolution culturelle des derniers anténéandertaliens., 2005.
- 1743 Valensi, P., Michel, V., El Guennouni, K., and Liouville, M.: New data on human behavior from a 160,000
1744 year old Acheulean occupation level at Lazaret cave, south-east France: An archaeozoological
1745 approach, *Quaternary International*, 316, <https://doi.org/10.1016/j.quaint.2013.10.034>, 2013.
- 1746 Vernot, B., Zavala, E., Gómez-Olivencia, A., Jacobs, Z., Slon, V., Mafessoni, F., Romagné, F., Pearson, A.,
1747 Petr, M., Sala, N., Pablos, A., Aranburu, A., Bermúdez de Castro, J.-M., Carbonell, E., Li, B., Krajcarz, M.,
1748 Krivoshapkin, A., Kolobova, K., Kozlikin, M., and Meyer, M.: Unearthing Neanderthal population history
1749 using nuclear and mitochondrial DNA from cave sediments, *Science*, 372, eabf1667,
1750 <https://doi.org/10.1126/science.abf1667>, 2021.
- 1751 Vidal-Matutano, P., Blasco, R., Sañudo, P., and Fernández Peris, J.: The Anthropogenic Use of Firewood
1752 During the European Middle Pleistocene: Charcoal Evidence from Levels XIII and XI of Bolomor Cave,
1753 Eastern Iberia (230–160 ka), *Environmental Archaeology*, 24, 269–284,
1754 <https://doi.org/10.1080/14614103.2017.1406026>, 2019.
- 1755 Voelker, A. H. L. and de Abreu, L.: A Review of Abrupt Climate Change Events in the Northeastern
1756 Atlantic Ocean (Iberian Margin): Latitudinal, Longitudinal, and Vertical Gradients, in: *Abrupt Climate*
1757 *Change: Mechanisms, Patterns, and Impacts*, American Geophysical Union (AGU), 15–37,
1758 <https://doi.org/10.1029/2010GM001021>, 2011.
- 1759 Wagner, B., Vogel, H., Francke, A., Friedrich, T., Donders, T., Lacey, J. H., Leng, M. J., Regattieri, E.,
1760 Sadori, L., Wilke, T., Zanchetta, G., Albrecht, C., Bertini, A., Combourieu-Nebout, N., Cvetkoska, A.,
1761 Giaccio, B., Grazhdani, A., Hauffe, T., Holtvoeth, J., Joannin, S., Jovanovska, E., Just, J., Kouli, K., Kousis,
1762 I., Koutsodendris, A., Krastel, S., Lagos, M., Leicher, N., Levkov, Z., Lindhorst, K., Masi, A., Melles, M.,
1763 Mercuri, A. M., Nomade, S., Nowaczyk, N., Panagiotopoulos, K., Peyron, O., Reed, J. M., Sagnotti, L.,
1764 Sinopoli, G., Stelbrink, B., Sulpizio, R., Timmermann, A., Tofilovska, S., Torri, P., Wagner-Cremer, F.,
1765 Wonik, T., and Zhang, X.: Mediterranean winter rainfall in phase with African monsoons during the
1766 past 1.36 million years, *Nature*, 573, 256–260, <https://doi.org/10.1038/s41586-019-1529-0>, 2019.
- 1767 Wainer, K., Genty, D., Blamart, D., Daëron, M., Bar-Matthews, M., Vonhof, H., Dublyansky, Y., Pons-
1768 Branchu, E., Thomas, L., Calsteren, P., Quinif, Y., and Caillon, N.: Speleothem record of the last 180 ka
1769 in Villars cave (SW France): Investigation of a large δ 18O shift between MIS6 and MIS5, *Quaternary*

- 1770 Science Reviews - QUATERNARY SCI REV, 30, 130–146,
1771 <https://doi.org/10.1016/j.quascirev.2010.07.004>, 2011.
- 1772 Wainer, K., Genty, D., Blamart, D., Bar-Matthews, M., Quinif, Y., and Plagnes, V.: Millennial climatic
1773 instability during penultimate glacial period recorded in a south-western France speleothem,
1774 *Palaeogeography, Palaeoclimatology, Palaeoecology*, 376, 122–131,
1775 <https://doi.org/10.1016/j.palaeo.2013.02.026>, 2013.
- 1776 Wang, Q., Wang, Y., Shao, Q., Liang, Y., Zhang, Z., and Kong, X.: Millennial-scale Asian monsoon
1777 variability during the late Marine Isotope Stage 6 from Hulu Cave, China, *Quat. res.*, 90, 394–405,
1778 <https://doi.org/10.1017/qua.2018.75>, 2018.
- 1779 Wang, Y. J., Cheng, H., Edwards, R. L., An, Z. S., Wu, J. Y., Shen, C. C., and Dorale, J. A.: A high-resolution
1780 absolute-dated late Pleistocene Monsoon record from Hulu Cave, China, *Science*, 294, 2345–2348,
1781 <https://doi.org/10.1126/science.1064618>, 2001.
- 1782 Wenzel, S.: Neanderthal presence and behaviour in central and Northwestern Europe during MIS 5e,
1783 in: *Developments in Quaternary Sciences*, 173–193, <https://doi.org/10.13140/2.1.2747.7442>, 2007.
- 1784 White, M. J. and Pettitt, P. B.: The British Late Middle Palaeolithic: An Interpretative Synthesis of
1785 Neanderthal Occupation at the Northwestern Edge of the Pleistocene World, *Journal of World*
1786 *Prehistory*, 24, <https://doi.org/10.1007/s10963-011-9043-9>, 2011.
- 1787 Willis, K. J., Bennett, K. D., Walker, D., Gamble, C., Davies, W., Pettitt, P., and Richards, M.: Climate
1788 change and evolving human diversity in Europe during the last glacial, *Philosophical Transactions of*
1789 *the Royal Society of London. Series B: Biological Sciences*, 359, 243–254,
1790 <https://doi.org/10.1098/rstb.2003.1396>, 2004.
- 1791 Wilson, G. P., Frogley, M. R., Hughes, P. D., Roucoux, K. H., Margari, V., Jones, T. D., Leng, M. J., and
1792 Tzedakis, P. C.: Persistent millennial-scale climate variability in Southern Europe during Marine Isotope
1793 Stage 6, *Quaternary Science Advances*, 3, 100016, <https://doi.org/10.1016/j.qsa.2020.100016>, 2021.
- 1794 Xue, G., Cai, Y., Ma, L., Cheng, X., Cheng, H., Edwards, R. L., Li, D., and Tan, L.: A new speleothem record
1795 of the penultimate deglacial: Insights into spatial variability and centennial-scale instabilities of East
1796 Asian monsoon, *Quaternary Science Reviews*, 210, 113–124,
1797 <https://doi.org/10.1016/j.quascirev.2019.02.023>, 2019.
- 1798 Yaworsky, P. M., Nielsen, E. S., and Nielsen, T. K.: The Neanderthal niche space of Western Eurasia 145
1799 ka to 30 ka ago, *Sci Rep*, 14, 7788, <https://doi.org/10.1038/s41598-024-57490-4>, 2024.
- 1800 Yravedra, J., Rubio-Jara, S., Panera, J., Made, J. van der, and Pérez-González, A.: Neanderthal diet in
1801 fluvial environments at the end of the Middle Pleistocene/early Late Pleistocene of PRERESA site in the
1802 Manzanares Valley (Madrid, Spain), *Quaternary International*, 520, 72–83,
1803 <https://doi.org/10.1016/j.quaint.2018.01.030>, 2019.
- 1804 Zahn, R., Comas, M. C., and Klaus, A. (Eds.): *Proceedings of the Ocean Drilling Program, 161 Scientific*
1805 *Results*, Ocean Drilling Program, <https://doi.org/10.2973/odp.proc.sr.161.1999>, 1999.
- 1806 Zhang, J., Zolitschka, B., Högrefe, I., Tsukamoto, S., Binot, F., and Frechen, M.: High-resolution
1807 luminescence-dated sediment record for the last two glacial-interglacial cycles from Rodderberg,
1808 Germany, *Quaternary Geochronology*, 82, 101535, <https://doi.org/10.1016/j.quageo.2024.101535>,
1809 2024.

1810 Ziegler, M., Tuenter, E., and Lourens, L.: The precession phase of the boreal summer monsoon as
1811 viewed from the eastern Mediterranean (ODP Site 968), *Quaternary Science Reviews*, 29,
1812 <https://doi.org/10.1016/j.quascirev.2010.03.011>, 2010.

1813